The Preparation, Functionalization and Biomedical Applications of Carbonaceous Nanomaterials

Jianfei Zhang

Dissertation submitted to the Faculty of Virginia Polytechnic Institute and State University in partial fulfillment of the requirements for the degree of

Doctor of Philosophy

In

Chemistry

Harry C. Dorn, Chair
Harry W. Gibson
Judy S. Riffle
Alfred L. Ritter
M. Nicole Rylander

March 21st, 2011

Blacksburg, Virginia

Keywords: Metallofullerene, Single-Walled Carbon Nanotube, Single-Walled Carbon Nanohorn, Peapod, Magnetic Resonance Imaging Contrast Agent

The Preparation, Functionalization and Biomedical Applications of Carbonaceous Nanomaterials

Jianfei Zhang

Abstract

Carbon nanomaterials have attracted significant attention in the past decades for their unique properties and potential applications in many areas. This dissertation addresses the preparation, functionalization and potential biomedical applications of various carbonaceous nanomaterials.

Trimetallic nitride template endohedral metallofullerenes (TNT-EMFs, $M_3N@C_{80}$, M = Gd, Lu, etc.) are some of the most promising materials for biomedical applications. Water-soluble $Gd_3N@C_{80}$ was prepared by the functionalization with poly(ethylene glycol) (PEG) and hydroxyl groups ($Gd_3N@C_{80}$[DiPEG$(OH)_x$]). The length of the PEG chain was tuned by changing the molecular weight of the PEG from 350 to 5000. The ^1H magnetic resonance relaxivities of the materials were studied at 0.35 T, 2.4 T and 9.4 T. Their relaxivities were found to increase as the molecular weight of the PEG decreased, which is attributed to the increasing aggregate size. The aggregate sizes were confirmed by dynamic light scattering. *In vivo* study suggested that $Gd_3N@C_{80}$[DiPEG$(OH)_x$] was a good candidate for magnetic resonance imaging (MRI) contrast agents. Another facile method was also developed to functinalize $Gd_3N@C_{80}$ with both carboxyl and hydroxyl groups by reaction with succinic acyl peroxide and sodium hydroxide thereafter. The product was determined to be $Gd_3N@C_{80}(OH)_{\sim 26}(CH_2CH_2COOM)_{\sim 16}$ (M = Na, H) by X-ray photoelectron spectrometry. The $Gd_3N@C_{80}(OH)_{\sim 26}(CH_2CH_2COOM)_{\sim 16}$ also exhibited high relaxivity, and aggregates in water. The research on both pegylated and

carboxylated $Gd_3N@C_{80}$ suggests that aggregation and rotational correlation time plays an important role in relaxation, and the relaxivities and aggregation of the water-soluble metallofullerenes can be tuned by varying the molecular weight of the functionality.

TNT-EMFs can be encapsulated inside single-walled carbon nanotubes (SWNTs) to form “peapod” structures by heating the mixture of TNT-EMFs and SWNTs in a vacuum. The peapods were characterized by Raman spectrometry and transmission electron microscopy (TEM). The peapods were then functionalized with hydroxyl groups by a high speed vibration milling (HSVM) method in the presence of KOH. The functionalized Gd-doped peapods exhibited high relaxivites and had an additional advantage of “double carbon wall” protection of the toxic Gd atoms from possible leaking.

The HSVM method was modified by using succinic acyl peroxide. The modified HSVM method could functionalize multi-walled carbon nanotubes (MWNT) and single-walled carbon nanohorns (SWNHs) with carboxyl groups. In the presence of N-(3-dimethylaminopropyl)-N’-ethylcarbodiimide hydrochloride (EDC), carboxylate MWNTs and SWNHs could be conjugated with CdSe/ZnS quantum dots (QDs).

TNT-EMFs were also encapsulated inside SWNHs to form SWNH peapods. SWNH peapods were functionalized by the modified HSVM method and then were conjugated with CdSe/ZnS QDs. The peapods were characterized by TEM. *In vitro* and *in vivo* studies indicated that SWNH peapods could serve as a multimodal diagnostic agent: MRI contrast agent ($Gd_3N@C_{80}$ encapsulated), radio-active therapeutic agent ($Lu_3N@C_{80}$ encapsulated) and optical imaging agent (QDs).

Acknowledgements

First, I would like to thank my research advisor, Prof. Harry C. Dorn, for his guidance, encouragement and support in the past five years. He encourages me to try new things as much as possible. I still remember the first time I talked to him. He told me “I will not give you one project. I will give you several projects. Naturally you will focus on one.” Then during my entire PhD period I tried a lot of things and was exposed to many areas. As he said, naturally I focused on the biomedical applications of carbonaceous nanomaterials as potential MRI contrast agents. He is always supportive to me. When I made mistakes in experiments, he comforted me; when I was unconfident and in a bad mood, he tried to cheer me up. I have learned so much from his guidance and become more confident than before. Thank you for everything!

I would also like to thank all of my committee members: Dr. Harry W. Gibson, Dr. Alfred L. Ritter, Dr. M Nicole Rylander, and Dr. Judy S. Riffle. They are from different research areas and helped me in different ways. Thanks for Dr. Gibson’s help on revising all my writings, from literature review to my published papers. He always responds quickly and corrects all the mistakes I make, however minor they are. I improved a lot in English writing with his help. He also provided lots of valuable suggestions. Thanks for Dr. Ritter’s instruction and training on 15 MHz NMR instruments. I learned from him that understanding “why” is more important than merely knowing “how”. Thanks for Dr. Rylander’s collaboration in biomedical study on carbonaceous nanomaterials. Through collaboration with her I learned the concept of biomedical engineering and the view of engineers. Thanks for Dr. Riffle’s good suggestions in my presentations. I still remember

that she asked me to explain the field-dependent relaxation without using equations in the departmental seminar. I didn't answer it very well, but later I spent a lot of time thinking of it. I learned a lot from this process and realized that it's very important to think scientific problems with a big picture and in a simple way.

I thank Dr. Chunying Shu for her extensive collaboration. She collaborated with me in all the work involving metallofullerenes and single-walled carbon nanohorns (SWNHs), both in functionalization and in characterization. She also provided useful discussion in this dissertation, and taught me a lot of experimental skills. I thank Prof. Panos P. Fatourous, Dr. Frank D. Corwin and Dr. Michael D. Shultz (VCU) for their collaboration with 2.4 T relaxivity measurement and *in vivo* MRI study. I thank Dr. Eunna Chung, Dr. Saugata Sarkar, Kristen Zimmerman and Jon Whitney in Prof. Rylander's group for the collaborations with the *in vitro* study of SWNTs and SWNHs based materials. I also thank Dr. David B. Geohegan, Dr. Alex Puretzky (Oak Ridge National Laboratory) for kindly providing SWNHs.

I would like to thank Lesley Owens for her help with ICP measurement. It's not her research work but she is always willing to help. I really appreciate Dr. John E. Bonevich (National Institute of Standards and Technology) and Dr. Gurpreet Singh for the help with HRTEM. Thanks to John McIntosh, Kathy Lowe for the help with TEM. I also thank Kim C. Harich and Dr. William Keith Ray for the help with mass spectrometry. Thanks to Dr. Brian Burke, Dr. Keith A. Williams (University of Virginia), Charles Farley and Dr. Robert J. Bodnar for the help with Raman spectroscopy. Thanks to Dr. Sayangdev Naha, Dr. Thomas Andrew Campbell and Steven C. Arzberger in ADA Technologies, Inc. for financial support of single-walled carbon nanotubes (SWNTs)

project and some Raman characterization. Thanks to Prof. Paul A. Deck for letting me use his vacuum line. I would also thank Frank Cromer for the help with X-ray photoelectron spectroscopy (XPS). Thanks to Tom Glass and Dr. Hugo Azurmendi for the help with the NMR. I also thank Tom Wertalik for all the help with glass work.

I am really grateful for the valuable help and discussion with former and current group members, Dr. Jennifer L. Russ, Xuelei Wang, Dr. Ting Cai, Dr. Tianming Zuo, Dr. Wujun Fu, Liaosa Xu, Jonathan E. Reid, Dr. Jiechao Ge, Jianyuan Zhang, Hunter Champion, Tim Fuhrer, Prof. James Duchamp (Emory and Henry College) and Xiaoling Wang. I also thank Stephanie Hurt for her administrative help.

Finally I would like to thank my parents for their continuing love and support. Thanks to all my friends that helped me a lot in the past.

Table of Contents

List of Figures

Chapter 2

Chapter 3

Chapter 6

Chapter 7

List of Tables

Chapter 2

Chapter 3

Chapter 4

Chapter 6

Chapter 1

Dissertation Overview

During the past decades carbonaceous nanomaterials, including fullerenes, carbon nanotubes and carbon nanohorns, exhibited great applications in biomedical area. In particular, the carbonaceous nanomaterials encapsulating paramagnetic metal atoms/ions (e.g. Gd^{3+}) can be used as potential magnetic resonance imaging (MRI) contrast agents. However, due to the hydrophobic property of the carbon cage, the solubility of thematerials in water is very poor, which limits their biomedical applications. This dissertation addresses the preparation and functionalization of various carbonaceous nanomaterials. Their biomedical applications were also studied *in vitro* and *in vivo*.

Chapter 1 is an overview of the dissertation. It addresses how our research was developed, from water-soluble metallofullerenes to more complicated peapods and quantum dots complexes. The content of each chapter is also introduced briefly.

Chapter 2 provides the background of this dissertation. First, the carbonaceous nanomaterials and some typical functionalization and modification methods of the materials are introduced. Then, the theory of MRI and MRI contrast agents are discussed in detail. Lastly, the potential biomedical applications of these carbonaceous nanomaterials are introduced.

In **Chapter 3**, we discussed the functionalization of a trimetallic nitride template endohedral metallofullerene (TNT-EMF) ($Gd_3N@C_{80}$) with poly(ethylene glycol) (PEG)

malonate and hydroxyl groups. Our group previously reported the synthesis and characterization of $Gd_3N@C_{80}[DiPEG5000(OH)_x]$.[1] The product had good water-solubility and higher relaxivities compared to commercial MRI contrast agents. However, the effect of the length of the PEG chain hasn't been studied and optimized. In Chapter 3, we discuss the functionalization of $Gd_3N@C_{80}$ with DiPEG and hydroxyls, in which the molecular weight of DiPEG was tuned. The relaxivities of $Gd_3N@C_{80}[DiPEG(OH)_x]$ with different molecular weights were studied. In this research we found that $Gd_3N@C_{80}[DiPEG(OH)_x]$ with lower molecular weight has higher relaxivity. This is attributed to the different aggregation behavior. Dynamic light scattering confirmed this conclusion. $Gd_3N@C_{80}[DiPEG350(OH)_x]$ and $Gd_3N@C_{80}[DiPEG750(OH)_x]$ have the largest hydrodynamic diameters and the highest relaxivities, while $Gd_3N@C_{80}[DiPEG5000(OH)_x]$ has the smallest hydrodynamic diameter and the lowest relaxivities. Dr. Panos P. Fatouros' group (Virginia Commonwealth University) did the *in vivo* experiment, which showed that $Gd_3N@C_{80}[DiPEG350(OH)_x]$ was a good candidate for potential MRI contrast agents with long-term effect. This work was published in *Bioconjugate Chemistry*: Zhang, J.; Fatouros, P. P.; Shu, C.; Reid, J.; Owens, L. S.; Cai, T.; Gibson, H. W.; Long, G. L.; Corwin, F. D.; Chen, Z. J.; Dorn, H. C. *Bioconjugate Chem.* **2010**, 21, 610-615. Unpublished results on the pH dependence of relaxivities are also discussed in this chapter.

In recent years much attention has been drawn to developing multimodal imaging and diagnostic agents.[2] To facilitate further conjugation with other moieties, the metallofullerenes were also functionalized with carboxyl groups, which can be conjugated with amino-terminated moiety in the presence of EDC (1-ethyl-3-(3-

dimethylaminopropyl)carbodiimide hydrochloride). Another issue with water-soluble metallofullerenes is that functionalization may potentially alter the stability of the carbon cage. Therefore, adding an additional graphitic layer is a better choice. Carbon nanotubes and carbon nanohorns are good candidates for this purpose. Gd-doped metallofullerenes can be encapsulated inside for MRI, and the outer shell can be used for functionalization and conjugation with other functional moieties. The following chapters focus on the realization of these two purposes.

In **Chapter 4**, an aqueous phase reaction using succinic acyl peroxide to functionalize TNT-EMFs in a facile way is discussed. The method was developed by Dr. Chunying Shu in the Dorn Research Group at Virginia Tech. With this method we obtained water-soluble TNT-EMFs, $Gd_3N@C_{80}(OH)_{\sim 26}(CH_2CH_2COOM)_{\sim 12}$ (M = Na or H). I measured the relaxivity of this material and compared the results with the pegylated samples. This chapter appears as part of the paper published in *Bioconjugate Chemistry*: Shu, C.; Corwin, F. D.; Zhang, J.; Chen, Z.; Reid, J.; Sun, M.; Xu, W.; Sim, J. H.; Wang, C.; Fatouros, P. P.; Esker, A. R.; Gibson, H. W.; Dorn, H. C. *Bioconjugate Chem*. **2009**, 20, 1186-1193.

In **Chapter 5**, we discuss the functionalization of tubular carbonaceous nanomaterials with a high speed vibration milling (HSVM) method using succinic acyl peroxide. Single-walled carbon nanotubes (SWNTs) can be functionalized with carboxyl groups by reacting with succinic acyl peroxide.[3, 4] However, the reactivity of SWNTs is not as good as the reactivity of fullerenes. The reaction was tedious and time consuming. Another way to functionalize SWNTs is known as the HSVM method, which is easier and faster.

The HSVM method can functionalize SWNTs with hydroxyl groups by milling them with KOH. We combined the advantage of both methods and developed a new way to functionalize tubular carbonaceous nanomaterials in collaboration. The method works well for multi-walled carbon nanotubes (MWNTs) and single-walled carbon nanohorns (SWNHs), but not for SWNTs. The carboxylated MWNTs and SWNHs were also conjugated with CdSe/ZnS quantum dots (QD). Functionalization of SWNHs by this method was published in *Chemistry of Materials*: Shu, C.; Zhang, J.; Ge, J.; Sim, J. H.; Burke, B. G.; Williams, K. A.; Rylander, M. N.; Campbell, T.; Puretrzky, A.; Rouleau, C.; Geohegan, D. B.; More, K.; Esker, A. R.; Gibson, H. W.; Dorn, H. C. *Chemistry of Materials*, **2010**, 22, 347-351.

In **Chapter 6**, we discuss the preparation of SWNT peapods. TNT-EMFs, $Gd_3N@C_{80}$ and $Lu_3N@C_{80}$, were encapsulated inside SWNTs. The peapods were functionalized with hydroxyl groups by the HSVM method in the presence of KOH. The samples were characterized and the relaxivities were measured. This work appears as a manuscript ready for submission: Zhang, J.; Bonevich, J. E.; Burke, B.G.; Williams, K. A.; Dorn, H.C.; The Preparation and Characterization of Functionalized Trimetallic Nitride Endohedral Metallofullerenes Single-Walled Carbon Nanotube Peapods, f-$M_3N@C_{80}$@SWNTs with high ^1H MRI relaxivity.

In **Chapter 7**, we discuss the preparation and characterization of SWNH peapods. Both $Gd_3N@C_{80}$ and $Lu_3N@C_{80}$ were encapsulated inside SWNHs. Gd-doped peapods can be used as potential MRI contrast agents. If ^{177}Lu is doped in the TNT-EMFs, the materials can be used as potential radioactive therapeutic agents. Collaborating with Dr.

Chunying Shu and Dr. Jiechao Ge, I also conjugated the SWNH peapods with CdSe/ZnS quantum dots, which is an optical imaging agent. Dr. M. Nicole Rylander's group (Virginia Tech) and Dr. Panos P. Fatouros's group studied the material both *in vitro* and *in vivo*. The results indicated the potential of the conjugate as a multimodal platform. This work was published in *Nano Letters*: Zhang, J.; Ge, J.; Shultz, M. D.; Chung, E.; Singh, G.; Shu, C.; Fatouros, P. P.; Henderson, S. C.; Corwin, F. D.; Geohegan, D. B.; Puretzky, A. A.; Rouleau, C. M.; More, K.; Rylander, C.; Rylander, M. N.; Gibson, H. W.; Dorn, H. C. *Nano Lett.* **2010**, 10, 2843-2848.

Chapter 8 summarizes the research discussed in this dissertation. There are a variety of experiments that can be performed in the future. Some of the future research is also discussed in this chapter. The references are listed at the end of the dissertation.

Some of my research results not included in this dissertation include: the relaxivities of $Gd@C_{82}O_6(OH)_{16}(NHCH_2CH_2COOH)_8$ with and without the antibody of green fluorescence protein (anti-GFP);[5] the relaxivities of $Gd@C_{82}O_2(OH)_{16}(C(PO_3Et_2)_2)_{10}$;[6] the applications of SWNHs as photothermal cancer agents;[7] the measurement of thermal conductivity of tubular carbon nanomaterials-phantom tissue composites (paper submitted and accepted); the size distribution of surfactants-suspended SWNTs, MWNTs and SWNHs; and the size distribution of SWNHs vs. temperature and concentration.

Chapter 2

Introduction and Background

2.1 New Carbonaceous Materials

Carbon is the sixth element in the periodic table and is well-known for its capability of self-bonding in three dimensions. This capability allows carbon to form various allotropes. The most well-known carbon allotropes are diamond and graphite. Carbon can also form materials at the nanoscale. Since 1980s, many carbon nanomaterials have been discovered, e.g, fullerenes, carbon nanotubes, etc. These materials open a new research area. Here we introduce four carbon nanomaterials: fullerenes, carbon nanotubes, carbon nanohorns and peapods.

2.1.1 Fullerenes

Fullerene is a spherical molecule composed of a closed carbon cage. Carbon atoms in the fullerenes are sp^2 type with some sp^3 character because of the high curvature of the molecules. The first fullerene, C_{60}, was discovered by Kroto et al. in 1985.[8] It contains 12 pentagons and 20 hexagons, which form a structure as a soccer ball (Figure 1). Other fullerene molecules were also discovered thereafter. At the early stage, fullerenes could only be produced at small quantities. This limited the study of the fullerenes. In 1990, Krätschmer, Huffman and co-workers developed a procedure that can produce fullerenes at the macroscale.[9] The Krätschmer-Huffman procedure makes the extensive studies of fullerenes possible.

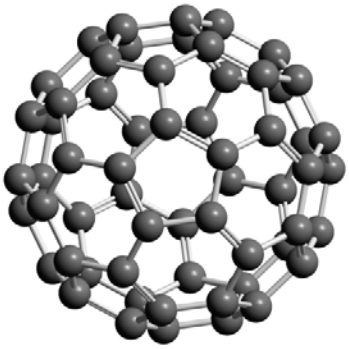

Figure 1. The structure of C_{60}.

Because the fullerene cage is hollow, atoms can be encapsulated. The first endohedral metallofullerene (EMF), La@C_{60}, was reported in 1985 by vaporizing a $LaCl_2$ impregnated graphite rod with a laser.[10] The symbol "@" was advocated to indicate that the atom is inside the fullerene cage.[11] Later many other metal atoms have also been encapsulated inside fullerene cages, including Group 2 (Ca, Sr, Ba) and Group 3 (Sc, Y, La) metals, alkali metals (Li, Na, K, Cs), and most of the lanthanide elements (La, Gd, Lu, etc).[12] The metallofullerenes can encapsulate not only mono metal atom (e.g. La@C_{60},[10, 11] Y@C_{82},[13] Ca@C_{82},[14] Gd@C_{82}[15]), but also multiple metal atoms (e.g. Ho_2@C_{82},[16] Sc_3@C_{84},[17] etc.) or metal carbides (e.g. Sc_2C_2@C_{84},[18] Sc_3C_2@C_{80}[19]).

In 1999, Stevenson, Dorn and coworkers discovered a novel endohedral metallofullerene molecule Sc_3N@C_{80} (Figure 2).[20] This molecule was formed by a trimetallic nitride template (TNT) process and produced in a high yield of 3-5% of the soluble extract.[20] Based on the TNT process, a new family of endohedral metallofullerenes (TNT-EMFs) was produced with different carbon cages and trimetallic nitride clusters.[21] The metal atoms inside the carbon cage can be either same metal atoms

(e.g. $Tb_3N@C_{80}$,[22] $Gd_3N@C_{80}$[23]) or combinations of various metal atoms (e.g. $CdSc_2N@C_{80}$,[24] $ScYErN@C_{80}$[25]).

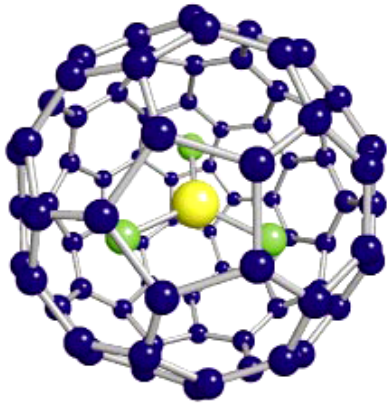

Figure 2. The structure of $Sc_3N@C_{80}$. Reprinted by permission from Macmillan Publishers Ltd: NATURE Reference[20], Copyright 1999.

2.1.2 Carbon Nanotubes

Carbon nanotubes are cylindrical carbon materials. In 1991 Iijima discovered double-walled and multi-walled carbon nanotubes (DWNTs and MWNTs).[26] Two years later Iijima and Bethune et al. also produced single-walled carbon nanotubes (SWNTs), which are composed of only one graphitic layer.[27, 28] Figure 3 shows high resolution transmission electron microscopic (HRTEM) images of various carbon nanotubes.

Since SWNTs can be considered as one rolled-up graphitic layer, they are usually named by a roll-up vector (n, m) as Figure 4 indicates. SWNTs with n=m are named as an "armchair" type while SWNTs with m=0 are named as a "zigzag" type. The other SWNTs are achiral. The roll-up vector determines many properties of SWNT, including diameter, helicity and band structure.[29] According to the calculation, about one-third of

SWNTs are one-dimensional metallic nanotubes(2n+m=3q, in which q is an integer), and the other two-third of SWNTs are one-dimensional semiconductive nanotubes (2n+q≠3q).[29]

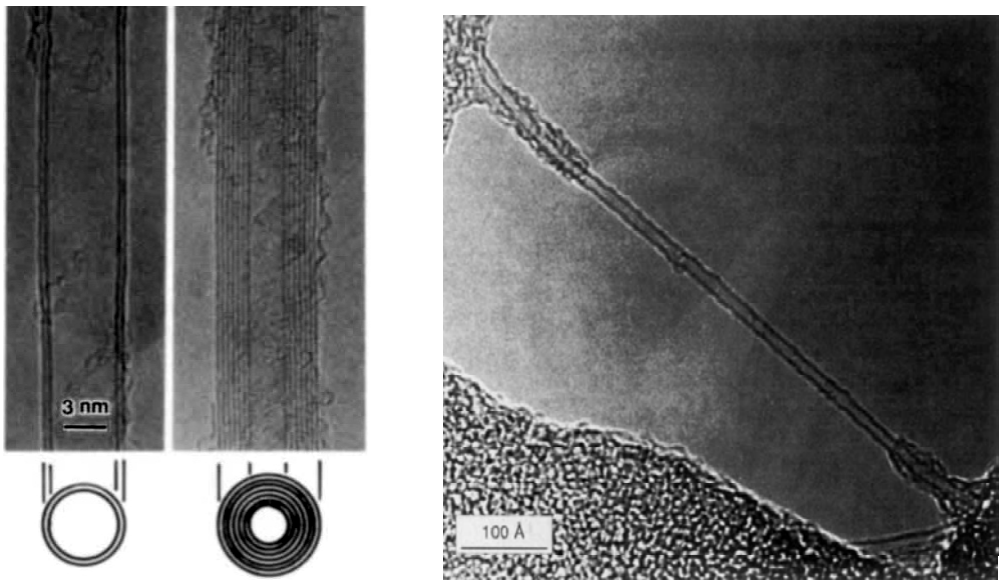

(a) (b)

Figure 3. High resolution transmission electron microscopic (HRTEM) images of (a) double-walled carbon nanotube (left) and multi-walled carbon nanotube (right); (b) single-walled carbon nanotube. Reprinted by permission from Macmillan Publishers Ltd: NATURE Reference[26] and Reference[28], Copyright 1991 and 1993.

2.1.3 Carbon Nanohorns

Single-walled carbon nanohorns (SWNH) were discovered in 1999.[30] SWNHs are produced by laser ablation of carbon at room temperature. Similar to SWNTs, SWNHs are also composed of one graphitic layer. The difference is that SWNH is terminated with one conical end. The typical size of SWNH is about 2-10 nm in diameter and 10-70 nm in length.[31] SWNH usually forms aggregates in diameter of 40~200nm. The structure of SWNH is shown by a HRTEM image in Figure 5.[32] The size of the aggregates depends on the length of individual SWNH and can be adjusted by changing the production

parameters.[33] SWNHs have a big advantage over SWNTs in that no metal catalyst is used in the production. Therefore, no purification is needed when using SWNHs.

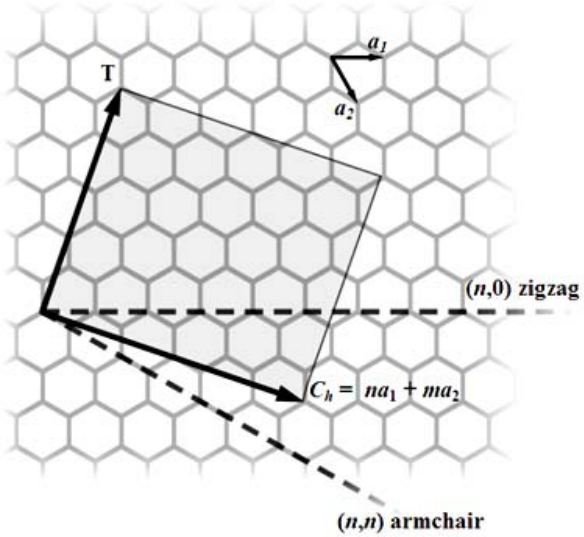

Figure 4. Single-walled carbon nanotubes naming scheme, where ***T*** denotes tube axis, and $\boldsymbol{a_1}$ and $\boldsymbol{a_2}$ are unit vectors of graphene in real space. (Reprinted from Wikipedia, image is in public domain.)

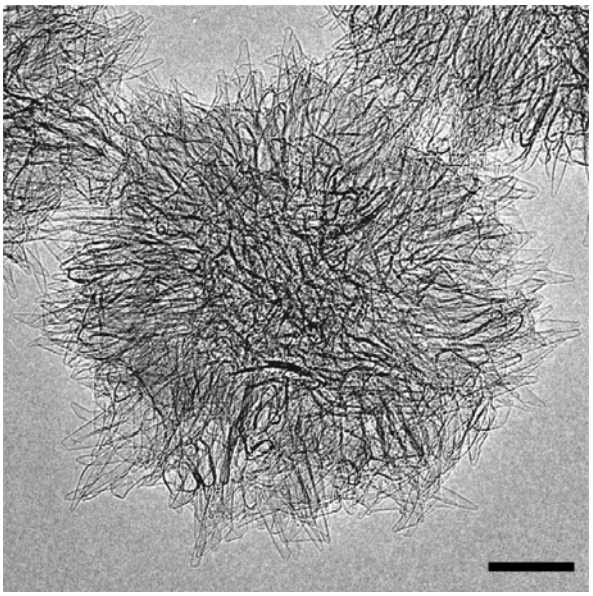

Figure 5. TEM image of dahlia-type SWNH aggregates. Scale bar represents 20 nm. Reprinted with permission from Reference[32]. Copyright 2008 American Chemical Society.

2.1.4 Peapods Structure

Both carbon nanotubes and nanohorns have interior space, which enables them to be filled by other atoms and/or molecules. In 1998 Smith and co-workers successfully encapsulated C_{60} inside SWNTs, as Figure 6 shows.[34] This new type of materials is called "peapod". Besides C_{60}, other fullerenes were also used to prepare peapods, such as C_{70},[35] Gd@C_{82}[36, 37] et al. Currently there are three methods to prepare peapods, which are discussed below:

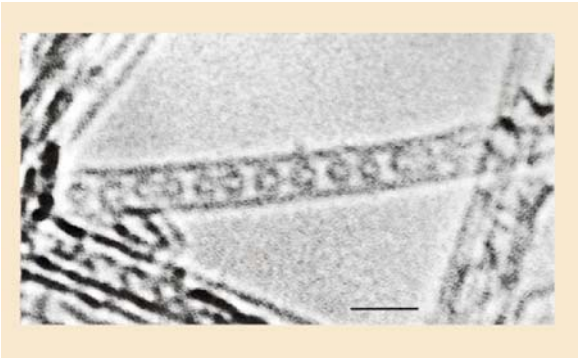

Figure 6. HRTEM image of C_{60}@SWNT. Reprinted by permission from Macmillan Publishers Ltd: NATURE Reference[34], copyright 1998.

i) Gas phase sublimation

This method is the most often used one.[35, 38-44] It is easy and straightforward. In this method the ends of SWNTs are opened first by heating the SWNTs in the air to about 400 ^{o}C. Then the open-ended SWNTs and fullerenes are placed together in a quartz tube. The tube is then sealed in high vacuum and heated to 400-600 ^{o}C. At this temperature fullerene molecules sublime and enter the SWNTs through the open ends.[45] This method can produce peapods in high yield (>80%).[45]

According to a theoretical study, there is no activation energy[46] or very low activation barrier[47] for the fullerenes to enter SWNT. Thus formation of peapods at room temperature is possible. The following two methods both produce peapods at room temperature. This is a great advantage for those molecules that are thermally unstable or nonvolatile.

ii) Liquid phase reaction

The liquid phase reaction usually involves putting open-ended SWNTs into a saturated solution of fullerene.[48, 49] A solvent in which fullerenes have low solubility and affinity was chosen. Due to the strong hydrophobic interaction between fullerenes and SWNTs, fullerene molecules can enter SWNTs. The yield of this method is not as high as the gas phase reaction.

iii) Supercritical Fluid

This method involves mixing fullerenes and open-ended SWNTs and placing the mixture in supercritical ethylene or carbon dioxide.[50-52] The pressure of the supercritical fluid (SCF) was cycled between 100 and 150 bar at 50 ^{o}C. The method has also the advantage of low temperature reaction.

2.2 Functionalization and Modification of Carbon Nanomaterials

Carbon nanomaterials typically have poor solubility in water. The solubility in organic solvents is also not satisfying. Carbon nanotubes and nanohorns do not dissolve even in any organic solvent. However, many applications of carbon nanomaterials need

good solubility in some solvents. Many efforts have been made to improve the solubility of carbon materials. This includes both covalent functionalizations and non-covalent modifications.

2.2.1 Covalent Functionalization

Many methods have been developed for covalent functionalization of SWNTs. Here several methods related to this dissertation are introduced below.

I. Bingel Reaction

The Bingel reaction is a classical reaction used to functionalize carbon nanomaterials with various functional groups. It was first applied to C_{60} (as shown in Figure 7).[53, 54] Fullerenes react with malonate in the presence of CBr_4 and DBU (1, 8-diazabicyclo[5,4,0]undec-7-ene). Later this reaction was also carried out on various metallofullerens, e.g. La@C_{82} [55-57] including TNT EMFs[1, 58, 59].

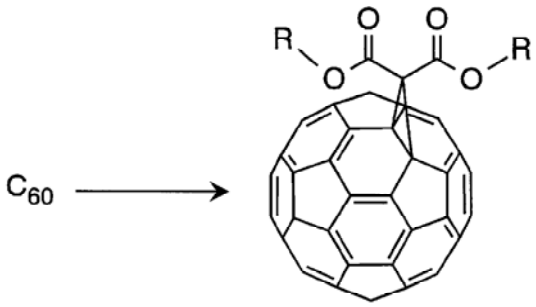

Figure 7. Bingel reaction. Reference[54]- Reproduced by permission of the Royal Society of Chemistry. http://dx.doi.org/10.1039/a702055d.

The Bingel reaction can also be used to functionalize carbon nanotubes[60-64] or nanohorns[65] to improve the solubility or for further conjugation reactions. Typically the

reaction occurs in some solvent. However, with the assistance of microwave radiation, the Bingel reaction can occur in a solvent-free environment.[65]

II. Hydroxylation

Solubility in water is important for all the medical applications. To facilitate biomedical applications, carbon nanomaterials must be functionalized with some hydrophilic groups, such as hydroxyl and/or carboxyl groups.

Fullerenes can be functionalized with hydroxyls by reaction with strong base. C_{60} with about 24-26 hydroxyl groups was prepared by stirring C_{60} in an aqueous solution of NaOH in the presence of phase transfer catalyst, such as TBAH (tetrabutylammonium hydroxide).[66, 67] A similar method was used to functionalize metallofullerene, $Ho_x@C_{82}$ (x=1,2), while the KOH was used instead of NaOH.[68] The first hydroxylated TNT-EMF was synthesized by Iezzi et al.[69] In their report, $Sc_3N@C_{80}$ was refluxed with sodium metal in toluene under the protection of argon. The procedure produced a black polyanionic radical precipitate. Exposing the precipitate to water and air produced the water-soluble TNT-EMF with hydroxyls.

The hydroxylation reaction can also be performed in a solvent-free environment, which reduces the effect of hazardous organic solvent. C_{60} was directly functionalized with about 16 hydroxyl groups by grinding the mixture of C_{60}, NaOH and H_2O_2 (Figure 8).[70] Single-walled carbon nanotubes (SWNT) were also functionalized by milling a mixture of SWNT and KOH at room temperature.[71]

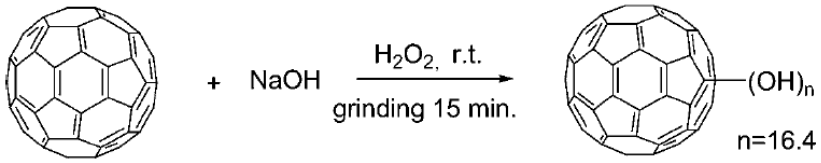

Figure 8. Solvent-free hydroxylation of fullerenes. Reprinted with permission from Reference[70]. Copyright 2005 Taylor and Francis.

III. Caboxylation

The carboxyl group is another hydrophilic group which is often used to functionalize carbon nanomaterials. Using the Bingel reaction, fullerene molecules can be directly functionalized with carboxyl groups by the reaction with malonic acid,[72, 73] but this method is not so efficient for SWNTs as fullerenes.[60] Single-walled carbon nanotubes can be easily functionalized with carboxyl groups when they are treated with strong oxidative acids, e.g. nitric acid or sulfuric acid.[74, 75] However, only ends and defect sites on SWNTs can be functionalized. Recently a one-step reaction was developed to functionalize SWNTs with carboxyl groups based on a free radical addition reaction (as shown in Figure 9).[3] In this reaction, SWNTs were stirred with succinic or glutaric acyl peroxide for ten days to produce carboxylated SWNTs.

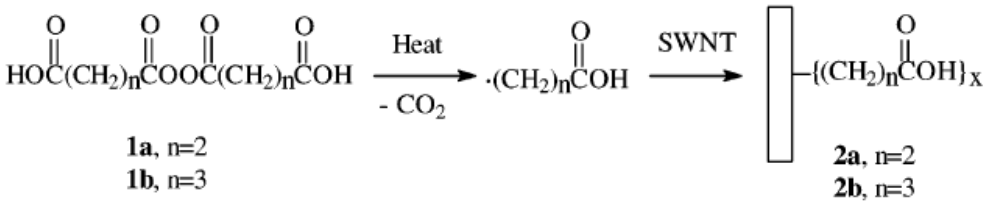

Figure 9. Sidewall functionalization of SWNTs. Reprinted with permission from Reference[3]. Copyright 2003 American Chemical Society.

The disadvantage of this method is that it is very time-consuming. Later a much faster solvent-free method was developed.[4] SWNTs were mixed with succinic acyl peroxide and heated at 110 ^{o}C, at which temperature the succinic acyl peroxide turned liquid. The half life of free radicals at this temperature is about 4 minutes. Therefore, the mixture was heated for 3-4 minutes to react. The procedure was repeated many times to make the functionalization complete. The method is demonstrated below in Figure 10.

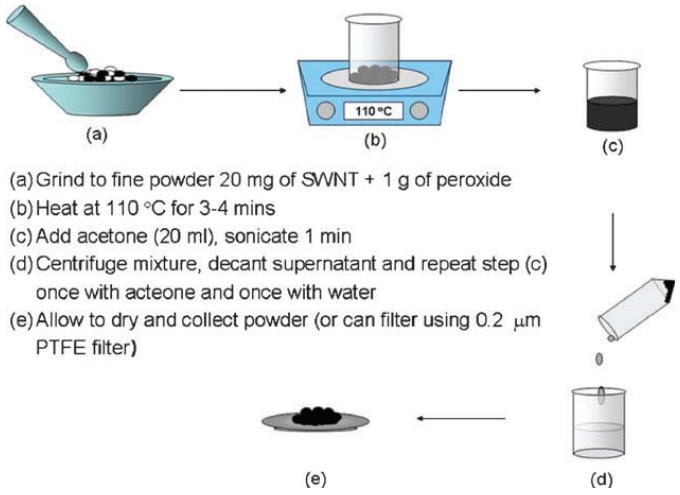

Figure 10. Carboxylic acid functionalization of SWNTs. Reference[4]-Reproduced by permission of the Royal Society of Chemistry. http://dx.doi.org/10.1039/b719380g.

IV. Conjugation

After functionalization, the carbon materials can be further conjugated with other functional moieties. In the presence of EDC (1-ethyl-3-(3-dimethylaminopropyl)carbodiimide hydrochloride), carboxylated carbon nanotubes can be conjugated with amine-terminated quantum dots (QDs) by amide bonds.[76] This procedure is demonstrated in Figure 11.

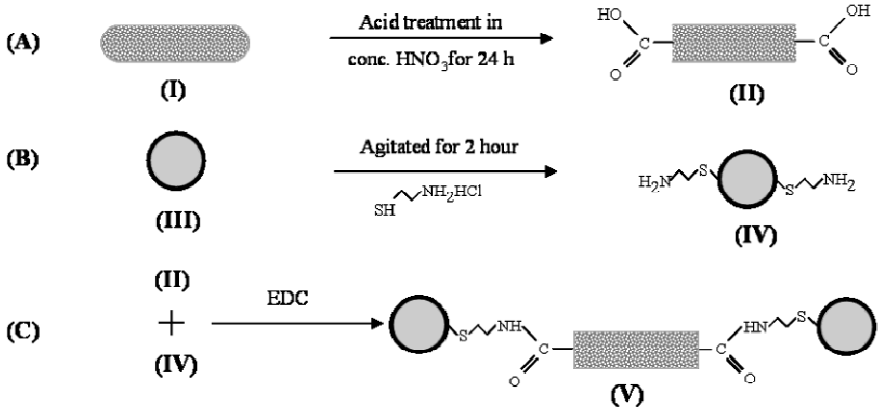

Figure 11. Schematic of the conjugation of carbon nanotubes to ZnS-capped CdSe quantum dots. Reprinted with permission from Reference[76]. Copyright 2003American Chemical Society.

2.2.2 Non-covalent Modification

Carbon nanotubes can also be exohedrally modified by non-covalent interaction.[77] They can be dispersed in aqueous phases by adding surfactants, such as benzylalkonium chloride,[78] sodium dodecylsulfate (SDS),[79] or Pluronic F108.[80] Wu et al. found that SWNTs modified by lysophospholipids, or single-chained phospholipids (shown in Figure 12), have an unprecedented solubility; however, the double-chained phospholipid modification is not so effective.[81]

Polymers were also used to modify carbon nanotubes to form composites.[82, 83] O'Connell and coworkers used poly(vinyl pyrrolidone) (PVP) and poly(styrene sulfonate) (PSS) to wrap SWNTs and prepared water-soluble SWNTs and discussed several ways of wrapping (shown in Figure 13).[84] They also found that the wrapping process is reversible if the solvent system is changed.

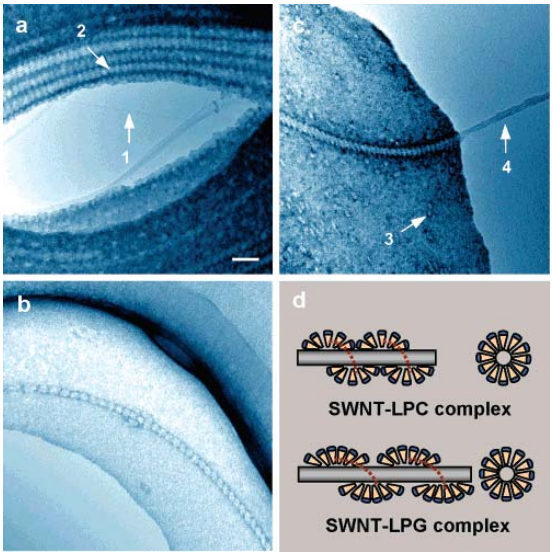

Figure 12. TEM images of SWNT-LPC (LPC: lysophosphatidylchlorine) (a and c) and SWNT-LPG (LPG: lysophosphatidylglycerol) (b) complexes. Arrow 2 in (a) indicates an LPC striation on a SWNT bundle. SWNT-LPG is less organized and has wider striations compared to SWNT-LPC. Scale bar: 20 nm (same for a-c). Figure d illustrates the lipid wrapping SWNTs from the side view and section view. Reprinted with permission from Reference[81]. Copyright 2006 American Chemical Society.

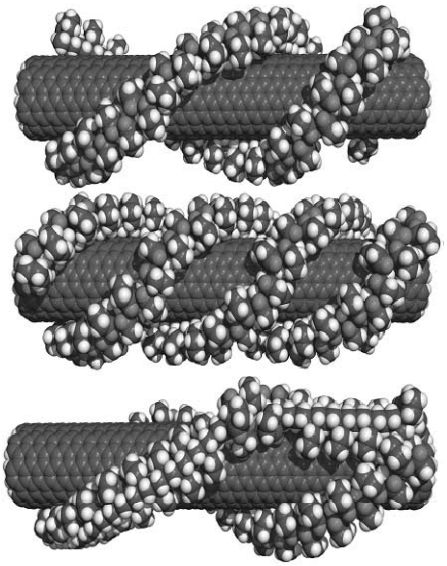

Figure 13. The schemes of three ways of wrapping PVP on SWNT. Top: double helix; middle: triple helix; bottom: multiple parallel wrapping strands. Reprinted from Reference[84], Copyright 2001, with permission from Elsevier.

2.3 Magnetic Resonance Imaging (MRI) and MRI Contrast Agents

2.3.1 Magnetic Resonance Imaging

Magnetic resonance imaging is a molecular imaging technique, which is noninvasive and harmless. It is widely used because of its high spatial resolution and great capacity of differentiating tissues. MRI is based on the same principles as nuclear magnetic resonance (NMR).[85] It detects the ^{1}H nuclei of water molecules in human bodies because 70% of the human body is water.

The ^{1}H nucleus has a magnetic moment. In an external magnetic field, $\boldsymbol{B_0}$, the magnetic moments of protons rotate around $\boldsymbol{B_0}$ incoherently at a Larmor frequency and form a net magnetization along $\boldsymbol{B_0}$ at equilibrium. When a radiation at the Larmor frequency is applied, a magnetic field $\boldsymbol{B_1}$ is produced perpendicular to $\boldsymbol{B_0}$ in the rotating frame. $\boldsymbol{B_1}$ perturbs the equilibrium and causes the magnetization to rotate around $\boldsymbol{B_1}$. After the radiation is removed, the magnetization recovers to its initial state. This relaxation process is exponential. The time constant of relaxation along $\boldsymbol{B_0}$ is T_1, which is called the longitudinal (or spin-lattice) relaxation time; while the time constant of relaxation perpendicular to $\boldsymbol{B_0}$ is T_2, which is called the transverse (or spin-spin) relaxation time.

The MRI signal intensity is determined by three factors: T_1, T_2 and the density of protons in water, ρ. The basic feature of MRI is that different tissues have different T_1 and T_2 values. The idea of MRI came out in 1971 when Damadian showed that normal tissues and tumors had different NMR relaxation times[86] and Hollis did similar

experiments.[87] This indicated that different tissues may have different NMR signal intensities, which encouraged scientists to develop an imaging technique based on it. In 1973 Lauterbur did the pioneering work[88] by introducing a linear gradient magnetic field and using projections along different directions. With these techniques two-dimensional images of objects were constructed. Later phase-encoding, frequency-encoding and slice-selection pulses were introduced into MRI[89], and form the basis of the modern MRI technique.

At the early stage of MRI, people expected that MRI, unlike X-ray based imaging, would never use contrast agents because the image contrast was strong and could be adjusted by varying different parameters.[90] However, plain MRI cannot produce satisfying images in many cases, e.g. tumors in the head, the loops of small bowels or some minor lesions. Currently more than 30% of MRI diagnoses must use contrast agents.[91, 92]

2.3.2 MRI Contrast Agents

MRI contrast agents are chemicals that can significantly change the relaxation times of water protons in tissues.[93, 94] In solutions with paramagnetic agents, the observed relaxation rates have two contributions as the equation 2.1 shows:[95]

$$\frac{1}{T_{i,obs}} = \frac{1}{T_{i,d}} + \frac{1}{T_{i,p}} = \frac{1}{T_{i,d}} + r_i[M], \quad \text{i=1, 2} \qquad (2.1)$$

$1/T_{i,obs}$ is the measured relaxation rate, $1/T_{i,\,d}$ is the relaxation rate of solvent nuclei without the paramagnetic contrast agents, $1/T_{i,\,p}$ is the contribution by the paramagnetic substance. [M] is the concentration of paramagnetic agent, and r_i is called the relaxivity

(r_1 is the spin-lattice or longitudinal relaxivity, while r_2 is the spin-spin or transverse relaxivity). Theoretically, the units of concentration should be molality (mol/kg solvent), but molarity (mol/L) is usually used for dilute solutions (mM^{-1} is often used).

In MRI image acquisition, the signal intensity can be described by:

$$\text{Signal Intensity} \propto \rho(1 - e^{-T_R/T_1})e^{-T_E/T_2} \qquad (2.2)^{96}$$

T_R is the pulse repetition time and T_E is the echo time. We can see that shorter T_1 produces greater signal intensity because the steady-state magnetization along $\boldsymbol{B_0}$ is greater with faster spin-lattice relaxation, while shorter T_2 generally decreases the signal intensity for the decreasing net transverse magnetization detected.[97, 98] Affecting T_1 and T_2 to different degrees can produce two kinds of images: T_1-weighted images and T_2-weighted images. Accordingly, the MRI contrast agents can be classified into two classes: T_1 agents and T_2 agents.

T_1 agents are paramagnetic substances. They affect T_1 strongly or affect both T_1 and T_2 by roughly the same amount. They usually have a r_2/r_1 ratio of 1~2[97] and produce positive images. Typical T_1 contrast agents are chelated gadolinium(III) ions. Figure 14 shows the structures of two representative MRI contrast agents: Magnevist® and Omniscan®.

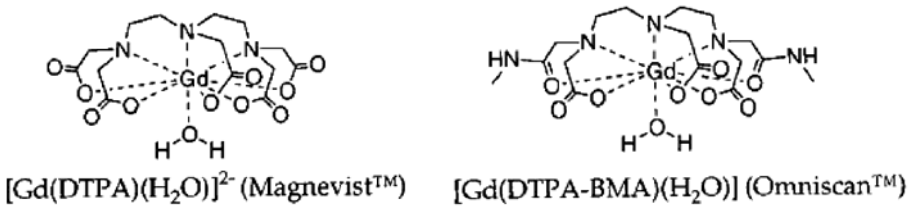

Figure 14. Structures of two commercial MRI contrast agents. Reprinted with permission from Reference[97]. Copyright 1999 American Chemical Society.

T_2 agents affect T_2 more greatly and produce negative images. The r_2/r_1 ratio for T_2 agents is typically as high as 10 or more.[97] They introduce a large local magnetic field inhomogeneity near the agents and thus affect the contrast.[99] Therefore, they have more long-range effect than gadolinium agents that interact with water protons directly. Typical T_2 agents are supermagnetic iron oxide particles coated by water-soluble shell-like dextrans.

Good contrast agents should have higher relaxivity to make superb contrast-enhanced images. Furthermore, to be clinically used, they must also be biocompatible, water-soluble, nontoxic and stable. Besides, the agents must have relatively longer intravascular duration and can be excreted after diagnosis.

2.3.3 Theories for MRI Contrast Agents

Commercial gadolinium based MRI contrast agents influence the relaxation through the large and fluctuating local magnetic field induced by Gd (III). The dipole-dipole interactions between the proton nuclear spins and the local magnetic fields result in the paramagnetic relaxation.[95] However, the local magnetic fields decay rapidly with the distance between water molecules and Gd ions. The random translational diffusion of water molecules and other interactions that bring the water molecules and Gd(III) ions near each other play a very important role to transmit the paramagnetic effect.[98] The effect on the water protons can be divided into three types: inner-sphere relaxation, second-sphere relaxation and outer-sphere relaxation. The three types of water are demonstrated in Figure 15.[97]

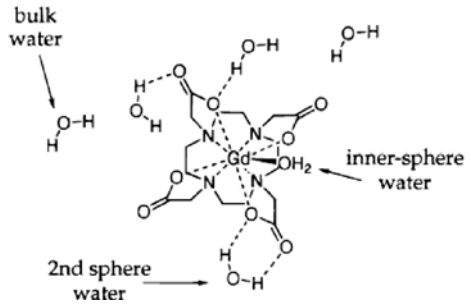

Figure 15. Three types of water: inner-sphere (directly coordinated to Gd (III)), second sphere (H-bonded to the complex), and bulk water. Reprinted with permission from Reference[97]. Copyright 1999 American Chemical Society.

The inner-sphere contribution to relaxivity is caused by the exchange of coordinated water molecules and bulk water molecules. The longitudinal and transverse relaxation rates are given by the following equations:[100, 101]

$$\frac{1}{T_1^{IS}} = \frac{qP_m}{T_{1m} + \tau_m} \qquad (2.3)$$

$$\frac{1}{T_2^{IS}} = qP_m \frac{1}{\tau_m}\left[\frac{T_{2m}^{-1}(\tau_m^{-1} + T_{2m}^{-1}) + \Delta\omega_m^2}{(\tau_m^{-1} + T_{2m}^{-1})^2 + \Delta\omega_m^2}\right] \qquad (2.4)$$

$$\Delta\omega_{obs}^{IS} = qP_m\left[\frac{\Delta\omega_m}{(1 + \tau_m T_{2m}^{-1})^2 + \tau^2\Delta\omega_m^2}\right] \qquad (2.5)$$

The superscript IS represents inner-sphere, P_m = [Gd]/55.6 is the mole fraction of the bound water molecules, q is the number of coordinated water molecules, τ_m is the residential time of the protons of bound water molecules, and $\Delta\omega_m$ is the chemical shift difference between the bound and the bulk water molecules. Usually $\Delta\omega_m$ is very small for aqueous solutions of Gd(III) complexes at magnetic field strengths higher than 0.2 T (which is the typical magnetic field strength for clinical use). Therefore, equation (2.4) can be simplified to (2.6):[102]

$$\frac{1}{T_2^{IS}} = \frac{qP_m}{T_{2m} + \tau_m} \qquad (2.6)$$

For hydrogen nuclei, the inner-sphere relaxation is governed by the dipole-dipole (DD) mechanism and scalar (SC) or contact mechanism. The dipole-dipole mechanism is influenced by the reorientation of nuclear spin – electron spin vector, the electron spin relaxation and the exchange of the water molecules. The scalar mechanism is affected by the electron spin relaxation and the water exchange.[95] Details about the two mechanisms are generally described by the Solomon-Bloembergen-Morgan (SBM) equations outlined below:[95, 97, 103-105]

$$\frac{1}{T_{i,m}} = \frac{1}{T_i^{DD}} + \frac{1}{T_i^{SC}} \quad \text{i} = 1, 2 \qquad (2.7)$$

$$\frac{1}{T_1^{DD}} = \frac{2}{15}\frac{\gamma_I^2 g^2 \mu_B^2 S(S+1)}{r^6}\left[\frac{3\tau_{c1}}{(1+\omega_I^2\tau_{c1}^2)} + \frac{7\tau_{c2}}{(1+\omega_s^2\tau_{c2}^2)}\right] \qquad (2.8)$$

$$\frac{1}{T_1^{SC}} = \frac{2}{3}S(S+1)\left(\frac{A}{\hbar}\right)^2\left[\frac{\tau_{e2}}{(1+\omega_s^2\tau_{e2}^2)}\right] \qquad (2.9)$$

$$\frac{1}{T_2^{DD}} = \frac{1}{15}\frac{\gamma_I^2 g^2 \mu_B^2 S(S+1)}{r^6}\left[\frac{3\tau_{c1}}{(1+\omega_I^2\tau_{c1}^2)} + \frac{13\tau_{c2}}{(1+\omega_s^2\tau_{c2}^2)} + 4\tau_{c1}\right] \qquad (2.10)$$

$$\frac{1}{T_2^{SC}} = \frac{1}{3}S(S+1)\left(\frac{A}{\hbar}\right)^2\left[\frac{\tau_{e2}}{(1+\omega_s^2\tau_{c2}^2)} + \tau_{e1}\right] \qquad (2.11)$$

$$\frac{1}{\tau_{ci}} = \frac{1}{T_{ie}} + \frac{1}{\tau_m} + \frac{1}{\tau_R} \qquad \text{i} = 1, 2 \qquad (2.12)$$

$$\frac{1}{\tau_{ei}} = \frac{1}{T_{ie}} + \frac{1}{\tau_m} \qquad \text{i} = 1, 2 \qquad (2.13)$$

γ_I is the nuclear gyromagnetic ratio, g is the electronic g factor, μ_B is the Bohr magneton, r is the electron spin-solvent nuclear spin distance, S is the spin of the nuclei,

ω_s and ω_I are the electron and nuclear Larmor precession frequencies, respectively. $\frac{A}{\hbar}$ is the electron-nuclear hyperfine coupling constant, T_{1e} and T_{2e} are the electronic relaxation times for longitudinal and transverse relaxation, and τ_R is the rotational correlation time corresponding to the metal ion-water proton nucleus vector.

From the equations above, we can see that several factors are very important in the enhancement of relaxation. These factors are further discussed below.

I. Rotation

Rotation is perhaps the most important factor that affects the relaxivity. Slowing the rotation of the Gd complex can significantly increase the relaxation rates. For the common Gd complexes at the clinical imaging magnetic field strength the rotational correlation time, τ_R, is on the order of 0.1 ns.[106] Figure 16 shows the nuclear magnetic relaxation dispersion (NMRD) profiles of the releaxivities at different rotational correlation times that are calculated by the SBM equations.[98] Typical values of other parameters for Gd(III) are used for calculation. The graph indicates that the height of the peak is significantly affected by rotation.

There are several factors that influence rotation: (1) The microviscosity of the tissues in which the Gd(III) contrast agents are distributed; (2) The covalent bonding between the agents and larger molecules such as proteins and antibodies; (3) The non-covalent binding of the Gd(III) agents and macromolecules.

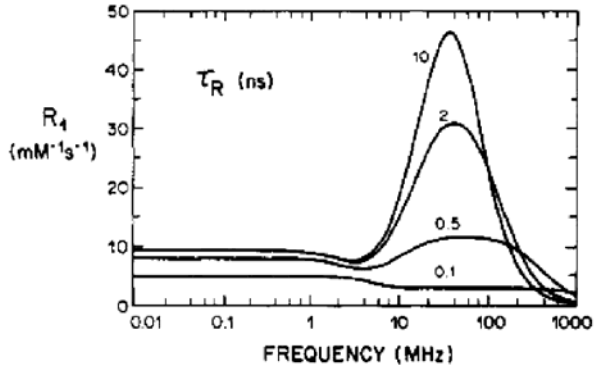

Figure 16. NMRD profiles of calculated inner sphere longitudinal relaxivities with different rotational correlation times. Typical parameters for Gd(III) complex were used. Reprinted with permission from Reference[98]. Copyright 1987 American Chemical Society.

Among the three factors, the viscosity is an important one. For spherical molecules, the effect of viscosity can be described by Debye-Stokes theory:[98]

$$\tau_R = 4\pi a^3 \eta / 3kT \qquad (2.14)$$

a is the radius of the molecules, η is the viscosity of the medium, k is Boltzmann constant and T is the absolute temperature. From the equation one can see that the rotational correlation time is directly proportional to the viscosity. The macroviscosity may differ from the microviscosity, which is hard to determine. Therefore, it is difficult to calculate τ_R directly. However, for similar systems with different molecular weights, the microviscosity can be assumed to be constant and the equation can be used to compare the rotational correlation times and the relaxivities.

One possible way to increase rotational correlation time, which leads to improved relaxivity, is attaching the Gd^{3+} chelate to a macromolecule through covalent or noncovalent interactions. This is one of the directions of current research. One thing

should be noticed that if the Gd^{3+} chelate has a motion that is independent on the macromolecule (internal motion), such as the rotation about a single axis, the relaxivity can be greatly reduced.[98] This explains why sometimes the relaxivity will not increase with the increasing molecular weight as expected. When designing the Gd-based contrast agents attached to macromolecules, two or more attachment sites are often helpful to reduce the internal flexibility.

A useful method to describe the rotational motion is the Lipari-Szabo approach.[107, 108] It is believed that two types of motion will affect the relaxation. One is rapid, local motion and the other is slow, global motion.[95] For Gd (III) chelates, the global rotation usually makes more contribution to the relaxivity.[95, 107, 108]

II. Proton exchange

The exchange rate of the protons of bound water molecules with bulk water is another important factor that affects relaxivity. It has dual effects on the relaxivity. On one hand, it modulates the efficiency of the exchange of bound water and bulk water, as equations (2.3) and (2.6) show; on the other hand, it makes a contribution to the overall correlation time, τ_c, as equations (2.8) and (2.12) demonstrate. The exchange of protons can be described by both the exchange of the whole water molecule and exchange of only hydrogen nuclei.[95] At physiological pH values, the proton exchange of Gd (III) agents has the same rate as the exchange rate of water molecules, and the residential time of protons, τ_m, is the reciprocal of water exchange rate constant, k_{ex}. However, if the pH is far away from the physiological pH, the proton may exchange faster than water molecules due to acid- or base- catalyzed pathways.[109, 110]

The dual effect can be demonstrated by Figure 17.[98] From the graphs we can see that both too long and too short τ_m can decrease the relaxivity. If τ_m is too long, which means that the exchange of water molecules is very slow, the Gd (III) ions will only influence a small fraction of water molecules and thus reduce the relaxivity. From equations (2.3) and (2.6), one can see that large τ_m will decrease relaxivity. If τ_m is too short, which represents very fast exchange of bound and bulk water molecules, the interaction time between Gd (III) ions and water molecules is not long enough to enhance relaxivity. Equation (2.12) shows that short τ_m, usually at the same order as τ_R and T_{ie}, can decrease τ_{ci}. Since τ_{ci} is short, $\omega_I^2\tau_{c1}^2$ and $\omega_s^2\tau_{c2}^2$ terms in equations (2.8) and (2.10) are usually much smaller than 1 and can be neglected. Thus we can see that T_i^{DD} gets larger. T_i^{SC} has similar dependence on τ_m. From equations (2.3) (2.4) (2.6) (2.7), we can conclude that short τ_m decreases relaxivity. This is more obvious at higher magnetic field strength where T_{ie} increases.[98]

The dual effects of water exchange on relaxivity require optimizing τ_m. Two factors should be considered. (1) The steric effect: one example is that the water exchange rate of the complex that undergoes dissociative exchange will increase with increasing steric bulk;[106, 111] (2) Charge effects: For a dissociative process, higher negative overall charge can increase the exchange rate because it helps water molecules to leave.[112, 113]

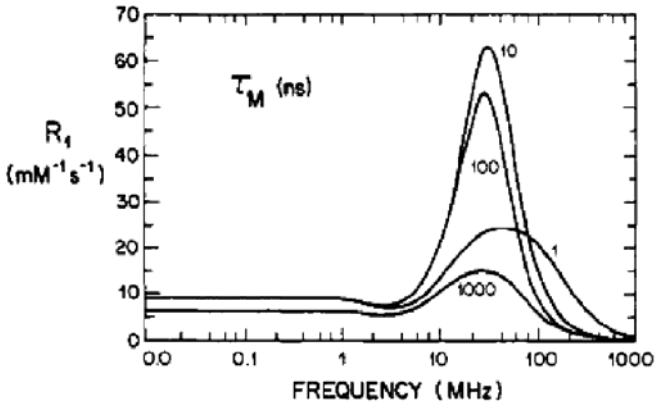

(a)

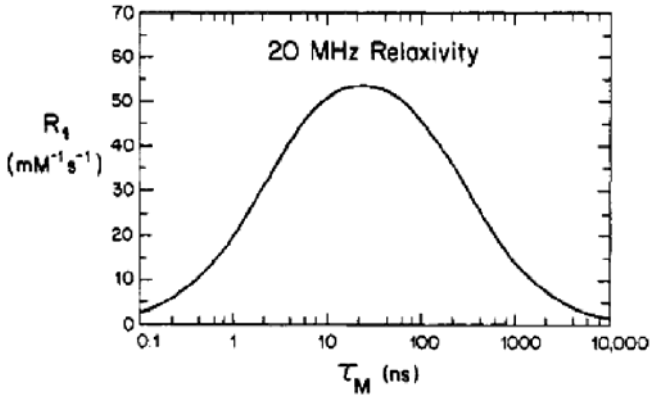

(b)

Figure 17. (a) NMRD profiles with different values of τ_m for immobilized complex. SBM theory was used with some typical values of other parameters for Gd (III) complex; (b) Calculated relaxivities with different τ_m for immobilized complex. The magnetic field is fixed at Larmor Frequency 20 MHz. Reprinted with permission from Reference[98]. Copyright 1987 American Chemical Society.

III. Electronic relaxation

The f orbitals of Gd (III) ions are half-filled, which makes the electronic relaxation relatively inefficient and the T_{1e} relatively long.[114] From equations (2.3) – (2.10) we can see that the longer T_e also contributes to the relaxivity. The electronic relaxation is

magnetic field dependent, which makes it difficult to determine. At low field, when $\omega_s^2\tau_v^2 \ll 1$, the electronic relaxation is monoexponential[104] and can be described as:

$$\frac{1}{T_{1e}} = B[\frac{1}{1+\omega_s^2\tau_v^2} + \frac{4}{1+4\omega_s^2\tau_v^2}], \quad B = \frac{1}{25}\Delta^2[4S(S+1)-3]\tau_V \qquad (2.15)$$

$$\frac{1}{T_{2e}} = B[\frac{5}{1+\omega_s^2\tau_v^2} + \frac{2}{1+\omega_s^2\tau_v^2} + 3], \; B = \frac{1}{10\tau_{so}} = \frac{\Delta^2}{50}[4S(S+1)-3]\tau_V \qquad (2.16)$$

Here Δ is the trace of zero field splitting (ZFS) tensor, τ_V is the correlation time for the modulation of ZFS. However, for Gd (III) ion, S=$\frac{7}{2}$ and the condition is not satisfied. The electronic relaxation becomes multiexponential.[115]

The physical meaning of this difference is that at the low field limit, the Zeeman energy is dominant and the electron spin precesses about the direction of external magnetic field. But at high field strength, the ZFS interaction is larger than that of Zeeman splitting, and the electron spin precesses about the principle axis of ZFS tensor, so that under the ZFS limit, the symmetry of molecules will also affect nuclear relaxivity.

IV. Hydration number and distance between nuclei and unpaired electron

Equations (2.3) and (2.4) indicate that the relaxation rates are directly proportional to the number of bound water molecules. However, it is impractical to increase the relaxivity by increasing q, because it will also decrease the thermal stability and kinetic inertness of the Gd(III) complex. The complex may release toxic Gd^{3+} ions. Therefore q is usually 1 for all the Gd(III) based MRI contrast agents.

The relaxivity is dependent on $1/r^6$. If we decrease the distance between unpaired electrons and protons, the relaxivity will increase significantly. However, this is also difficult to measure and control. The Gd-O distance of a bound water molecule can be measured.[116, 117] It has been verified that the distance is unlikely to change from solid state to solution,[116] but the angle between the plane of water molecule and Gd-O vector varies very much in aqueous solutions. Direct measurement of Gd-H distance has been obtained for very concentrated solutions,[118, 119] and the distance was found to be independent of ligand and total charge. Therefore, it is difficult to enhance relaxivity by shortening the Gd-H distance. The bonding in Gd(III) complexes is predominantly ionic; thus, electron delocalization onto the ligand to shorten the relaxivity is also infeasible.[103]

2.3.4 Measurement of Relaxivity

Measurement of relaxivity is realized by measuring the relaxiation times of a series of samples with different paramagnetic agent concentrations. A plot of relaxation rate vs. concentration is made. According to equation (2.1), the plot is linear, and the slope is the relaxivity. Therefore, the key point for measuring relaxivity is to measure relaxation times. Below is the description for measuring T_1 and T_2, respectively.

I. Measurement of T_1

In this dissertation, measuring T_1 is realized by an inversion-recovery method. In this method, a π pulse is first applied to flip the nuclear magnetization to $-z$ direction, which is opposite to the direction of the external magnetic field. The nuclear magnetization then returns to its original state via spin-lattice relaxation process. Before it reaches the

equilibrium state, a $\pi/2$ pulse is applied. The nuclear magnetization is flipped to the transverse plane, and starts to process about the external magnetic field, $\boldsymbol{B_0}$. Free induction decay (FID) signal can be measured for variable delay time τ. The pulse sequence is shown in the Figure 18.

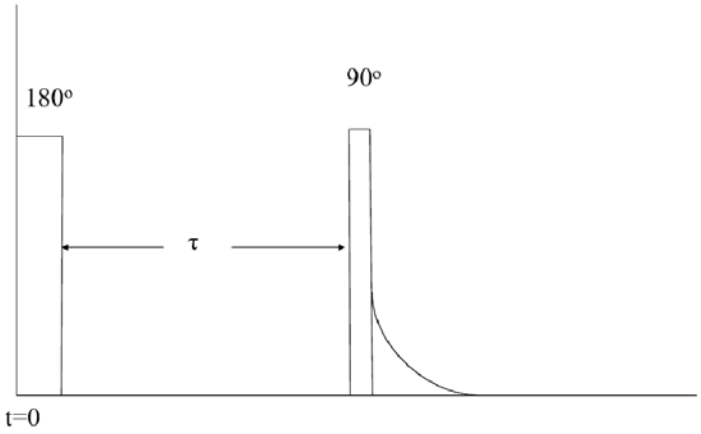

Figure 18. Inversion-recovery pulses sequence.

With this pulse sequence, the magnetization at any time τ is

$$M(\tau) = -2M_0 e^{(-\frac{\tau}{T_1})} + M_0$$

M_0 is the magnetization at equilibrium state (t = 0). At 9.4 T, the $M(\tau)$ is measured and plotted vs. τ. T_1 is then obtained by exponential fitting. At 0.35 T, a different method was used. The difference of magnetization at time τ and equilibrium state is measured:

$$\Delta = M_0 - M(\tau) = 2M_0 e^{(-\frac{\tau}{T_1})}$$

Taking the natural log of the equation yields

$$\ln \Delta = \ln 2M_0 - \frac{\tau}{T_1}$$

$\ln\Delta$ is plotted vs. τ, the slope is $1/T_1$ and T_1 can be calculated.

II. Measurement of T_2

T_2 is measured with a spin-echo pulse sequence, which is shown in Figure 19. In this method, a $\pi/2$ pulse is applied to rotate the nuclear magnetization onto the *XY* plane. The magnetization then starts to precess about the external magnetic field, $\boldsymbol{B_0}$, and fans out due to the spin-spin relaxation process and the inhomogeneity of the magnetic field. After time τ, a π pulse is applied to flip the magnetization. Then at time 2τ an echo signal forms. The π pulse reduces the signal decay caused by the inhomogeneity of the external magnetic field. Therefore, the measured echo signal is only affected by the spin-spin relaxation. In real measurements, a series of π/-π pulses are applied at time equals τ, 3τ, 5τ… alternatively, and echo signal can be measured at times 2τ, 4τ, 6τ….. The alternative π/–π pulses are used to compensate the slight discrepancy of each pulse from 180°. This method is called Carr-Purcell-Meiboom-Gill (CPMG) method. When spin-echo pulses are used, the magnetization measured at time t is

$$M(t) = M_0 e^{-\frac{t}{T_2}}$$

Taking the natural log of the equation, we can obtain

$$\ln M(t) = \ln(M_0) - \frac{t}{T_2}$$

M(t) is measured at t = 2τ, 4τ, 6τ… T_2 can be obtained either by exponential fitting (9.4 T) or by plotting lnM(t) vs. t and calculating from the slope (0.35T).

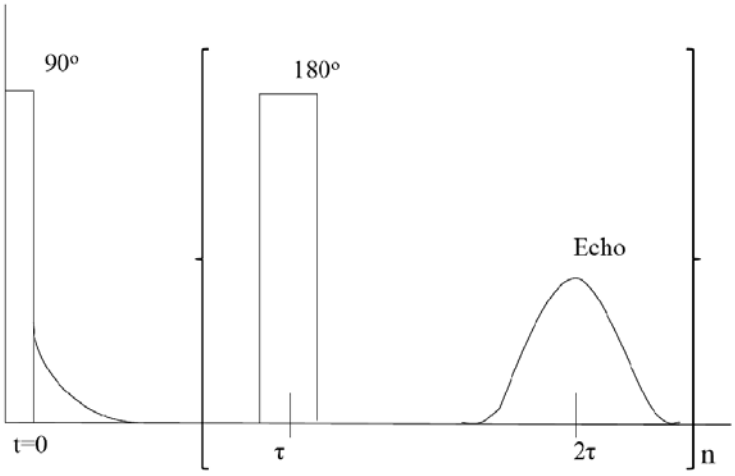

Figure 19. Spin-echo pulses sequences.

2.4 The Potential Applications of Carbonaceous Nanomaterials

2.4.1 MRI Contrast Agents

2.4.1.1 Fullerenes

Since the discovery of fullerenes, many applications have been proposed. Medical applications are one of the promising areas. In this section the potential application of endohedral metallofullerenes and their derivatives as potential MRI contrast agents will be discussed.

Endohedral metallofullerenes encapsulate one or more metal atoms inside the carbon cage. The metal atoms in the cage are usually lanthanides. One important advantage of these materials is that the carbon cage of fullerene is very stable. Therefore the internal metal atoms have no chance of being released into the body. Different combinations of the metal atoms inside the fullerenes can provide various characteristics, so that metallofullerenes can be used as potential X-ray contrast agents (Lu doped), MRI

contrast agents (Gd doped) et al. As shown in Figure 20, there is a substantial overlap of the metals that can both form metallofullerenes and have nuclear applications,[120] which makes metallofullerenes very attractive materials for biomedial applications. Gadolinium is often encapsulated inside the fullerenes for applications as potential MRI contrast agents. Other metals, such as holmium, are also studied for this purpose.

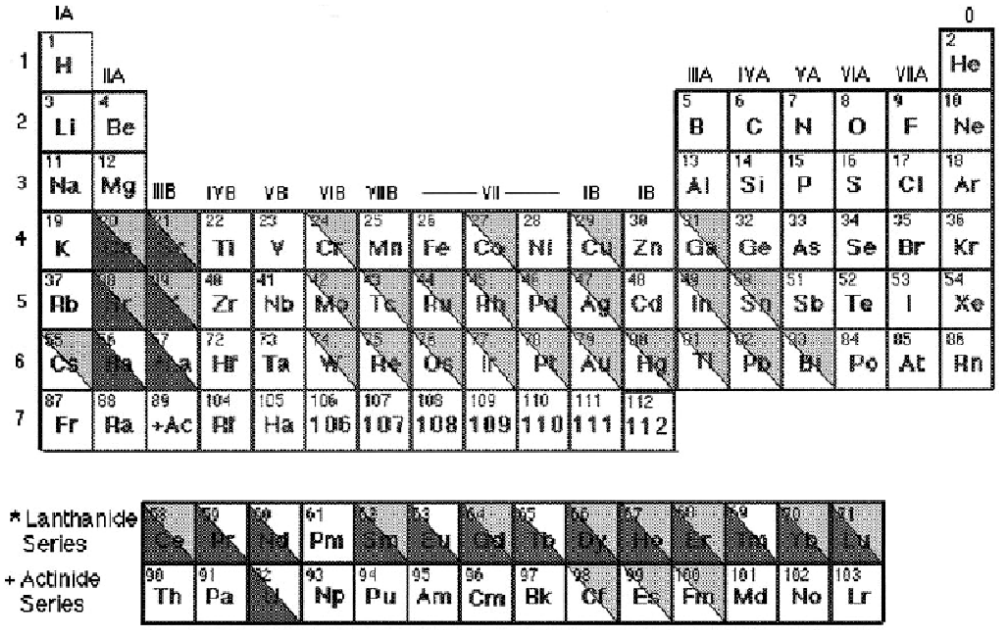

Figure 20. Metals that can form endohedral metallofullerenes (dark shading) and those are useful for nuclear medicine (light shading). Reprinted with permission from Reference[120]. Copyright 1999 Elsevier.

There is one disadvantage of metallofullerenes: they are usually insoluble in water, so they cannot be used directly *in vivo*. Fortunately, the rich chemistry in functionalizing fullerenes makes it possible to obtain water-soluble metallofullerenes by attaching water-soluble groups to the carbon cage. Many efforts have been developed to produce water-soluble metallofullerenes for biomedical applications.

I. Current research progress

Water-soluble lanthanoid metallofullerenes have great relaxivity and are good candidate as potential MRI contrast agents. There are mainly two types of water-soluble metallofullerene derivatives: polyhydroxylated and polycarboxylated metallofullerenes. Other functional groups can be attached to obtain fullerenes with some specific characteristics.[121, 122]

(1) Relaxivity. Polyhydroxylated lathanoid metallofullerenes usually have much higher relaxivity compared to commercial Gd chelates. Kato et al. studied the relaxivities of various lanthanoid fullerenols $M@C_{82}(OH)_n$ and other compounds.[96] The results are listed in the table 1.

Ln compds	r_i	La	Ce	Gd	Dy	Er
ions[b]	r_1	0.0	0.0	12	0.5	0.4
	r_2	0.0	0.0	14	0.6	0.5
M-DTPA[b]	r_1	0.0	0.0	4.4	0.1	0.1
	r_2	0.0	0.0	5.0	0.1	0.1
fullerenols	r_1	0.8	1.2	73	1.1	1.3
	r_2	1.2	1.6	80	1.9	1.5

Table 1. Relaxivitities of Lanthanoid compounds at 0.47 T, pH=7 and 19 ^{o}C. Reprinted with permission from Reference[96]. Copyright 2003 American Chemical Society.

From the table we can see that the relaxivities of metallofullerenols are much higher than those of DTPA chelates and bare metal ions. Substantial relaxivities were observed even for the metallofullerenols encapsulating metals with low magnetic moments, such as La^{3+} and Ce^{3+}， which usually show no relaxivities for bare ions and DTPA chelates. *In vivo* phantom study of the metallofullerenols shows that sufficient MRI signal

enhancement can be obtained at lower concentration for metallofullerenols, as Figure 21 shows[96].

Carboxylated metallofullerens do not have such high relaxivities, but their relaxivities are comparable to those of commercial MRI contrast agents.[123-125] Other water-soluble metallofullerene derivatives, such as amino acid derivatives of Gd (III) endohedral metallofullerenes (AAD-EMFs), also exhibit significant relaxivities.[121, 122] All the research shows that water-soluble metallofullerenes derivatives can significantly enhance the contrast of MRI images.

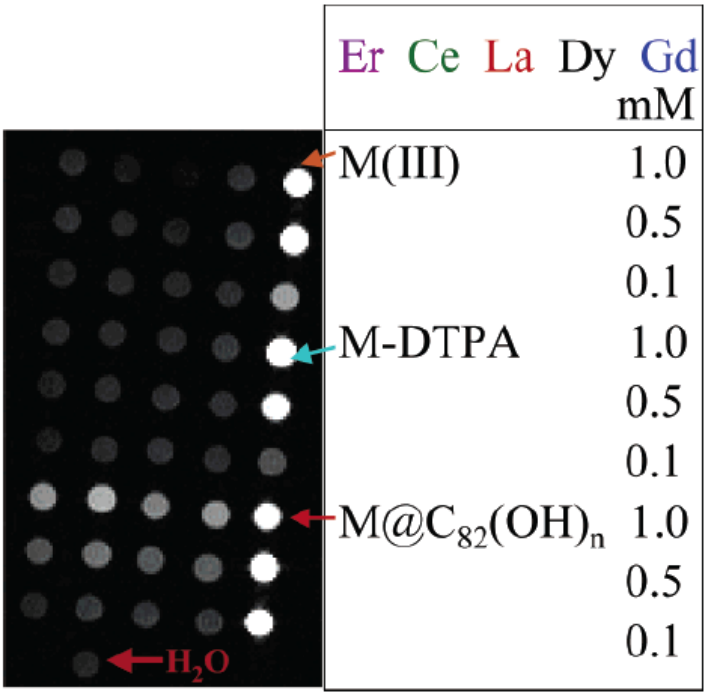

Figure 21. Phantom MRI images of various lanthanoid compounds. Reprinted with permission from Reference[96]. Copyright 2003 American Chemical Society.

(2) Biodistribution. Biodistribution is another important factor for MRI contrast agents because the agents must be biocompatible. Although metallofullerenols have higher

relaxivities, they also show high reticuloendothelial system (RES) uptakes, which are unfavorable for common MRI examinations. However, the carboxylated metallofullerenes show both low RES uptakes and good relaxivities comparable to commercial agents.[125] Figure 22 shows the *in vivo* MRI intensity distribution of $Gd@C_{60}[C(COOH)_2]_{10}$,[125] which has a higher kidney uptake and is easily excreted out of the body.

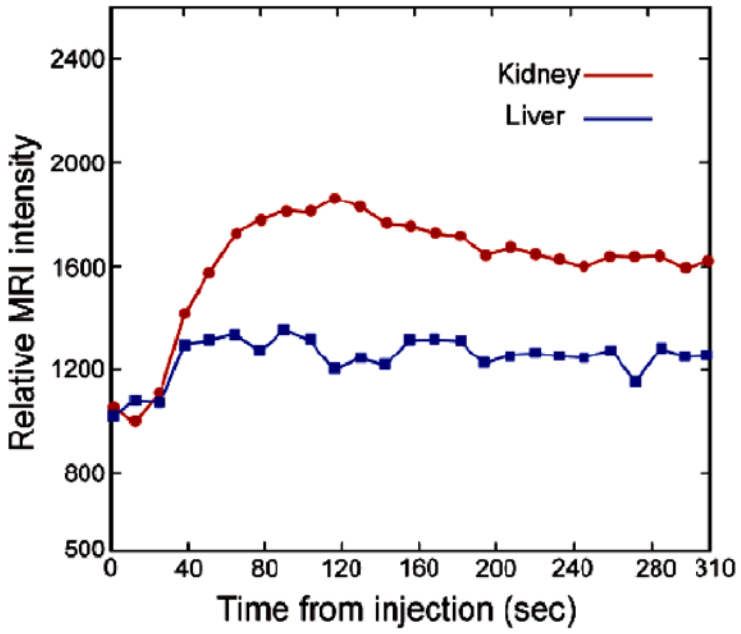

Figure 22. *In vivo* MRI intensity biodistribution. Reprinted with permission from Reference[125]. Copyright 2003 American Chemical Society.

II. Possible mechanisms

There are no water molecules directly coordinated to the Gd^{3+} ions inside metallofullerenes, so the inner-sphere model is not applicable in explaining the high relxivities. The only contribution comes from the outer sphere. Several factors have been proposed to explain the high relaxivity.

Studies have shown that both the hydroxylated and carboxylated metallofullerenes exhibit intermolecular aggregation in the solution. The results are listed in Table 2.[124] The aggregation results in increased rotational correlation times, which lead to high relaxivity. The hydroxylated fullerenes show more aggregation than the carboxylated ones, so they have much higher relaxivities. The aggregation may also lead to the formation of clusters large enough to be absorbed by RES. This explains why the hydroxylated metallofullerenes have higher RES uptake.

sample	Conc. C (mg/mL)	Average molecular weight M_w (g/mol)	Monomeric molecular weight M (g/mol)	Average aggregation number M_w/M	2nd virial coefficient A_2 (mL mol/g^2)
$Gd@C_{60}(OH)_x$	1-5	3.26×10^5	1269	257	-0.01×10^{-5}
$Gd@C_{60}[C(COOH)_2]_{10}$	5-8	1.27×10^5	2458	51	0.04×10^{-5}
	8-10	2.57×10^5	2458	105	0.03×10^{-5}

Table 2 Properties obtained from SLS data for $Gd@C_{60}(OH)_x$ and $Gd@C_{60}[C(COOH)_2]_{10}$. Reprinted with permission from Reference[124]. Copyright 2004 American Chemical Society.

Another possible reason is the negative charge on carbon cage. The metal atoms inside metallofullernes usually transfer electrons to the cage.[126] The negative charge on the carbon cage will attract the hydrogen end of water molecules. Thus the unpaired electrons in the metal ions can relax more water molecules.

There is also one hypothesis[127] that for monatomic metallofullerenes, three electrons are transferred to the cage so one of them is unpaired. The unpaired electron makes a significant contribution to the relaxivity. However, this cannot explain the high relaxivity of trimetallic nitride template endohedral metallofullerenes (TNT-EMF) derivatives,[1]

because TNT-EMFs transfer an even number of electrons (six electrons) to carbon cage. Recent research shows that the relaxivitity of $Gd_3N@C_{80}(OH)_m(O)_n$ is approximately three times that of $Gd@C_{60}(OH)_x$.[128] The relaxivities per gadolinium atom are nearly the same so the unpaired electron on the cage may make little contribution to the total relaxivity.

2.4.1.2 Carbon Nanotubes and Nanohorns

Carbon nanotube/nanohorn-based materials have also been studied as potential MRI contrast agents. Lon Wilson's group used ultrashort single-walled carbon nanotubes (SWNT) embedded with Gd^{3+} as potential MRI contrast agents.[129-131] In their experiments the Gd^{3+} clusters were formed near the defects on the walls of SWNTs, as shown in Figure 23. Similarly, Gd clusters were also prepared inside single-walled carbon nanohorns, which can be used as potential MRI contrast agents.[132]

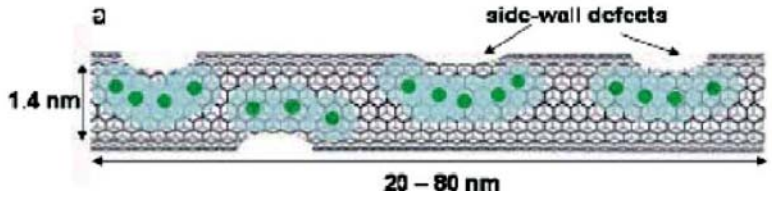

Figure 23. Depiction of a single ultra-short single-walled carbon nanotube loaded with hydrated Gd^{3+} ions. Gd^{3+} ions are near side-wall defects, which are created by cutting full-length nanotubes. Reference[130]- Reproduced by permission of The Royal Society of Chemistry. http://dx.doi.org/10.1039/b504435a.

Gd^{3+} ions were also noncovalently attached to the outer surface of carbon nanotubes (as shown in Figure 24).[133] Richard et al prepared amphiphilic Gd^{3+} chelates (GdL), and the amphiphlic chelated were linked with carbon nanotubes via van der Waals interaction.

This structure enabled direct access of water molecules to Gd^{3+}, and the relaxivities can be controlled by adjusting the concentration of GdL.

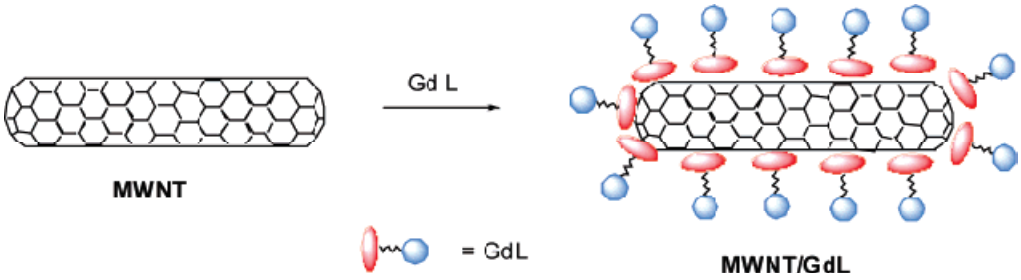

Figure 24. Carbon nanotubes noncovalently functionalized by amphiphlic Gd^{3+} chelates. Reprinted with permission from Reference[133]. Copyright 2008 American Chemical Society.

The high relaxivities of carbon nanotubes modified by gadolinium (both internally and externally) not only come from paramagnetic Gd ions, but also come from carbon nanotubes themselves. Lon Wilson's group studied raw, purified and shortened SWNTs' effect on shortening T_2.[134] They found all the materials show significant spin-spin relaxivities (r_2). The superior relaxivities of these SWNTs materials cannot be completely explained only by the metal impurities. Contributions also come from nanotubes themselves. This may be explained by the paramagnetic[135] or superparamagnetic properties[134] of SWNTs.

2.4.2 Drug Delivery

Single-walled carbon nanotubes and nanohorns have large interior space and surface area, which can encapsulate, adsorb or conjugate with other molecules. Therefore, they are good candidates for drug delivery systems. Theoretical studies indicate that drug molecules can be encapsulated inside single-walled carbon nanotubes. The minimum

radii to accept drug molecules and the radii with maximum suction energy for cisplatin were calculated as 4.785 Å and 5.27 Å respectiviely.[136, 137] The radii range which provides highest probability of efficient encapsulation was also determined as 9.134<a<12.683 Å for paclitaxel and 8.855<a<10.511 Å for doxorubicin.[138]

Experimentally, Guo et al loaded anticancer agent paclitaxel (PTX) into multi-walled carbon nanotubes coated with ultra-thin acrylic acid or poly (lactic-*co*-glycolic acid (PLGA) film. The material exhibits antitumor effects against human PC3MM2 prostate cancer cells.[139] Dai's group conjugated PTX to poly(ethylene glycol) on SWNTs as Figure 25 shows.[140] The conjugate is water-soluble and can suppress tumor growth of murine 4T1 breast cancer cell. The efficiency in suppressing tumor growth is higher than clinical Taxol. They also found that drug molecules, doxorubicin, can bind to the SWNTs via π-stacking, and the release of drug molecules can be controlled by using nanotubes with suitable diameters.[141] Tumor-targeting modules can also be attached to the drug-SWNTs conjugate system to deliver anti-cancer drug molecules to cancer cells more selectively and efficiently.[142]

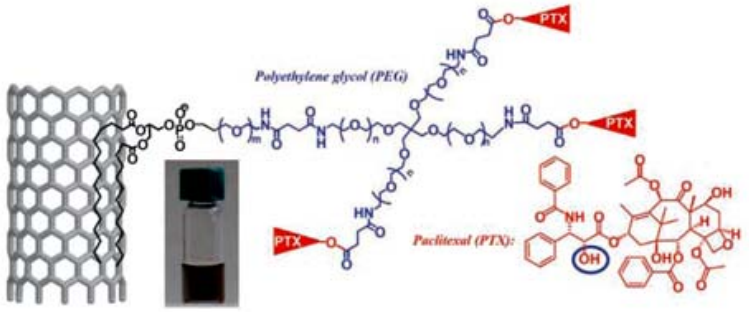

Figure 25. Schematic illustration of PTX conjugation to SWNT functionalized by phospholipids with branched PEG chains. PTX can be released from nanotubes by cleaving ester *in vivo*. The SWNT-PTX conjugate forms a stable suspension in normal physiologic buffer (PBS, as shown in the photo) and serum without aggregation. Reprinted from Reference[140] with the permission from the corresponding author.

Single-walled carbon nanohorns have also applications in drug delivery.[143, 144] Murakami et al. found that anti-inflammatory glucocorticoid dexamethasone, was adsorbed on both SWNHs and oxidized SWNHs (ox-SWNHs).[145] The adsorbed dexamethason was released after incubation at 37 ^{o}C in phosphate buffer saline (PBS). Cisplatin, an anticancer agent, was encapsulated inside ox-SWNHs and later slowly released in PBS or cell-culture media. The released cisplatin terminated the growth of human lung-cancer cells.[146] Further study found that cisplatin@SWNHs have better anticancer effects than cisplatin itself.[147] The reason is that cisplatin can be slowly released locally in tumor tissues, and ox-SWNHs also have anticancer effect. The cisplatin-loaded SWNHs can be well dispersed in aqueous solutions with the help of a peptide aptamer and poly(ethylene glycol).[148]

2.4.3 Laser Therapeutic Agents

Unlike biological systems, which are transparent to near-infrared (NIR) light,[149] carbonaceous tubules have strong absorptions in this window.[150] Carbon tubules also have good thermal conductivity.[151] The absorption of NIR light produces heat locally and enables the carbon materials to kill cells. This is the photothermal or photohyperthemia effect.

Kim et al. first studied the application of carbon nanotubes as photothermal agents.[152] In this study, both MWNTs and SWNTs were incubated with E. *coli* K12 strain and irradiated by pulsed laser. Carbon nanotubes exhibited great potential as photothermal contrast agents and caused irreparable damage to disease-causing pathogens. The photothermal effect was tuned by doping atoms or changing the length of carbon

nanotubes.[153] Coating carbon nanotubes with gold further enhanced the abruption at near-infrared wavelengths and minimized toxicity.[154] Tumor-targeting modules were also conjugated to SWNTs.[155] The effect of SWNTs as photothermal agents were studied *in vivo*.[156] SWNTs dispersed with poly(ethylene glycol) (PEG) was injected into human epidermoid mouth carcinoma KB tumor cells implanted in mice. With NIR irradiation, the tumors treated with SWNTs by injection were completely destroyed without harmful side effect over six months and the mice were alive. However, the tumors treated with only SWNTs by injection or NIR irradiation continuously grew till the death of the mice. The SWNTs injected into mice bodies were excreted in about two months. The *in vivo* study demonstrates the great potential of SWNTs as effective photothermal therapeutic agents.

Miyako et al. prepared complexes of molecular recognition elements (MRE) and SWNHs, which can selectively eliminate yeast and bacteria by laser NIR radiation.[157] The process is shown in the Figure 26. Further research also indicate that the complex can also eliminate virus.[158]

Zhang et al. loaded zinc pothalocyanine (ZnPc) inside SWNHs and conjugated bovine serum albumin (BSA) to SWNHs.[159] ZnPc serves as photodynamic therapeutic (PDT) agent while SWNHs themselves perform as photohyperthermia (PHT) agents. BSA provides the biocompatibility. The complex system was injected into tumors in mice. The tumors disappeared when irradiated with a 670 nm laser.

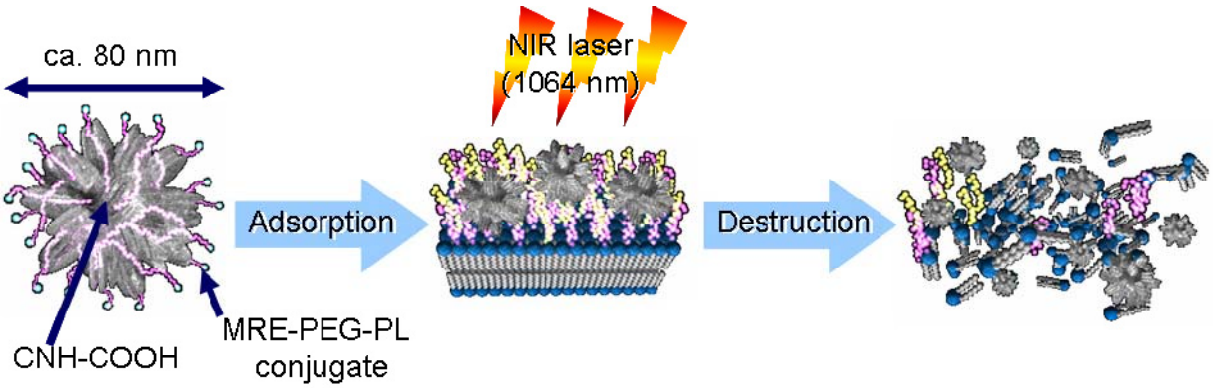

Figure 26. Method for the elimination of microorganisms using MRE–SWNH complexes and NIR laser irradiation (1064 nm). The MRE selectively targets the microbe, the PEG chains and phospholipid (PL) moiety were used to improve the solubility. Reprinted from Reference[157].

Chapter 3

High Relaxivity Trimetallic Nitride ($Gd_3N@C_{80}$) Metallofullerene MRI Contrast Agents with Optimized Functionality

3.1 Introduction

Magnetic resonance imaging (MRI) contrast agents are widely employed in clinical MRI studies. Currently, the most widely used MRI contrast agents are gadolinium chelates. However, the possibility of potential leaking of toxic Gd^{3+} ions has not been completely removed. It has been recently reported that nephrogenic systemic fibrosis (NSF), a painful and debilitating disorder of the skin and systemic tissues in patients with renal insufficiency, is associated with exposure to Gd^{3+} ions from contrast agents [160, 161]. New contrast agents with higher relaxivity and lower toxicity are an important target of current investigations.

Endohedral metallofullerenes (EMFs) represent ideal next generation nanoparticles as diagnostic biomedical nanoprobes because they can isolate the toxic Gd^{3+} ions from the

bioenvironment. Several new classes of MRI contrast agents, water-soluble endohedral metallofullerenes, have been reported [1, 5, 6, 96, 121-125, 162-165]. EMFs have been functionalized with hydrophilic groups, e.g., -OH or –COOH [96, 123-125, 162]. These water-soluble EMF derivatives show significantly greater relaxivities than the chelated Gd^{3+} compounds in current clinical use.

Our group has previously reported the synthesis of trimetallic nitride templated (TNT) EMFs, $A_xB_{3-x}N@C_{80}$ (A, B = metal, x = 0-3) [20]. The TNT EMFs have an additional advantage: they can encapsulate up to three Gd^{3+} ions inside the cage, resulting in higher relaxivity. If different metal atoms/ions are encapsulated, e.g., Lu, Tb, Ho, and so forth, TNT EMFs can also act as multimodal platforms with the same biodistribution. Previously, our group synthesized $Gd_3N@C_{80}$[DiPEG5000$(OH)_x$] (PEG = poly(ethylene glycol)) [1], which is water-soluble and exhibits high relaxivity. *In vitro* and *in vivo* studies demonstrated the potential applicability of this MRI contrast agent. More recent studies have also demonstrated high relaxivity for related TNT EMFs with different functionalities [5, 163, 164]. The high relaxivity of the TNT EMFs derivative arises from the following factors: (1) the large number of exchangeable water molecules coordinated to the hydroxyl groups which are attached to the carbon cage and are simultaneously relaxed by the $(Gd_3N)^{6+}$ endohedral cluster, (2) the slow rotational correlation time caused by the long PEG chains and aggregation effects.

In this chapter, we introduce the synthesis of pegylated and hydroxylated $Gd_3N@C_{80}$ with different PEG chain lengths (350-5000 MW). The MRI relaxivities of these derivatives were measured at three different magnetic field strengths. The optimum PEG

chain is discussed. It is known that cancerous tissues have significantly lower pH values than healthy tissues. Therefore, MRI contrast agents with pH responsive behavior are very important in cancer imaging. The relaxation of $Gd_3N@C_{80}$[DiPEG350$(OH)_x$] at different pH was also studied. To demonstrate the *in vivo* applicability of these high-relaxivity contrast agents, a convection-enhanced delivery (CED) method was used to infuse $Gd_3N@C_{80}$[DiPEG$(OH)_x$] directly into brain-tumor-bearing rats.

3.2 Materials and Methods

3.2.1 Synthesis of $Gd_3N@C_{80}$[DiPEG$(OH)_x$]

$Gd_3N@C_{80}$ was produced by the standard Krätschmer-Huffman (K-H) method with the introduction of nitrogen gas into the K-H generator [20]. The product was purified by HPLC as previously reported [166]. 1,8-Diazabicyclo(5.4.0)undec-7-ene (DBU, FW 152.24), 98%, was purchased from Sigma-Aldrich; 99% CBr_4, 99% 18-crown-6, 50% sodium hydroxide solution, and 30 wt % hydrogen peroxide were used as obtained from Aldrich Chemical Co. Di{ω-methyl-poly(ethylene glycol)} malonates (DiPEG) 350, 750, 2000, and 5000 (MW. 768, 1568, 4068, 10068, respectively) were prepared from ω-methyl-poly(ethylene glycol)s (PEGs) as follows: To a solution of PEG and triethylamine (TEA) in CH_2Cl_2, a solution of malonyl dichloride in CH_2Cl_2 was added dropwise. The molar ratio of PEG/TEA/malonyl dichloride was 2:2:1. The solution was stirred at room temperature under N_2 protection for 3 h, concentrated and dropped into a large amount of ethyl ether, and then fractionated by a silica gel column.

$Gd_3N@C_{80}$, DiPEG, DBU, and CBr_4 were dissolved in chlorobenzene in molar ratio 1:20:20:67. After deaeration by bubbling argon for 30 min, the solution was stirred overnight at room temperature. The resultant mixture was evaporated, and the residue was dissolved in toluene. To this solution, 18-crown-6 and 50% sodium hydroxide solution were added, and the resultant solution was stirred for 4 h. 1.5 mL hydrogen peroxide was added drop by drop, and more water was added. The mixture was stirred overnight at room temperature. The resultant solution was concentrated and separated on a Sephadex G25 (Pharmacia) size-exclusion gel column with distilled water as eluent to afford a narrow golden band (first fraction, pH=7). (See Figure 1)

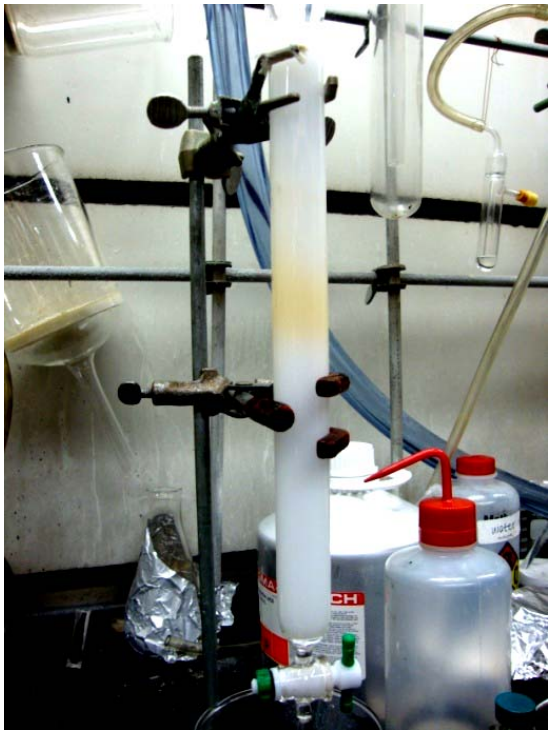

Figure 1. Picture of purifying $Gd_3N@C_{80}[DiPEG(OH)_x]$ with Sephadex G25 size-exclusion gel column. The diameter of the column is 2.5cm and the length is 42cm. Elution time is 55 minutes.

3.2.2 Relaxivity Measurements

The concentrations of Gd^{3+} ions were determined by inductively coupled plasma optical emission spectroscopy (ICP-OES, Perkin-Elmer Optima 5300DV) at 342.247 nm. The instrument was calibrated by a 10 ppm ICP standard solution. Each molecule was assumed to encapsulate three Gd^{3+} ions, so the concentration of $Gd_3N@C_{80}[DiPEG(OH)_x]$ was assumed to be one-third of the Gd^{3+} ion concentration. The ^1H relaxation times were measured at three different magnetic field strengths: 0.35 T (TEACH SPIN PS1-B), 2.4 T (Bruker/Biospec), and 9.4 T (Varian Inova 400). The inversion recovery method was used to measure T_1 and the Carr-Pucell-Meiboom-Gill method was used for the measurement of T_2. The relaxivities were extracted from linear fits of plots of relaxation rates ($1/T_1$ and $1/T_2$) vs. the concentrations of the paramagnetic species.

To study the pH dependence of the relaxivity, $Gd_3N@C_{80}[DiPEG350(OH)_x]$ solutions were prepared at the same concentration (15.6 μM) with different pH values. The pH values of the solutions were adjusted with NaOH (1.000M, VWR) and HCl (1.000M, VWR) solutions. A Beckman *Φ*240 pH meter was used to determine pH values. Before measurement the pH-meter was calibrated with standard solutions of pH = 4.00 and 7.00.

3.2.3 Dynamic Light Scattering

Dynamic light scattering (DLS) measurements were carried out with an ALV/CGS-3 compact goniometer system and ALV/LSE-5003 multi-τ digital correlator at 25 °C. He-Ne laser producing vertically polarized light of λ_0 = 632.8 nm was used as a light source. Each sample was filtered with a 0.5 μm cellulose acetate membrane filter.

3.2.4 Animal Studies

We used a convection-enhanced delivery method [1] to infuse 0.0235 mM $Gd_3N@C_{80}$[DiPEG350$(OH)_x$] into a live rat brain tumor and followed the functionalized EMF redistribution over the course of several days. Infusion was applied for 180 min at a rate of 0.2 μL/min with a total infusion volume of 36 μL.

3.3 Results and discussion

3.3.1 ^{1}H NMR

^{1}H NMR spectra of $Gd_3N@C_{80}$[DiPEG$(OH)_x$] were obtained on an Inova 400. Figure 2 displays the ^{1}H NMR spectra of $Gd_3N@C_{80}$[DiPEG$(OH)_x$] and malonyl DiPEG350 in D_2O. In $Gd_3N@C_{80}$[DiPEG$(OH)_x$] the $–OCH_3$ and $–OCH_2CH_2–$ signals appeared at 3.35 ppm (s, 6H) and 3.67ppm (m, 52H), respectively; the signals for $–COOCH_2$ and $COOCH_2CH_2–$ centered at 4.32 ppm (t, 4H) and 3.78 ppm (t, 4H) in the malonate disappeared in the TNT EMFs derivative apparently due to the strong paramagnetic effect of the Gd^{3+} ions. The NMR spectra of other PEG derivatives gave similar results.

3.3.2 UV-Vis

The UV-Vis spectra of $Gd_3N@C_{80}$ and $Gd_3N@C_{80}$[DiPEG2000$(OH)_x$] are shown in Figure 3. For $Gd_3N@C_{80}$, there is an absorption peak at about 710 nm and a second absorption occurs at 410 nm [167], and these absorptions are attributed to the $\Pi \rightarrow \Pi^*$ transitions [168]. For the functionalized metallofullerenes, however, these characteristic features are significantly reduced. This indicates that the conjugated π structure of the

carbon cage has been significantly altered. Similar results were obtained with other samples with different molecular weights ($Gd_3N@C_{80}$[DiPEG5000, 750, 350$(OH)_x$]).

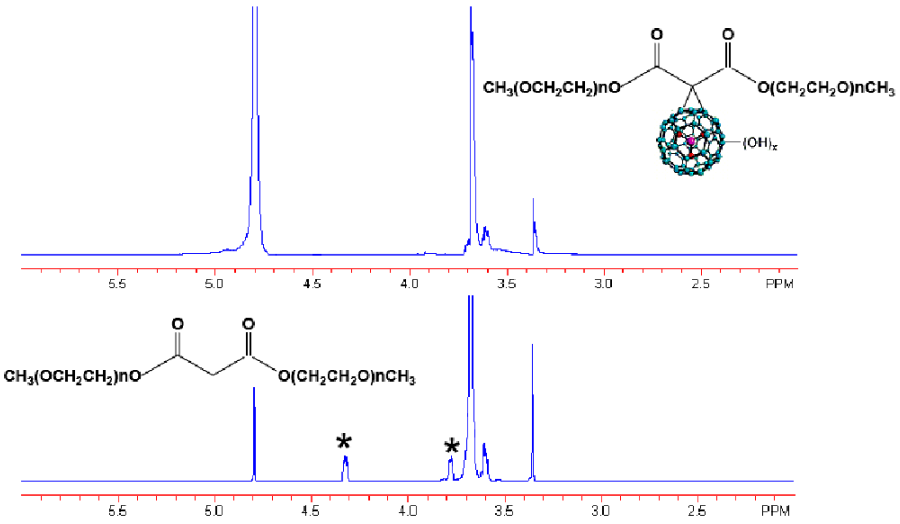

Figure 2. 400MHz ^{1}H NMR spectra of $Gd_3N@C_{80}$[DiPEG350$(OH)_x$] (top) in comparison with DiPEGM350 malonate (bottom) in D_2O.

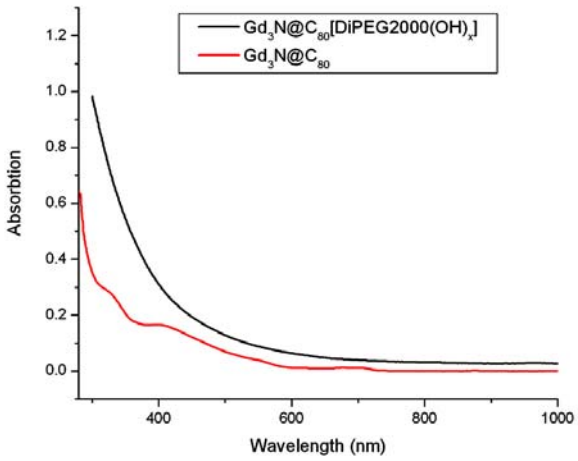

Figure 3. UV-Vis spectra of $Gd_3N@C_{80}$ and $Gd_3N@C_{80}$[DiPEG2000$(OH)_x$]. Note the disappearance of the characteristic peaks at 330 and 410 nm in the derivative.

3.3.3 Mass Spectra

To confirm the functionalization, matrix-assisted laser desorption/ionization time-of flight (MALDI-TOF) mass spectra were obtained for DiPEG750, $Gd_3N@C_{80}$[DiPEG750], and $Gd_3N@C_{80}$[DiPEG750$(OH)_x$]. Figure 4 shows the spectrum for DiPEG 750 that contains a series of peaks centered at about m/z ~1388. The peaks were separated by m/z ~ 44, which is the mass of the (CH_2CH_2O) unit. The spectrum of $Gd_3N@C_{80}$[DiPEG750] was a series of peaks centered at about m/z 2907 (Figure 5). The separation of m/z ~ 1 is attributed to the isotope effect of $Gd_3N@C_{80}$. We can clearly see that $Gd_3N@C_{80}$ was successfully functionalized with DiPEG750. However, in the mass spectrum of $Gd_3N@C_{80}$[DiPEG750$(OH)_x$] (Figure 6) we only observed peaks for metallofullerene (m/z~ 1447) and PEG fragments (centered at m/z ~ 759 and separated by 44). Even though the molecular ion peak was not observed, the metallofullerene and PEG fragments indicate successful functionalization.

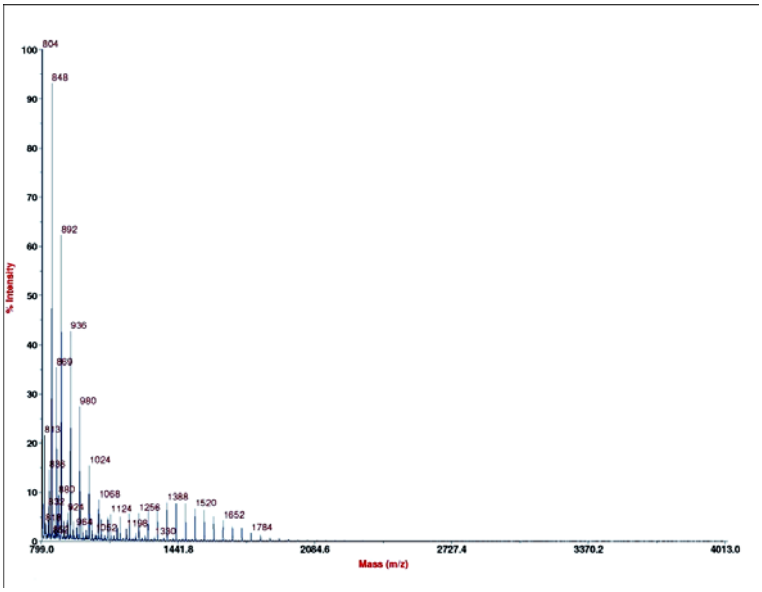

Figure 4. MALDI-TOF mass spectra of DiPEG750 (2,5-dihydroxybenzoic acid was used as the matrix).

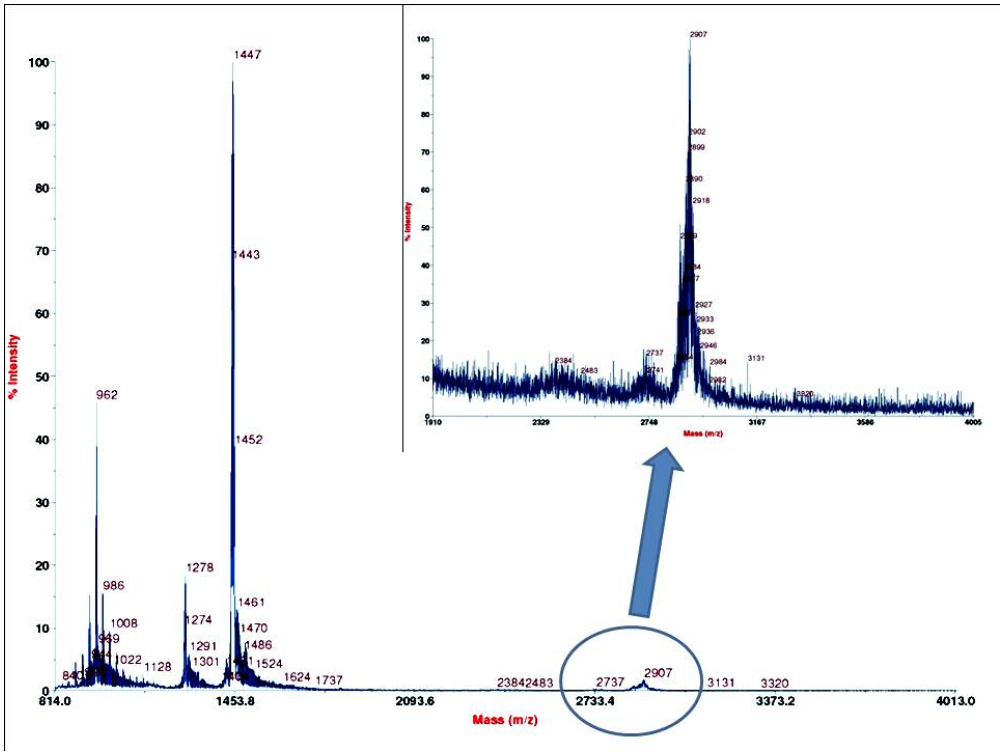

(a)

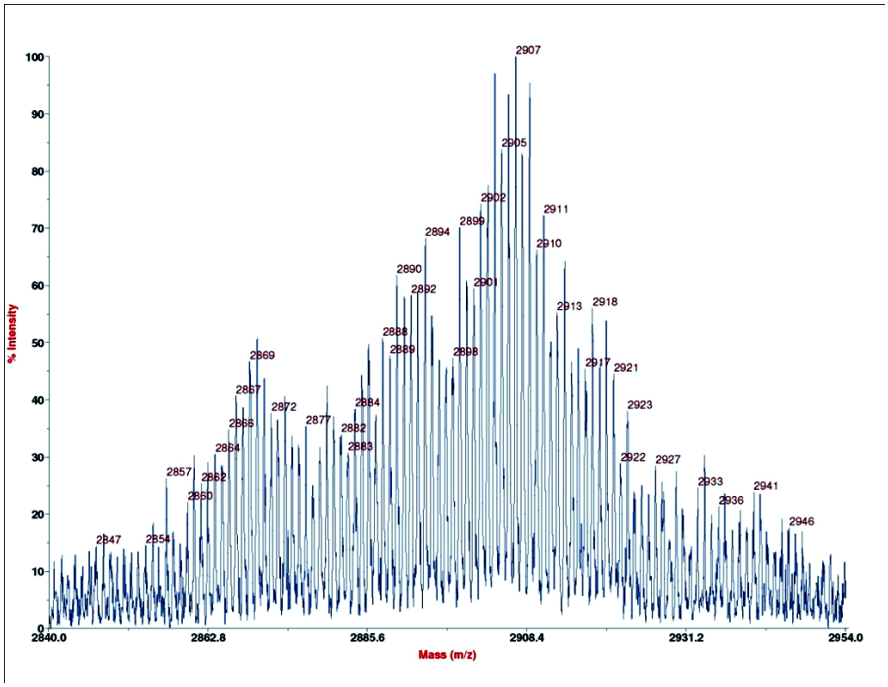

(b)

Figure 5. MALDI-TOF Mass spectra of $Gd_3N@C_{80}$[DiPEG750] (9-nitroanthracene was used as the matrix) at lower resolution (a) and higher resolution (b).

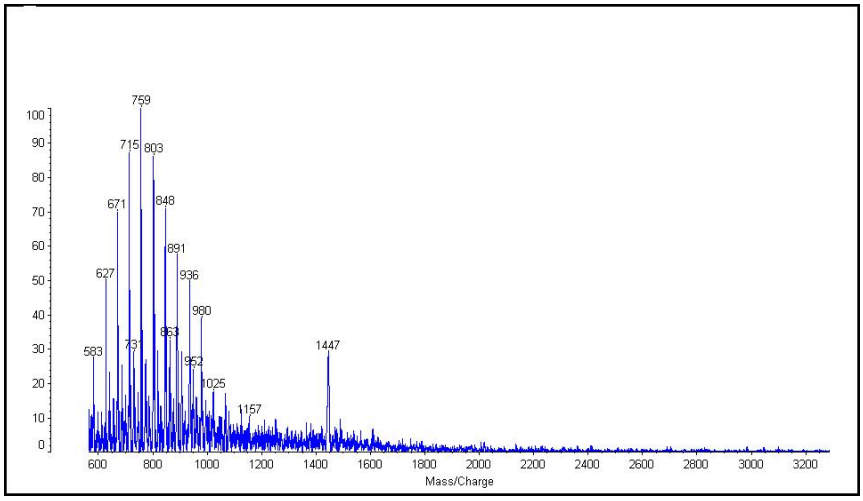

Figure 6. MALDI-TOF Mass spectra of $Gd_3N@C_{80}$[DiPEG750$(OH)_x$] (9-nitroanthracene was used as the matrix).

3.3.4 MRI Relaxivity

In the present investigation, the relaxivities of all the $Gd_3N@C_{80}$[DiPEG$(OH)_x$] samples were measured. The results are summarized in Table 1. Our previously reported relaxivities for $Gd_3N@C_{80}$[DiPEG$(OH)_x$] [1] are also listed, and they agree with the current data. All the $Gd_3N@C_{80}$[DiPEG$(OH)_x$] samples have high r_1 and r_2 values at all three magnetic field strengths. The r_1 values range from 139 $mM^{-1}s^{-1}$ (Gd^{3+} based relaxivity 46.3 $mM^{-1}s^{-1}$) to 237 $mM^{-1}s^{-1}$ (Gd^{3+} based relaxivity 79.0 mM^{-1} s^{-1}) for the different PEG chains at 2.4 T compared to the value of about 4 $mM^{-1}s^{-1}$ for commercially available Gd^{3+} ion chelated contrast agents. Several other groups have also reported r_1 values of mono gadofullerene derivatives, that is, one Gd^{3+} ion per fullerene cage. These r_1 values are typically higher than those of commercial MRI contrast agents. In our work, the relaxivities of all the $Gd_3N@C_{80}$[DiPEG$(OH)_x$] samples are significantly higher on a per molecule basis. A summary of these other studies and the relaxivities of $Gd_3N@C_{80}$[DiPEG350$(OH)_x$] in the current study are presented in Table 2 [122-125, 162, 169].

TABLE 1. Relaxivity data of $Gd_3N@C_{80}[DiPEG(OH)_x]$ series[a]

Mol. Weight of PEG	Conc. Range (μM)	r_1 (0.35T) ($mM^{-1}s^{-1}$)	r_2 (0.35T) ($mM^{-1}s^{-1}$)	r_1 (2.4T) ($mM^{-1}s^{-1}$)	r_2 (2.4T) ($mM^{-1}s^{-1}$)	r_1 (9.4T) ($mM^{-1}s^{-1}$)	r_2 (9.4T) ($mM^{-1}s^{-1}$)
5000	0.4-6.5	107±8	127±36	139±6	221±11	52.5±2.4	186±12
5000[1]	1.6-12.6	102	144	143	222	32	137
2000	1.0-15.2	130±4	148±8	158±6	249±12	41.9±3.0	218±11
750	1.1-17.4	152±5	169±20	232±10	398±22	63.3±1.8	274±9
350	1.5-23.5	227±31	268±19	237±9	460±23	68.2±3.3	438±5

[a] The relaxivities were measured at room temperature in water.

TABLE 2. Relaxivity data of $Gd_3N@C_{80}[DiPEG(OH)_x]$ series[a]

Metallofullerene Derivatives	r_1 ($mM^{-1}s^{-1}$)	Magnetic Field Strength (T)
$Gd@C_{82}O_6(OH)_{16}(NH_2CH_2CH_2COOH)_8$[122]	9.1	1.5
Gadofullerenol[169]	47	9.4
$Gd@C_{82}(OH)_{40}$[162]	67	0.47
	81	1.0
	31	4.7
$Gd@C_{60}(OH)_x$[170]	83.2	1.4
$Gd@C_{60}[C(COOH)_2]_{10}$[125, 170]	24.0	1.4
	4.6	0.47
$Gd_3N@C_{80}[DiPEG750(OH)_x]$	150 (50.0 Gd^{3+} based)	0.35
	246 (82.0 Gd^{3+} based)	2.4
	58.1 (19.7 Gd^{3+} based)	9.4

[a] The relaxivities were measured at room temperature in water.

As previously indicated, a primary reason for the high molar relaxivity of the $Gd_3N@C_{80}[DiPEG(OH)_x]$ samples in comparison with other endohedral metallofullerenes derivatives originates from the presence of three Gd^{3+} ions within the cage: the charge transfer between the $(Gd_3N)^{6+}$ cluster and the $(C_{80})^{6-}$ cage leads to a very stable nanoparticle. Previous studies have confirmed that ferromagnetic coupling in this cluster gives rise to a large magnetic moment, 21 μB [171]. The dipolar electron-nuclear

spin interaction between the fluctuating Gd^{3+} electron magnetic moment and the large number of exchangeable water hydrogen atoms induces efficient proton relaxation. This is in contrast with the conventional Gd-DTPA complex, which has a single water molecule bound in the first coordination sphere of the metal ion, exchanges rather slowly with the bulk water, and the entire complex tumbles very rapidly.

Further factors contributing to the relaxation process relate to the unique property of the fullerenes to aggregate and form large nanoclusters. Aggregation occurs frequently for water-soluble metallofullerenes and affects the relaxivity significantly as previous studies have shown [121, 124]. For the low molar mass $Gd_3N@C_{80}[DiPEG(OH)_x]$ samples, the aggregates are formed by hydrogen bonding between -OH groups; however, the hydrophobic fullerene-fullerene interactions are also strong. Hence, fullerene aggregates can be formed. According to the Debye-Stokes equation for rigid spherical particles:

$$\tau_R = 4\pi\eta r_{eff}^3 / 3k_B T$$

the rotational correlation time τ_R increases as the particle radius increases, which is an important parameter influencing relaxivity as a function of magnetic field strength. It has also been postulated that the presence of these aggregates might lead to a "confined" pool of water molecules in the interstitial spaces between individual gadofullerenes, which exchanges rapidly with the bulk waters increasing again the relaxivity [172]. Depending on the PEG length and aggregate size, different restricted pools of water would be created as mentioned above, influencing the measured overall relaxivities.

In the limit of $\tau_M << T_{1M}, T_{2M}$ for eqs 2 and 3, we obtain

$$r_2/r_1 = [3+4(1+\omega_H^2 \tau_C^2)]/6 \quad (1)$$

At low field, $\omega_H^2 \tau_C^2 << 1$ and the ratio approaches the value7/6=1.17. Our measured ratios of r_2/r_1 are listed in Table 3. On the basis of equation 1, the ratios at 0.35 T are consistent with the predicted value. Another result of the SBM equations is $\omega_H \tau_C \approx 1$ at maximum r_1. According to equation 1, this leads to $r_2/r_1 \approx 11/6 = 1.83$ for the peak. The ratios for the 750 and 350 PEGs at 2.4 T are close to 11/6 = 1.83 and hence the maximum r_1 values should occur near 100 MHz (2.4 T). We can also see that at 2.4 T the 750/350 Da species has the maximum r_1 of all the samples. Hence, at 2.4 T for the 750/350 samples we obtain $\tau_C = 1/\omega_H = 1.59$ ns, which is significantly longer than the commercial contrast agent, e.g., τ_R = 66 ps for the [Gd(DTPA-BMA)] [97]. This assumes that τ_C is dominated by a rotational component.

TABLE 3. The r_2/r_1 ratios of the pegylated/hydroxylated samples

Sample	**r_2/r_1 (0.35T)**	**r_2/r_1 (2.4T)**	**r_2/r_1 (9.4T)**
5000	1.19	1.59	3.54
2000	1.14	1.58	5.20
750	1.11	1.72	4.33
350	1.18	1.94	6.42

The aggregation behavior was studied by DLS experiments. The DLS results for all $Gd_3N@C_{80}$[DiPEG(OH)$_x$] samples are shown in Figure 7. The mean peak positions are 75 nm, 76 nm, 58 nm, and 37 nm for $Gd_3N@C_{80}$[DiPEG350(OH)$_x$], $Gd_3N@C_{80}$[DiPEG750(OH)$_x$], $Gd_3N@C_{80}$[DiPEG2000(OH)$_x$], and $Gd_3N@C_{80}$[DiPEG5000(OH)$_x$], respectively. The 350PEG and 750PEG samples have the largest average aggregation size (~75 nm), while the 5000PEG sample is much smaller (~37 nm). The trend of decreasing aggregation size with increasing molecular weight is

consistent with the relaxivity trend. It should also be noted that these pegylated particles clearly deviate from spherical shape and the ones with longer PEG chains might exhibit internal flexibility. This could be an important additional factor for the observed reduced relaxivities for these larger molecules due to increased anisotropic rotation described by a fast local motion component that controls relaxivity and a slow global motional component [173].

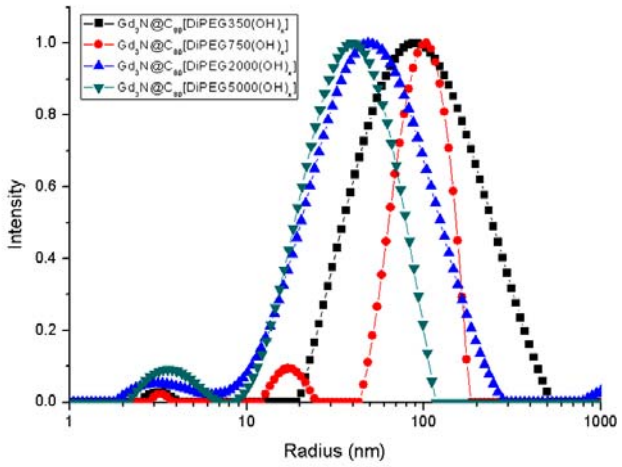

Figure 7. Size distribution function (intensity weighted) of $Gd_3N@C_{80}[DiPEG(OH)_x]$ from DLS experiment. The mean peak positions are 75nm, 76nm, 58nm and 37nm for $Gd_3N@C_{80}[DiPEG350(OH)_x]$, $Gd_3N@C_{80}[DiPEG750(OH)_x]$, $Gd_3N@C_{80}[DiPEG2000(OH)_x]$ and $Gd_3N@C_{80}[DiPEG5000(OH)_x]$, respectively.

3.3.5 The pH dependence of Relaxivity

The spin-lattice and spin-spin relaxation rates of $Gd_3N@C_{80}[DiPEG350(OH)_x]$ were measured at 0.35 T and 9.4 T respectively and plotted vs. pH in Figure 9. From the figure we can see that both R_1 and R_2 are almost constant within the range pH = 2~9. For pH < 2, precipitation was observed and the relaxation rates decreased significantly.

On one hand, the pH of solutions influences the water exchange process and changes the residence time of water molecules, τ_M. The relaxivity-independence on pH indicates that τ_M doesn't dominate the total correlation time, and makes little contributions to final relaxivity. On the other hand, pH can also affect the aggregation behavior. In the pH range 2~9, a small change in rotational correlation time has little effect on the relaxivity. Further increasng the rotational correlation time may not significantly increase relaxivity. $Gd_3N@C_{80}$[DiPEG(350$(OH)_x$] should be the optimized sample for pegylated and hydroxylated TNT-EMFs. In basic solutions of pH > 9, deprotonation will cause a negative charge on the molecule, which makes the aggregation more difficult. The deaggregating effect makes τ_R shorter and leads to a decrease in relaxivity. In acidic solutions with pH < 2, the precipitation caused a sifnificant decrease in the actual concentration of $Gd_3N@C_{80}$[DiPEG350$(OH)_x$]. This can explain the small relaxation rates measured.

3.3.6 Animal Infusion Study

Pure T_1 computed images of three consecutive brain slices of a live rat brain following infusion of 0.0235 mM $Gd_3N@C_{80}$[DiPEG350$(OH)_x$] into the brain tumor are shown in Figure 9. The middle column indicates the slice with the tumor, while the left and the right columns are slices without tumor used as controls. Immediately after the infusion is terminated ("3.5 h"), the $Gd_3N@C_{80}$[DiPEG350$(OH)_x$] nanoparticles have been distributed throughout the tumor, reducing the tissue T_1 values. The tumor appears as a dark area, as the white circle indicates. As time progresses, the brain tumor grows and the $Gd_3N@C_{80}$[DiPEG350$(OH)_x$] nanoparticles appear to be pushed out into the tumor periphery. This is illustrated at day 7 in the T_1 map, which shows aggregates on the

surface, and the T_1-weighted image shows an enhancement ring around the tumor. These results illustrate the enhanced *in vivo* relaxivity of this optimized $Gd_3N@C_{80}$[DiPEG350$(OH)_x$] system at low molar concentrations. It should also be noted that after 7 days the nanoparticles can still enhance the MRI contrast, which indicates that these metallofullerene agents can be used for long-term imaging diagnostic applications. In addition, these metallofullerene agents provide a platform for effective brachytherapy applications when Gd is replaced and/or combined with radioactive agents (^{177}Lu).

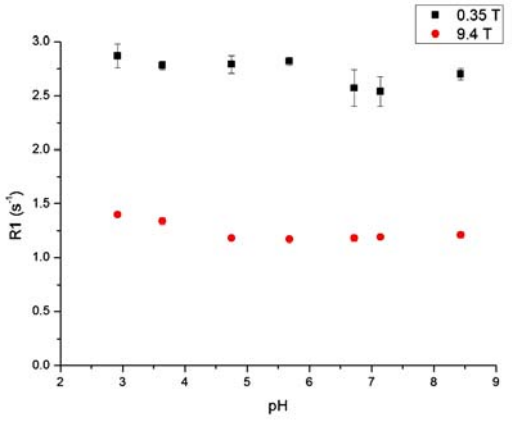

(a)

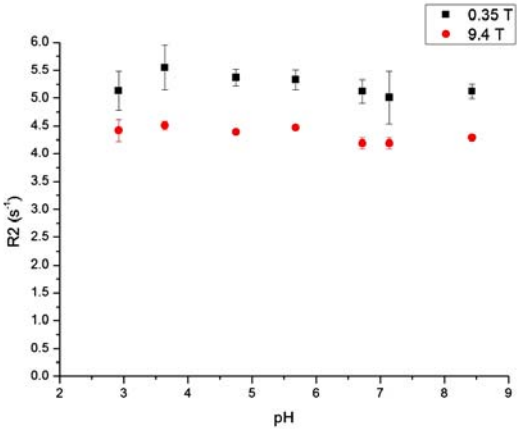

(b)

Figure 8. The pH dependence of relaxation rates of $Gd_3N@C_{80}$[DiPEG(350$(OH)_x$] at different magnetic field strengths.

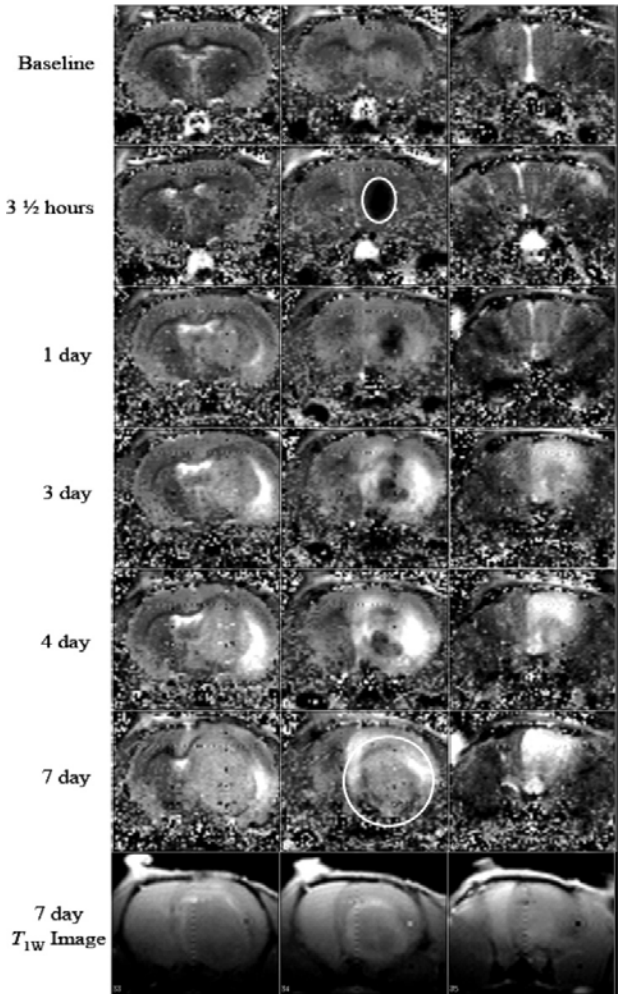

Figure 9. T_1 computed images and T_{1W} image of a live rat brain after direct infusion into the tumor of 0.0235 mM $Gd_3N@C_{80}[DiPEG350(OH)_x]$.

3.4 Conclusions

We synthesized hydroxylated and pegylated Gd-containing TNT EMFs, $Gd_3N@C_{80}[DiPEG(OH)_x]$, with different chain lengths of PEG. The relaxivities were measured at three magnetic field strengths. All the samples show significantly higher r_1 and r_2 values compared to commercially available Gd-chelates, and show considerable promise as a new class of contrast agents. They represent some of the highest relaxivities reported in the literature for commercial and investigational MRI contrast agents.

Analyzing the field dependence of r_1, r_2, r_2/r_1 indicates reasonable agreement with the predictions of the SBM theory under the assumption that the rotational correlation time τ_R dominates the relaxation process. The relaxivity and aggregation size can be tuned by varying the length of PEG chains. The $Gd_3N@C_{80}$[DiPEG350$(OH)_x$] didn't exhibite obvious pH dependent relaxivities. The Direct infusion of $Gd_3N@C_{80}$[DiPEG350$(OH)_x$] into the live tumor-bearing rat brain demonstrates an initial uniform distribution and hence the potential for effective brachytherapy applications when Gd is replaced with radioactive ^{177}Lu.

Chapter 4
Functionalization of TNT EMFs with Carboxyls and Hydroxyls

4.1 Introduction

In Chapter 3 the pegylated and hydroxylated TNT metallofullerenes were discussed. TNT fullerenes can also be funtionalized with carboxyls, which facilitate further conjugation with other materials. Recently, a method using succinic acyl peroxide was developed to functionalize single-walled carbon nanotubes.[3] Similar to this method, Dr. Chunying Shu in our group developed a new facile method to functionalize TNT-EMFs with carboxyls and hydroxyls, which are highly water-soluble and produced in a high yield.[163] In this chapter, we will discuss the synthesis of carboxylated and hydroxylated $Gd_3N@C_{80}$ and the measurement of its relaxivities.

4.2 Experimental Section

4.2.1 Synthesis of Succinic Acyl Peroxide

Succinic acyl peroxide was synthesized similar as the literature describes.[3] Briefly, 4 mL 50% hydrogen peroxide was diluted to 20 mL and cooled in an ice bath. 10 g succinic anhydride was added to the hydrogen peroxide and stirred for 1 h, when all the powder dissolved and a gel-like solution formed. The solution was filtered with a 0.20 μm PTFE membrane and the solid was washed with a small amount of water. Then the solid was transferred into a glass vial and dried in a vacuum for 24 h.

4.2.2 Functionalization of Metallofullerenes

4 mg $Gd_3N@C_{80}$ was dissolved in 5 mL of *o*-dichlorobenzene, and 3.2 mg succinic acyl peroxide was added. Deaeration by nitrogen stripping was performed for 30 min, and the solution was then heated at 84 °C for 48 h. More succinic acyl peroxide was added (total mass added was 3.2 mg) every 12 h. After the reaction, the water-soluble product was extracted by adding 8 mL of 0.2 M NaOH aqueous solution. Two layers were obtained; a deep brown layer was on the top and a colorless layer was at the bottom. The top layer was concentrated, and the residue was purified via a Sephadex G-25 (Parmacia) size-exclusion gel column. A neutral narrow brown band was obtained. The synthesis of both succinic acyl peroxide and f-TNT-EMFs is shown in Figure 1. The sample was characterized by FTIR, etc., and the structure was determined by XPS to be $Gd_3N@C_{80}(OH)_{\sim 26}(CH_2CH_2COOM)_{\sim 16}$, (M = H, Na).[163]

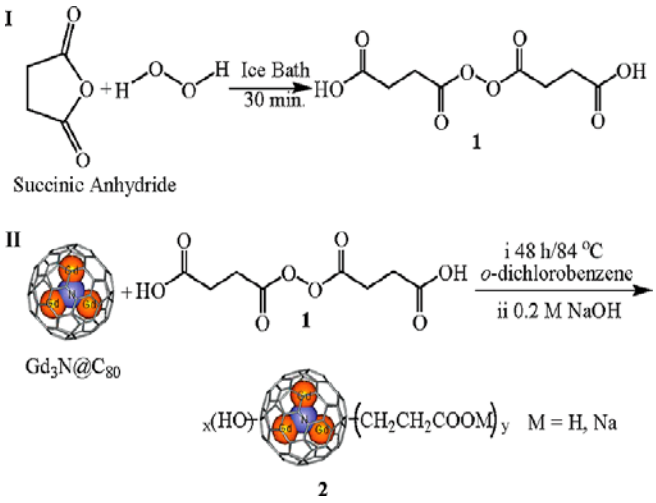

Figure 1. Synthesis of succinic acyl peroxide and $Gd_3N@C_{80}(OH)_{\sim 26}(CH_2CH_2COOM)_{\sim 16}$ (M = Na, H).

4.2.3 Characterization

The concentration of Gd^{3+} ion in the aqueous solutions was determined by inductively coupled plasma atomic emission spectroscopy (ICP-OES, VARIAN) at 342.247 nm. The relaxation times were measured at three different magnetic field strengths: 0.35 T (TEACH SPIN PS1-B), 2.4 T (Bruker/Biospec), and 9.4 T (Varian Inova 400). The inversion-recovery method was used to measure T_1 and the Carr-Pucell-Meiboom-Gill method was used for the measurement of T_2. The relaxivities (r_1 and r_2 in $mM^{-1}s^{-1}$) in aqueous solution (pH = 7) and phosphate buffered saline (PBS, pH = 7.4) solution were obtained from linear fitting of the plots of relaxation rates ($1/T_1$ and $1/T_2$) vs [Gd_3N].

Dynamic light scattering (DLS) measurements were carried out with an ALV/CGS-3 compact goniometer system and ALV/LSE-5003 multi-τ digital correlator at 25 °C. He-Ne laser producing vertically polarized light of λ_0 = 632.8 nm was used as a light source.

Each sample was filtered with a 0.5 μm cellulose acetate membrane filter. Each sample was filtered with a 0.2 μm cellulose acetate membrane filter before measurement.

4.3 Results and discussion

The relaxivities were measured at three magnetic field strengths: 0.35T, 2.4T and 9.4T in both water and PBS. The results are shown in Table 1. From the table we can see that the relaxivities of carboxylated $Gd_3N@C_{80}$ are much higher than the commercial MRI contrast agents (e.g. Ominscan®, whose $r_1$and r_2 are 4.1 $mM^{-1}s^{-1}$ and 4.7 $mM^{-1}s^{-1}$, respectively[163]). In contrast the relaxivity decreases significantly in PBS. This is attributed to the deaggregation in PBS, which leads to smaller aggregation size and faster tumbling rate. Therefore the decreased rotational correlation time leads to smaller relaxivities as the equations in Chapter 2 indicate. This behavior also indicates that the rotational correlation time dominates the relaxivity, which obeys the SMB theory.

Table 1 Relaxivities and r_2/r_1 ratios of $Gd_3N@C_{80}(OH)_{\sim 26}(COOM)_{\sim 16}$ in both water and PBS.

	0.35T(15 MHz)			2.4 T (100 MHz)			9.4 T (400 MHz)		
	r_1	r_2	r_2/r_1	r_1	r_2	r_2/r_1	r_1	r_2	r_2/r_1
Water	154±7	204±22	1.3±0.2	207±9	282±31	1.8±0.2	76±3	231±25	3.0±0.4
PBS	29±1	37±4	1.3±0.2	35±2	62±7	1.6±0.2	18±1	72±8	4.1±0.5

Dynamic light scattering confirmed the deaggregation. The size distribution functions of $Gd_3N@C_{80}(OH)_{\sim 26}(COOM)_{\sim 16}$ in water rand PBS are shown in Figure 2. It indicates that the the hydrodynamic diameter of $Gd_3N@C_{80}(OH)_{\sim 26}(COOM)_{\sim 16}$ is ~90 nm in water and ~50 nm in PBS. If we compare $Gd_3N@C_{80}(OH)_{\sim 26}(COOM)_{\sim 16}$ with

$Gd_3N@C_{80}[DiPEG(OH)_x]$ discussed in Chapter 3, we can find that $Gd_3N@C_{80}(OH)_{\sim 26}(COOM)_{\sim 16}$ has a similar hydrodynamic diameter as $Gd_3N@C_{80}[DiPEG350(OH)_x]$ and $Gd_3N@C_{80}[DiPEG750(OH)_x]$ in water, and the relaxivities are also similar. Different attached moieties, carboxyls and PEG chains, do not have too much effect on the relaxivities. Therefore, for both types of functionalized TNT-EMFs, we conclude that relaxivities are mainly dominated by the aggregation size, which affects the rotational correlation time.

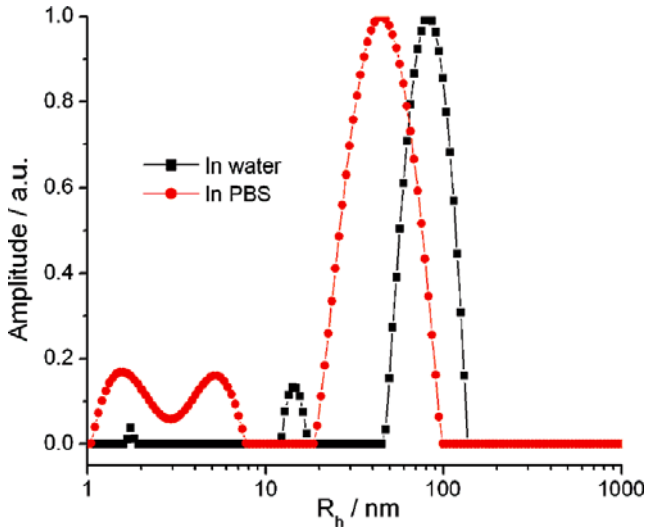

Figure 2. The intensity-weighted size distribution function of $Gd_3N@C_{80}(OH)_{\sim 26}(COOM)_{\sim 16}$ in water and PBS.

4.4 Conclusion

TNT-EMFs were functionalized by carboxyls and hydroxyls by a facile new method in high yield. The new material exhibited high relaxivity and is a good candidate as a potential MRI contrast agents. The carboxyl groups provide possibilities of coupling with tissue targeting moieties. DLS confirmed the importance of aggregation size and the relaxivities are determined mainly by the rotational correlation time.

Chapter 5

Functionalization and Conjugation of Tubular Carbonaceous Nanomaterials

5.1 Introduction

Since the discovery of fullerenes, many other types of carbon nanomaterials have also been discovered. Among these new carbon nanomaterials, two types of tubular carbon nanomaterials, carbon nanotubes and carbon nanohorns, have attracted great attentions. These tubular carbon nanomaterials are very promising as biomaterials for applications in nanomedicine.[174] However, the applications of these materials are limited because of their hydrophobic property. Dispersion of the hydrophobic carbon nanomaterials in aqueous media is a foremost challenge and prerequisite to facilitate applications in biomedical areas. A wide variety of methods have been reported to disperse carbon nanomaterials in water, both covalently and non-covalently.[175-177] The non-covalent modification includes using surfactants,[150, 178-181] polymers,[148, 179, 182-185] and biopolymers[186-190]. Compared to non-covalent modification, covalent functionalizations

have the advantage of being more robust during manipulations and processing. The covalent functionalization of tubular carbon nanomaterials includes oxidation by strong acid[157, 191] and functionalizations based on addition reactions[3, 192-200]. Recently a one-step reaction utilizing acyl peroxide was developed to functionalize single-walled carbon nanotubes (SWNTs) with carboxyl groups.[3] However, this method is very time-consuming because of the relatively low solubility of both free radicals and SWNTs in organic solvents. The method was later improved by heating the mixture of SWNTs and succinic acyl peroxide at 110 ^{o}C, at which temperature succinic acyl peroxide turns into liquid.[4] The improved method increases the concentration of radicals significantly and is much faster. Another new method to functionalize SWNTs is the high speed vibration milling (HSVM) method.[71] SWNTs were mixed with KOH and vigorously shaken for 2 h. The method leads to hydroxylated SWNTs. The advantage of this method is that it is solvent-free and very time-efficient.

SWNT peapods functionalized by HSVM with KOH and their properties will be discussed in Chapter 6. In this chapter, we will discuss combining the ideas of the HSVM and the liquid-phase reactions using succinic acyl peroxide, and developing a facile new method to functionalize tubular carbon nanomaterials with carboxyl groups easily and fast. The carboxylated carbonaceous nanomaterials were further conjugated with CdSe/ZnS quantum dots (QDs), which can be used for optical imaging.

5.2 Experimental Section

5.2.1 Purification

Single-walled carbon nanohorns (SWNHs) were produced without the use of metal catalyst, and multi-walled carbon nanotubes (MWNTs) contain little metal catalyst. Therefore, they can be used without purification. As-received SWNTs contain a lot of metal catalyst and must be purified before use. The SWNTs used in this dissertation were purified by the following procedure: SWNTs were placed in a crucible and heated in air in a furnace at 350 ^{o}C for 2 h to remove amorphous carbon. After that SWNTs were treated with microwaves for 5 min. The microwave couples to the metal catalyst particles in the sample and produces heat locally, which leads to the significantly increased temperature. The carbon passivation layers wrapping the metal particles were either oxidized or ruptured.[201] Then the SWNTs were refluxed in concentrated HCl solutions at 80 ^{o}C for 2 h. The metal catalysts can be easily removed by the strong acid. The whole procedure was repeated four times. The obtained purified SWNTs were dispersed in 1, 2-dichloroethane by sonication and dropped onto lacey carbon copper TEM grids for morphological characterization.

5.2.2 Functionalization

Succinic acyl peroxide was synthesized as described in Chapter 4. Then 1 mg carbon nanomaterial (SWNTs, MWNTs, or SWNHs) was mixed with 100 mg succinic acyl peroxide in a stainless steel capsule. A stainless steel milling ball is also put in the capsule. The capsule was vigorously shaken for 2 h (SPEX 8000 Mixer/Mill, 1725 rpm).

After the milling procedure, acetone was added to suspend the solid product, and the suspension was transferred into a small test tube and centrifuged for 20 min. The supernatant was decanted. This procedure was repeated four times so that succinic acyl peroxide was completely removed. The final solid product was washed with water twice and sonicated in pure water (or culture media for cell experiments) for 20 min. A dark homogeneous suspension was obtained.

5.2.3 Conjugation with CdSe/ZnS Quantum Dots

CdSe/ZnS QDs were conjugated with carboxylated carbon nanomaterials. The method was similar to a published procedure.[76] The first step was to prepare amine-terminated QDs (f-QDs). Briefly, CdSe/ZnS QDs (emission: 577 nm, FWHM < 24 nm, Ocean Nano Tech LLC) were sonicated in chloroform for 30 min. Aqueous 1.0 M AET (2-aminoethanethiol hydrochloride) solution was added to the QDs mixture. Two layers were formed: the organic layer of chloroform-QDs suspension and the aqueous layer with AET. The mixture was stirred vigorously over night and allowed to settle for a few minutes. An equal volume of phosphate buffered saline (PBS) was then added, and the mixture was stirred over night. The f-QDs were all transferred into the aqueous phase, which was collected and centrifuged. The precipitated f-QDs were then resuspended in PBS. To prepare QD-conjugated carbon nanomaterials, 1 mg of carboxylated carbon nanomaterial was suspended in 4 mL of PBS by sonication. N-(3-Dimethylaminopropyl)-N'-ethylcarbodiimide hydrochloride (EDC, 115 mg) and N-hydroxysulfosuccinimide (Sulfo-NHS, 2.8 mg) were added, and the mixture was stirred for 5 min. Then 2 mL of f-QDs (2 mg/mL) in PBS were added and the resulting suspension was stirred at 50 °C for

20 h. The suspension was filtered through a 0.2 μm Nylon membrane. The solid was washed with pure water.

5.3 Results and Discussion

5.3.1 SWNTs

TEM images of SWNTs after purification are shown in Figure 1. After purification, metal particles were seldom observed in the sample. The SWNTs form bundles, and individual nanotubes can occasionally be seen, whose diameter was estimated to be about 1.2 nm. However, after functionalization with the HSVM method in the presence of succinic acyl peroxide, the functionalized SWNTs (f-SWNTs) do not form a stable homogeneous solution. Precipitation occurred soon after the functionalization. One possibility is that the residual ferromagnetic metal impurities quench the free radicals during the milling procedure. Therefore, the HSVM method using succinic acyl peroxide is not the best way to functionalize SWNTs and SWNT peapods.

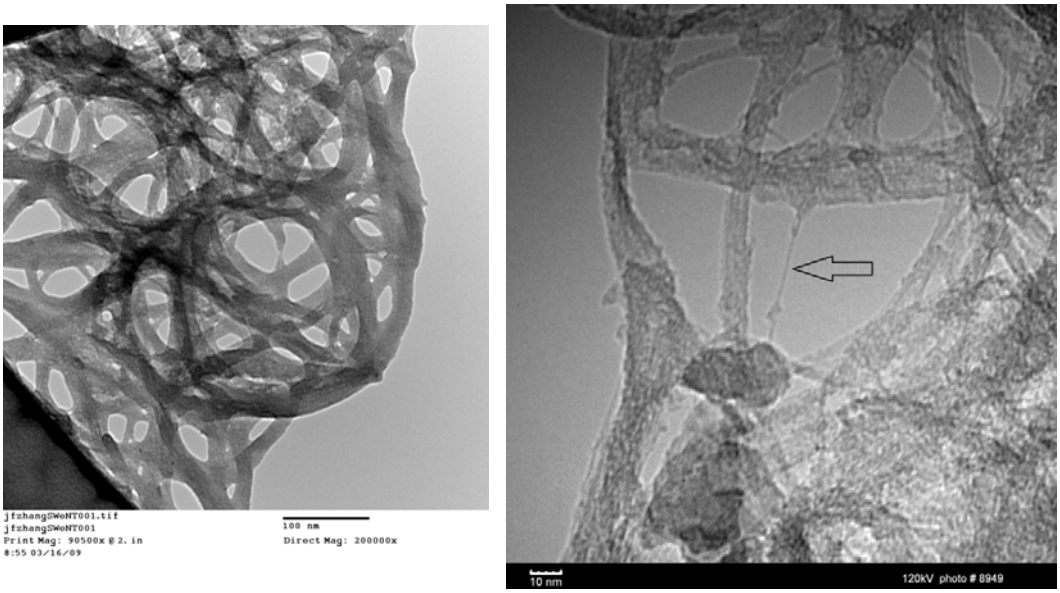

(a) (b)

Figure 1. TEM images of SWNTs. Most SWNTs form bundles (a), but individual SWNT can be occasionally observed as the arrow indicates in (b).

5.3.2 MWNTs

MWNTs were used as received. Figure 2a shows the TEM image of MWNTs. The diameter of MWNTs is estimated to be about 15 nm, and the thickness of the walls is estimated to be about 5 nm, which corresponds to about 14 layers. Unlike SWNTs, MWNTs don't form bundles. MWNTs were functionalized by the HSVM method using succinic acyl peroxide, and a stable suspension formed. A TEM image of functionalized MWNTs is shown in Figure 2b below. The tubular structures were well retained.

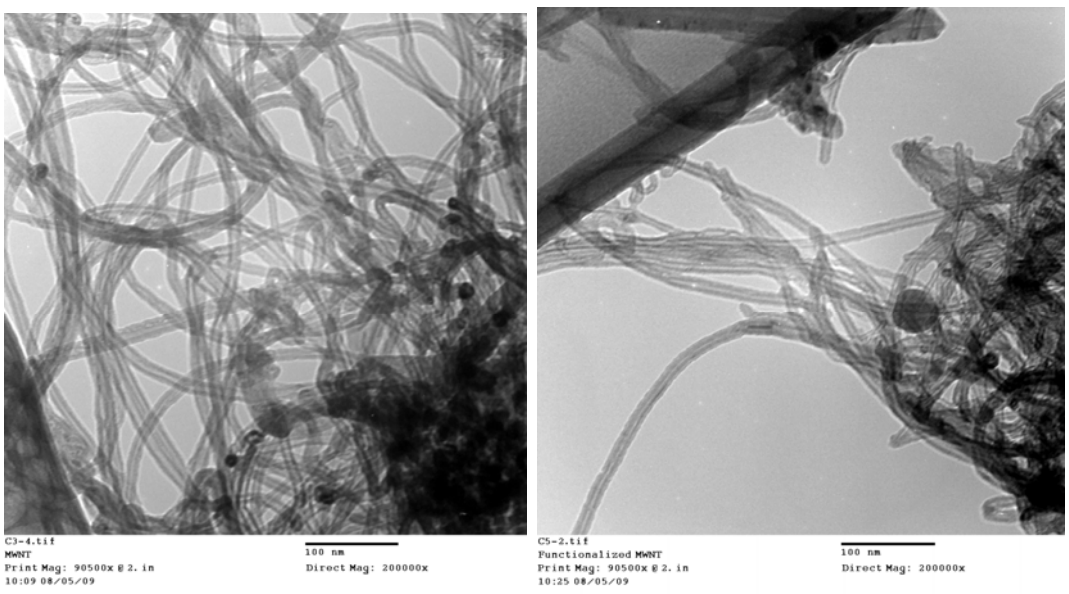

(a) (b)

Figure 2. TEM Images of MWNTs before (a) and after (b) functionalization.

XPS elemental survey (Figure 3) shows that no obvious oxygen for the as-received MSNTs. The O/C atomic ratio increased significantly after functionalization, which indicates the introduction of oxygen-containing groups.

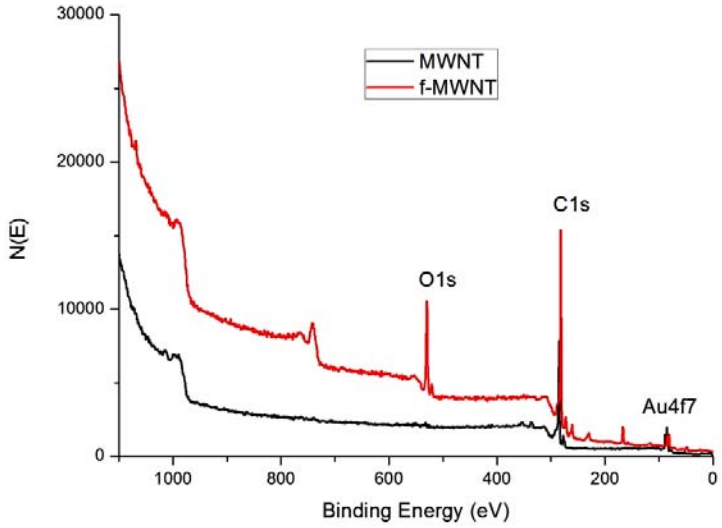

Figure 3. XPS survey of MWNT (black) and functionalized MWNT (red line).

The f-MWNTs were further conjugated with QDs as described in the experimental section. Before the conjugation, QDs were functionalized with AET first. The diameter of CdSe/ZnS QDs was estimated to be about 4.4 nm before functionalization and about 5.2 nm after functionalization from the TEM images of QDs (Figure 4). The f-MWNTs then reacted with the f-QDs in the presence of EDC. The TEM image of MWNT-QDs (Figure 5) clearly show the QDs attached to the MWNTs, which proves the successful conjugation. QDs can be used as optical imaging agents, which provide another method to study the biodistribution of the carbon materials.

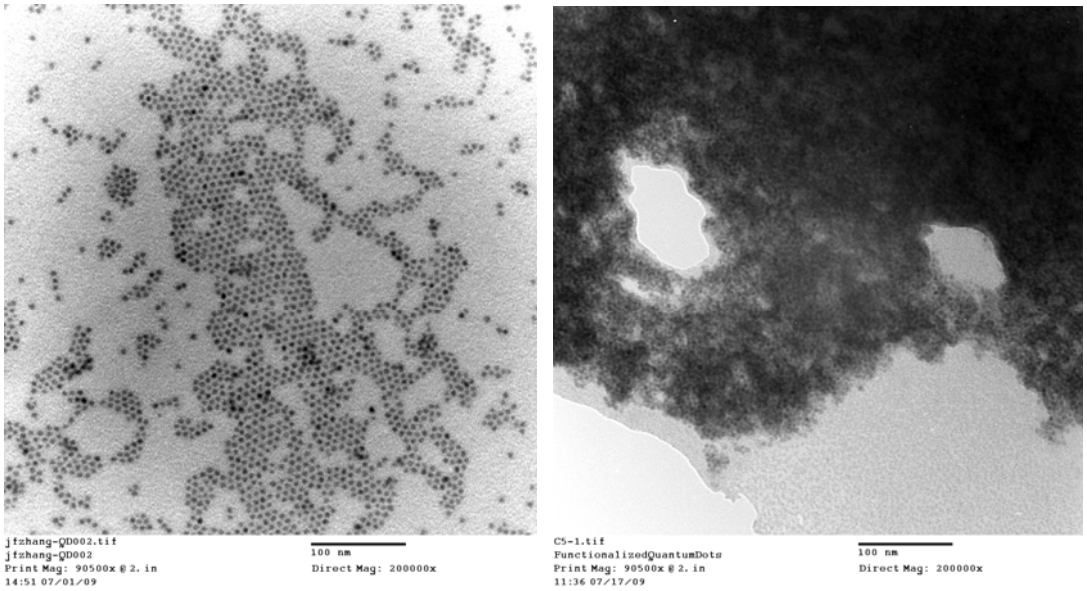

(a) (b)

Figure 4. TEM images of CdSe/ZnS quatum dots before (a) and after (b) functionalization with AET.

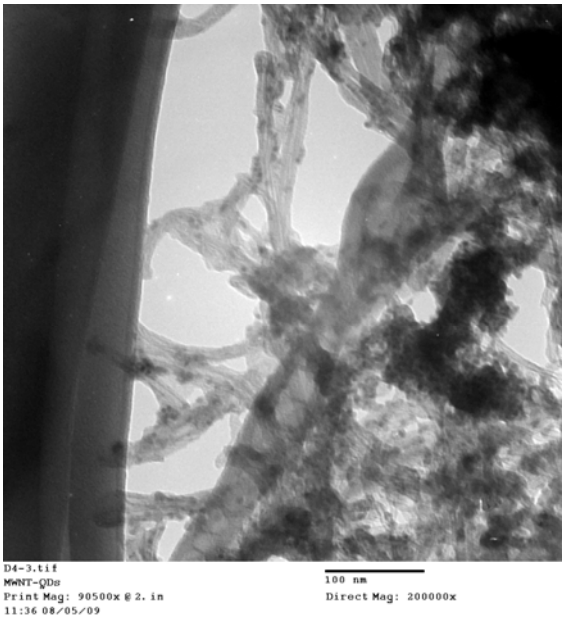

Figure 5. TEM image of MWNT-QDs complex.

5.3.3 SWNHs

SWNHs are more preferred for biomedical applications because they don't have metal impurities and they have bio-compatibility. Figure 6 and Figure 7 show some TEM images of SWNHs at various magnifications. Figure 6a is a typical image of SWNH aggregates. Some beautiful Dalia-like structures can occasionally be observed (Figure 6b). Scrutinizing these aggregates at higher magnification reveals the conical shape of individual SWNH (Figure 7a, b). Functionalization of SWNHs or SWNHs peapods by HSVM with succinic acyl peroxide worked pretty well. Suspensions were obtained and were stable for more than one year (Figure 8). TEM images of functionalized SWNHs at both low and high magnifications are shown in Figure 9, which show that the milling procedure didn't alter the morphology of SWNHs.

The aggregation behavior of f-SWNHs (the short SWNHs) was studied by dynamic light scattering (DLS). Figure 10 exhibits the intensity-weighted size distribution function of f-SWNHs in both water and PBS at 0.1 mg/mL. The peak position of hydrodynamic radius is at about 82 nm in water and increases to 1188 nm in PBS. This is different with carboxylated TNT-EMFs, whose aggregate size decreases in PBS. The different behavior of f-SWNHs relative to TNT-EMFs may be explained by different surface charge and ξ potential, which are under investigation.

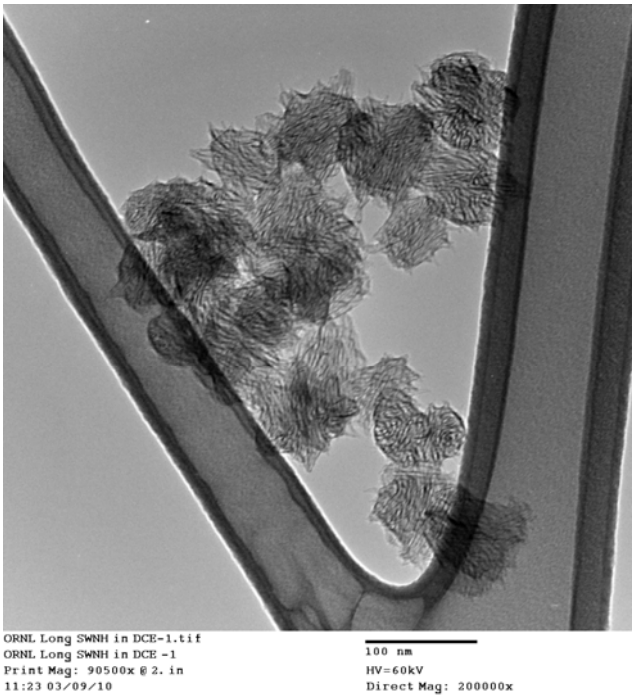

(a)

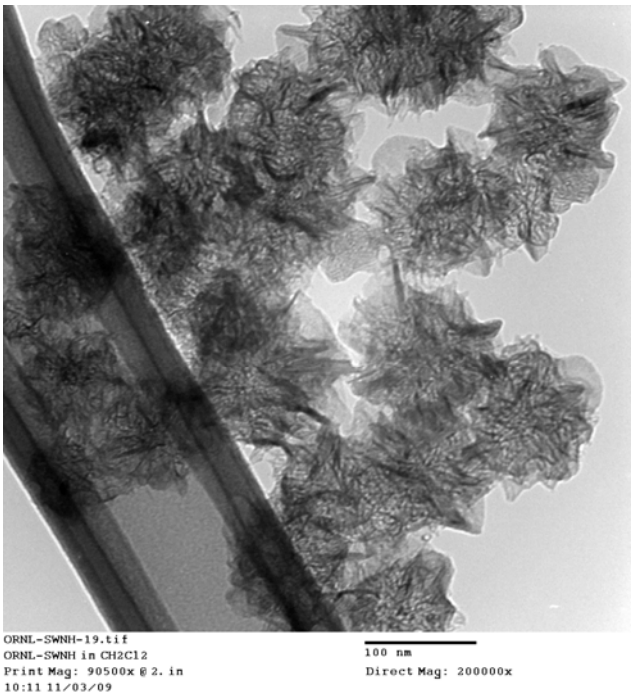

(b)

Figure 6. TEM images of SWNHs at lower magnification.

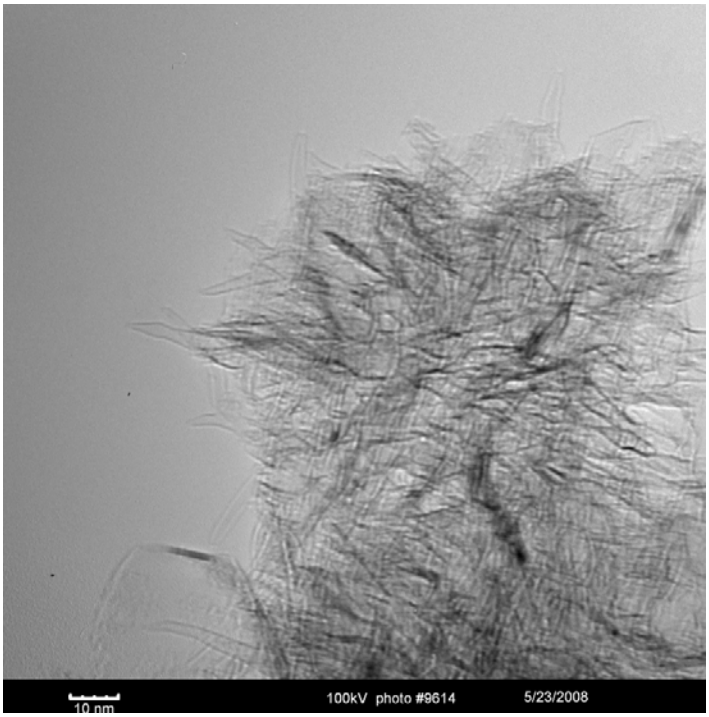

(a)

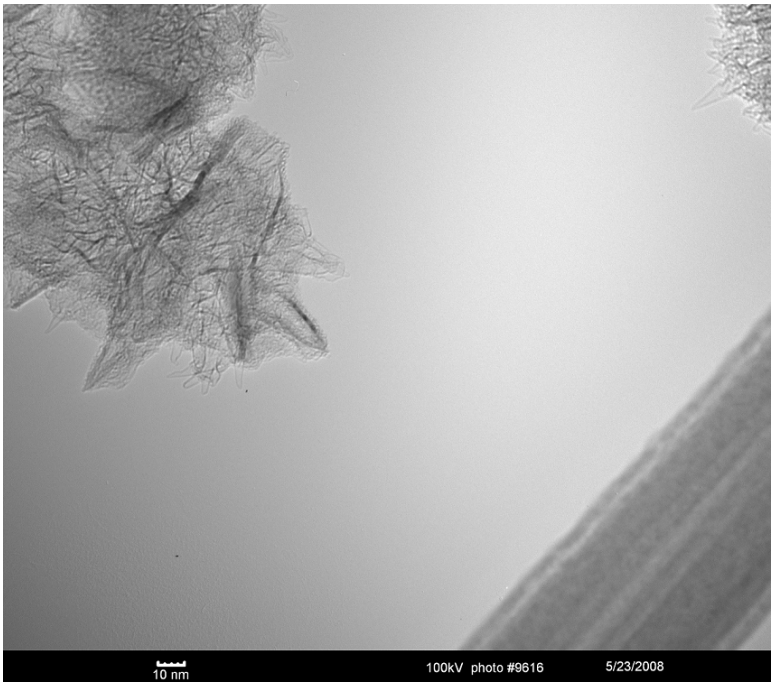

(b)

Figure 7. TEM images of SWNHs at higher magnification.

Figure 8. Pictures of SWNHs materials: raw SWNHs, f-SWNHs, f-$Gd_3N@C_{80}$@CNH and f- $Lu_3N@C_{80}$@CNH (in the order from left to right).

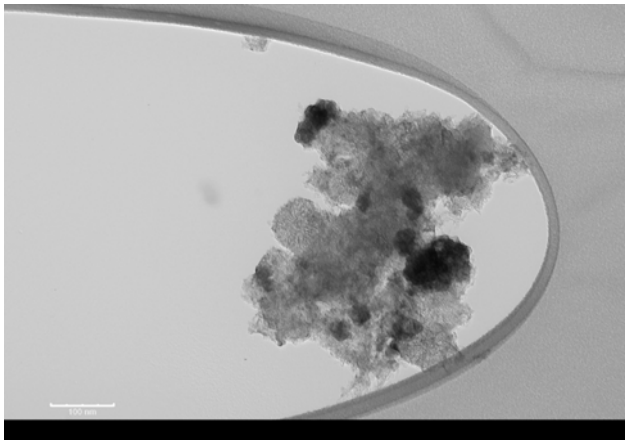

(a)

(b)

Figure 9. TEM images of functionalized SWNHs at lower (a) and higher (b) magnification. Scale bar: (a) 100nm; (b) 10nm.

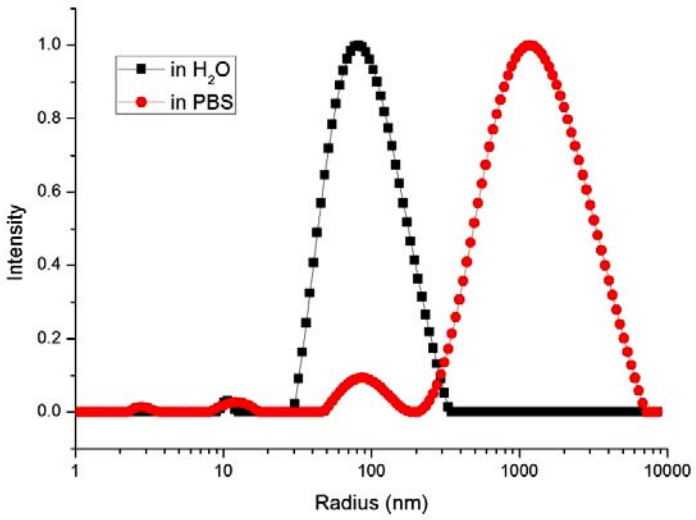

Figure 10. The Intensity-weighted size distribution of functionalized SWNHs in water (black) and PBS (red) at 0.1 mg/mL.

5.4 Conclusion

Tubular carbon nanomaterials, SWNTs, MWNTs and SWNHs, can be functionalized with carboxyl groups by the HSVM method. The carboxylated materials can be further conjugated with QDs, which are used as optical imaging agents. Other molecules can also be encapsulated inside these tubular materials, and make them good candidates for multifunctional platforms. In Chapter 7, SWNHs encapsulating TNT fullerenes and conjugated with QDs will be described in detail.

Chapter 6

The Preparation and Characterization of Functionalized Trimetallic Nitride Endohedral Metallofullerenes Single-Walled Carbon Nanotube Peapods: f-$M_3N@C_{80}$@SWNTs with High ^1H MRI Relaxivity

6.1 Introduction

Magnetic resonance imaging (MRI) is a powerful diagnostic technique with high spatial resolution and great capacity of differentiating soft tissues. MRI contrast agents are commonly employed to improve the image quality of MRI images and more than 30% of clinical MRI examinations use gadolinium based chelate contrast agents, such as Omniscan® and Magnevist®.[91, 92, 97, 98] In recent years, there is growing recognition of the association between the use of these gadolinium-containing MRI contrast agents and a serious dermal and systemic disease, nephrogenic fibrosing dermopathy/nephrogenic systemic fibrosis (NFD/NSF).[160, 161] A clear advantage of the fullerene and nanotube carbon cage in the design of next generation MRI contrast agents is the high stability and characteristic resistance to release of the free Gd^{3+} ion by any potential metabolic fullerene and/or nanotube cage-opening process. These new gadolinium-doped carbon nanomaterials have emerged as promising new MRI contrast agents. One example is endohedral metallofullerenes (EMFs) encapsulating gadolinium atoms/ions inside inert carbon cages, which prevent the potential leaking of gadolinium atoms/ions. This

potential application of EMFs is limited by the hydrophobic property of the carbon cage. Many efforts have been made to functionalize EMFs with hydrophilic groups, such as carboxyl or hydroxyl groups, and the prepared water-soluble EMFs appeared to be good candidates for MRI contrast agents.[1, 5, 6, 96, 121-124, 162-164, 202] Another example is single-walled carbon nanotubes (SWNTs) based materials. Paramagnetic Gd atoms/ions can be either encapsulated inside SWNTs[129-131, 203] or attached outside SWNTs[133], but the possibility of Gd leaking is not completely eliminated.

When fullerene caged molecules are encapsulated inside SWNTs, a structure named "peapod" is formed[34] and various fullerenes have been used to prepare peapods[204]. The inner carbon cage encapsulates Gd atoms and the outer carbon wall can be functionalized with hydrophilic groups[3, 4, 192, 205] or modified with tissue-targeting moieties. Recently a solid phase mechanochemical reaction was developed to functionalize SWNTs with hydroxyl groups in a facile way.[71]

In this chapter, we have prepared SWNTs encapsulated with trimetallic nitride template (TNT) EMFs, $M_3N@C_{80}$ (M = Gd, Lu, Sc). These $M_3N@C_{80}$@SWNTs peapods were then functionalized with hydroxyl groups by a high speed vibration milling (HSVM) method in the presence of KOH and characterized by transmission electron microscopy (TEM), X-ray photoelectron spectroscopy (XPS), UV-Vis, and Raman spectroscopy. In addition, we have measured the ^1H magnetic resonance (MR) relaxivity of the new $M_3N@C_{80}$@SWNT$(OH)_x$ peapods as potential next generation diagnostic MRI contrast agents.

6.2 Materials and Methods

The TNT EMFs, $M_3N@C_{80}$ (M = Gd, Lu, Sc), were produced by the Krästchmer-Huffman method and purified as reported previously.[166] Two different types of SWNTs were used in the study: one is Carbolex® nanotubes purchased from Sigma-Aldrich (SWNTs-1), the other is SWeNT® (SWNTs-2) nanotubes manufactured by SouthWest NanoTechnologies, Inc.

Transmission electron microscopic (TEM) images were obtained with a Zeiss 10 CA microscrope at 60kV accelerating voltage. High angle annular dark-field (HAADF) images were obtained using a 300 kV field-emission scanning transmission electron microscope (FE-STEM). The sample was imaged at 300 kV accelerating voltage. UV-Vis spectra were measured with a Cary 50 (Bio, Varian Inc.) Raman spectra were obtained from a JY Horiba LabRam. ^1H relaxivities were measured at two magnetic fields: 0.35T (TEACH SPIN PS1-B) and 9.4T (Varian Inova 400). The XPS measurements were performed utilizing a Perkin-Elmer 5400 X-ray photoelectron spectrometer calibrated with surface Au lines ($4f_{7/2}$ and $4f_{5/2}$) at 83.8 and 87.45 eV, respectively. The concentrations of metal elements were determined by induced coupled plasma optical emission spectroscopy (ICP-OES, Perkin-Elmer Optima 5300DV) at 342.247 nm (Gd), 261.542 nm (Lu) and 361.383 nm (Sc). Dynamic light scattering (DLS) measurements were carried out with an ALV/CGS-3 compact goniometer system and ALV/LSE-5003 multi-τ digital correlator at 25 ^oC. He-Ne laser producing vertically polarized light of λ_0 = 632.8 nm was used as a light source.

The $M_3N@C_{80}@$SWNTs peapods were prepared using a procedure similar to earlier reports.[206, 207] SWNTs were purified by heating at 300 ^oC in air for 2 h and subsequently irradiated with microwave radiation for 5 min. Then the SWNTs were refluxed in a concentrated HCl solution at 80 ^oC for 8 h followed by a filtration with a 0.45μm PTFE membrane filter. SWNTs left on the membrane were carefully collected and dried, and then heated again at 300 ^oC. The whole process was then repeated four times, and the last time a solution of 0.1 M HCl was used. The purified SWNTs were then heated to 420 ^oC for 20 min to open the ends of tubes and create defects in the walls. The samples were cooled and the CS_2 solutions of TNT EMFs were dropped onto the purified SWNTs and then the solvent was evaporated. The mixture of SWNTs and TNT fullerenes was sealed in quartz tubes under a vacuum of 10^{-4} Pa (10^{-6} Torr) and heated at 450 ^oC for four days. The products were sonicated in toluene for 20 min and filtered with 0.45 μm PTFE membrane filters. Then the solid was washed several times with toluene until the extract was clear.

The peapods were functionalized in a fashion similar to the procedures previously described.[71] Specifically, the peapods were mixed with KOH (mass ratio of $M_3N@C_{80}@$SWNTs:KOH=1:100). The mixture was put into a stainless steel capsule. A stainless steel milling ball was added and shaken vigorously for 2 h (SPEX 8000 Mixer/Mill, 1725 rpm). The product was washed with pure water to remove excess KOH and sonicated in water for 20 min. A homogeneous black suspension was obtained and was stable for months.

6.3 Results and Discussion

TEM

The unfunctionalized $M_3N@C_{80}$@SWNTs were dispersed in 1,2-dichloroethane and dropped onto lacey carbon coated TEM copper grids. **Figure 1** shows a regular TEM image (1a, made of SWNTs-2) and high angle angular dark field (HAADF) images (1b, c, made of SWNTs-1) of the $Gd_3N@C_{80}$@SWNTs peapods. The $Gd_3N@C_{80}$ molecules aligned densely inside SWNTs as indicated by the bright spots due to high atomic number, Z, contrast. The distance between fullerene molecules is about 0.8 nm, which corresponds to the diameter of fullerenes. Similar results were obtained for $Lu_3N@C_{80}$@SWNTs peapods and peapods made with both types of SWNTs.

The functionalized peapods, $M_3N@C_{80}$@SWNT$(OH)_x$, were dissolved in a mixture of water:methanol (Vol. 1:10) and dropped onto TEM grids. **Figure 2** is a TEM image of a functionalized sample, $Gd_3N@C_{80}$@SWNT$(OH)_s$. (made of SWNTs-2) The $M_3N@C_{80}$@SWNT$(OH)_x$ peapods more readily formed aggregates, but the tube structure was retained after functionalization.

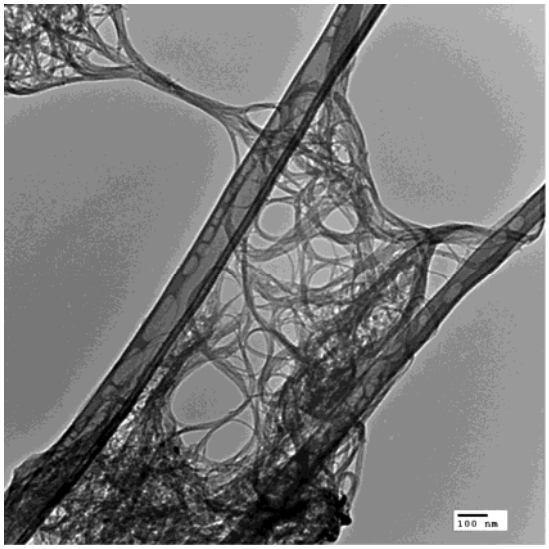

(a)

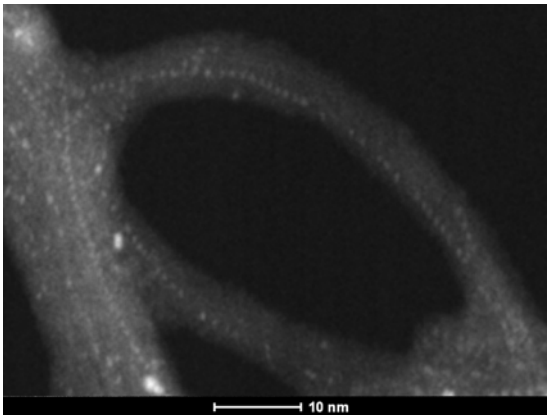

(b)

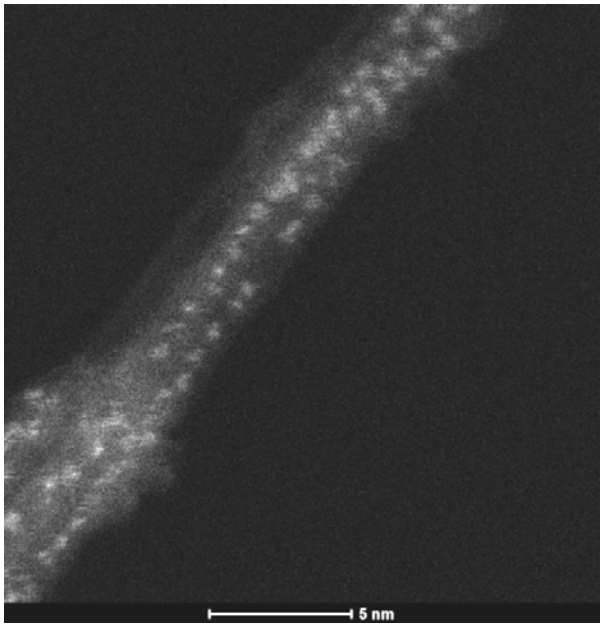

(c)

Figure 1. TEM images of $Gd_3N@C_{80}@SWNT$. (a) At low magnification and (b) (c) High angle annular dark field (HAADF) STEM images at high magnification.

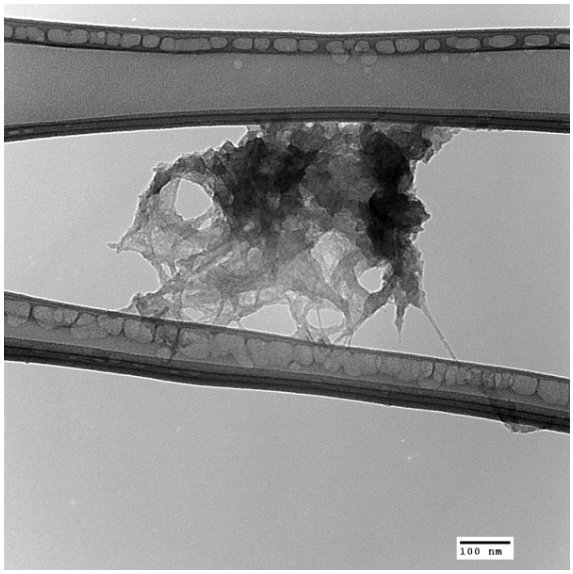

Figure 2. TEM image of $Gd_3N@C_{80}@SWNT(OH)_x$.

XPS

In order to further characterize the $M_3N@C_{80}@SWNT$ peapods, the peapods were analyzed by XPS. **Figure 3** illustrates the C 1s binding energy profiles of both functionalized and unfunctionalized $Lu_3N@C_{80}@SWNT$ made of SWNTs-1. The profiles are fitted by several Gaussian shape curves and the intensities were estimated from the integration of the peak areas under each line. The peaks centered at 286.3 eV, 287.6 eV and 289.4 eV are tentatively assigned as C(-OH), C=O and –C(O)O-, respectively. These oxygen-containing groups were observed for $Lu_3N@C_{80}@SWNT$ (**Figure 3a**) because of the heating procedure before the preparation of peapods. The intensity of the C-OH peak (286.3 eV) increased significantly from 14.3% to 23.1% after functionalization (**Figure 3b**), which clearly indicates the introduction of hydroxyl groups to SWNT peapods. Accordingly, the intensity of the peak corresponding to nonfunctionalized sp^2 and sp^3 carbon (285 eV) decreased from 77.1% to 64.9%. The payload of functional groups was

estimated as ca. 1 OH per 11 carbon atoms. This result agrees well with the previously reported value ca. 1 OH per 10 carbon atoms[71] considering the fullerene molecules encapsulated inside carbon nanotubes.

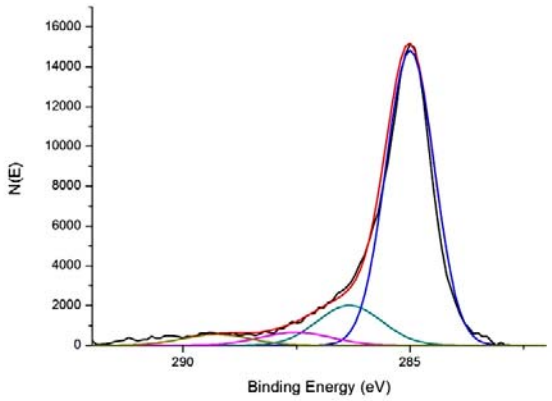

(a)

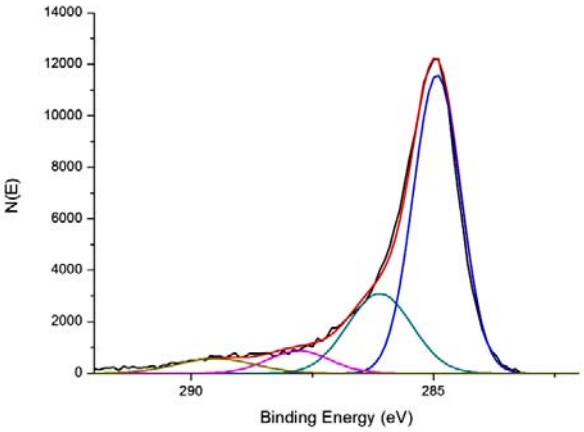

(b)

Figure 3. XPS C 1s binding energy spectrum of (a) $Lu_3N@C_{80}@SWNT$ and (b) $Lu_3N@C_{80}@SWNT(OH)_x$.

Raman

Raman spectroscopy is a valuable tool to characterize carbon nanotubes. The Raman spectra of $Gd_3N@C_{80}@SWNT$ and $Gd_3N@C_{80}@SWNT(OH)_x$ (made of SWNT-2) are shown in Figure 4a. A strong high frequency peak at 1591 cm^{-1} and a shoulder peak at 1553 cm^{-1} correspond to the tangential shear mode (G band) of SWNTs. The D band at about 1300 cm^{-1} representing defects on the SWNTs and G' band at 2610 cm^{-1} originating from a second order process involving a second longitudinal optical phonons were also observed at lower intensity.[208] The increased intensity of D band of the $Gd_3N@C_{80}@SWNT(OH)_x$ at about 1300 cm^{-1} indicates the break-down of sp2 structure of graphite, which is due to the functional group on the carbon wall. Radial breathing modes (RBM), which are in the lower frequency region at around 200 cm^{-1} and related to the diameters of SWNT, were also studied and shown in Figure 4b. Unlike regular peapods that exhibited red shifts of RBM peaks after encapsulation,[209-211] blue shift was observed for RBM peaks after the encapsulation of TNT metallofullerenes. The blue shift was most significant for the peaks at about 190 cm^{-1} and about 215 cm^{-1}. The blue shift can be explained by the stress of the inside fullerenes[212] and the different interactions between SWNT and encapsulated species as in earlier reports of SWNTs filled with organic molecules[213, 214] and fullerenes derivatives[215]. Therefore, it indicates the successful encapsulation of fullerene molecules and also suggests the diameter limit of SWNT encapsulating TNT metallofullerenes.[212] The tubular structure of peapods was retained after functionalization as indicated by the remaining RBM peaks. The peaks at higher frequency that did not shift represent the empty SWNTs, whose diameters are too

small to be filled with fullerene molecules. The decreased intensity may indicate partial damage of SWNTs after functionalization.

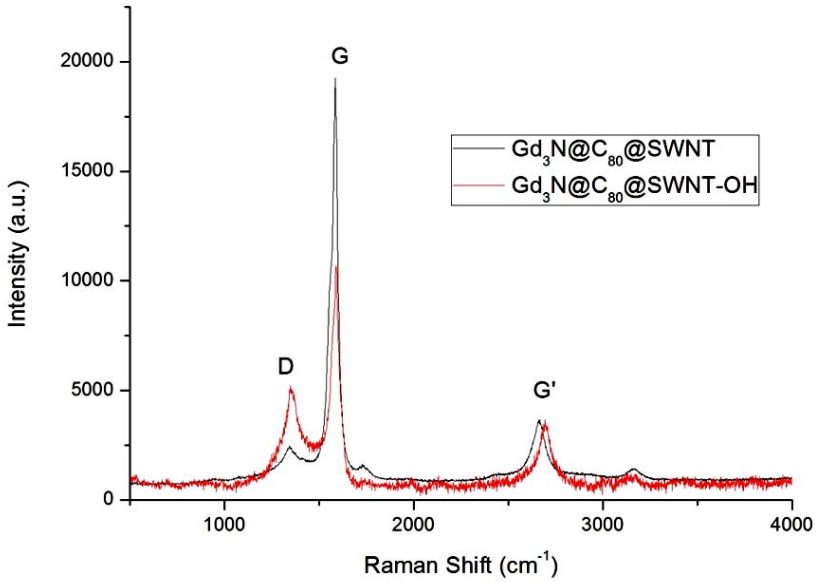

(a)

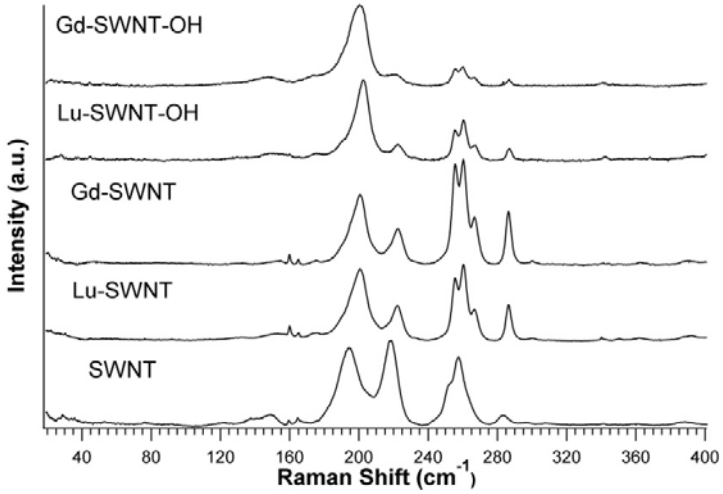

(b)

Figure 4. (a) Raman spectra of D, G and G' band of $Gd_3N@C_{80}@SWNT$ and $Gd_3N@C_{80}@SWNT(OH)_x$; (b) Raman spectra of RBM peaks of purified SWNTs, SWNT peapods and functionalized peapods.

UV-Vis

Figure 5 contains the UV-Vis spectra of purified SWNTs-1 and $Gd_3N@C_{80}@SWNT(OH)_x$ (made of SWNTs-1). The peaks at higher frequency originate from π plasmons.[208] A blue shift was observed for the water soluble peapods. This may indicate a change of the electronic structure of the SWNTs, possibly due to the stress and functionalization, because covalent functionalization removes π electrons from carbon nanotubes and transforms carbon atoms from sp^2 to sp^3 hybridization.[216]

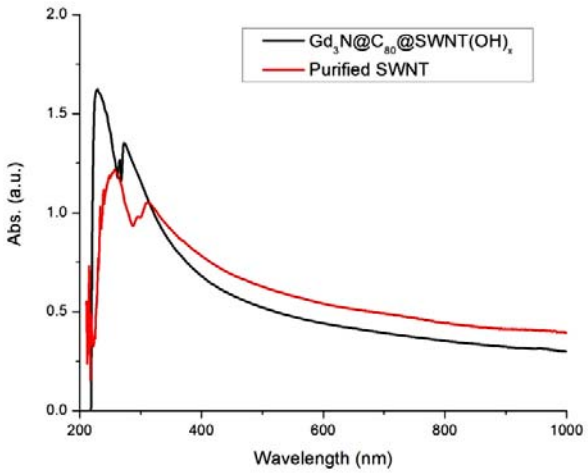

Figure 5. UV-Vis spectra of purified SWNT and $Gd_3N@C_{80}@SWNT(OH)_x$.

DLS

The aggregation of $Gd_3N@C_{80}@SWNT(OH)_x$ (made of SWNTs-2) was studied by DLS as shown in **Figure 6**. The mean value of the size distribution function of $Gd_3N@C_{80}@SWNT(OH)_x$ is determined as 146 nm. A similar result was obtained for $SWNT(OH)_x$ (data not shown), which suggests that encapsulation of TNT EMFs does not

have a significant effect on aggregation behavior. The mean size of $Gd_3N@C_{80}@SWNT(OH)_x$ is significantly larger than that of our previously reported $Gd_3N@C_{80}(OH)_{\sim 26}(CH_2CH_2COOH)_{\sim 16}$[163] and $Gd_3N@C_{80}$[DiPEG750$(OH)_x$] (~76 nm).[202] It is also significantly larger than the mean size (~105 nm) of functionalized single-walled carbon nanohorns (SWNHs) using the HSVM method in the presence of succinic acid acyl peroxide as reported previously.[217] The larger aggregation size of $Gd_3N@C_{80}@SWNT(OH)_x$ in comparison with the functionalized TNT-EMFs and SWNHs is a significant factor that could contribute to the higher ^1H magnetic resonance relaxivity discussed below.

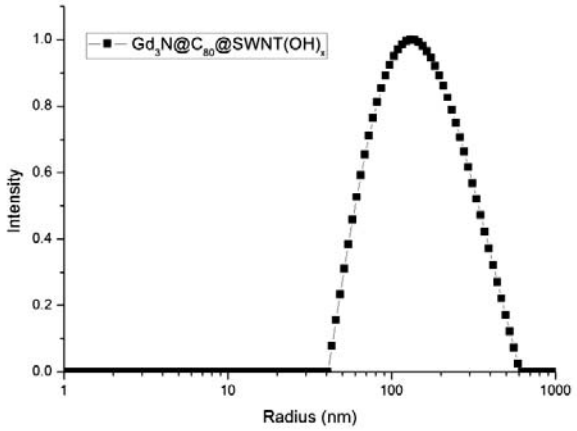

Figure 6. The intensity-weighted size distribution function of $Gd_3N@C_{80}@SWNT(OH)_x$ at 0.1 mg/mL.

^1H MR Relaxivities

The ^1H MR spin-lattice and spin-spin relaxation times (T_1 and T_2) and corresponding relaxivities ($1/T_1$ and $1/T_2$, $mM^{-1}s^{-1}$) of $M_3N@C_{80}@SWNT(OH)_x$ (M = Gd, Lu) were

measured at 0.35 T and 9.4 T. Since the $Lu_3N@C_{80}$ sample is diamagnetic, the Lu peapods were used as a diamagnetic control sample. The spin-lattice relaxivity (r_1) and spin-spin relaxitivy (r_2) data are listed in **Table 1**. For comparison, the relaxivity data of $Gd_3N@C_{80}(OH)_{\sim 26}(CH_2CH_2COOH)_{\sim 16}$ and $Gd_3N@C_{80}$[DiPEG750$(OH)_x$] previously reported are also listed in **Table 1.**[163, 202] The $Gd_3N@C_{80}@SWNT(OH)_x$ peapods prepared from both SWNTs sources exhibit consistent high spin-lattice relaxivities at the two magnetic fields. It is surprising that these $Gd_3N@C_{80}@SWNT(OH)_x$ peapods exhibit these high relaxivities in view of the "double carbon cage" separation between the encapsulated paramagnetic $(Gd_3N)^{6+}$ cluster and the water molecules. However, it is well recognized that carbon nanotubes are good transporters of water and protons[218, 219] which could facilitate ready exchange of water between the inside and outside of SWNTs. Protons and hydrogen-bonding defects also couple via long-range electrostatics.[218] In addition, the $Gd_3N@C_{80}@SWNT(OH)_x$ peapods readily form aggregates leading to increases in the rotational correlation time (τ_c) and this could also contribute to the higher spin-lattice relaxivity (r_1). As shown in **Table 1**, $Gd_3N@C_{80}@SWNT(OH)_x$ exhibited slightly higher spin-lattice relaxivity (r_1) than functionalized TNT-EMFs at 0.35 T which is consistent with the larger aggregate size distribution obtained from the DLS analysis. The spin-lattice relaxivity (r_1) of $Gd_3N@C_{80}@SWNT(OH)_x$ decreased much faster than functionalized TNT EMFs at high magnetic field (9.4 T). This is also consistent with the longer rotation correlation time (τ_c) of $Gd_3N@C_{80}@SWNT(OH)_x$ in comparison with the functionalized TNT-EMFs. A detailed nuclear magnetic resonance dispersion (NMRD) profile is needed to further understand the mechanistic details for these nanoparticles. The functionalized peapods also exhibited high spin-spin relaxivities (r_2). The high spin-

spin relaxivities could result from several additional factors. First, the residual paramagnetic metal impurities were not completely removed from the sample. ICP analysis indicated that purified SWNTs-1 still contained significant amounts of Ni impurities, but purified SWNTs-2 contained much less paramagnetic metal impurities than SWNTs-1 (see supporting information). This is consistent with much higher spin-spin relaxivity of peapods made of SWNTs-1 compared to peapods made of SWNTs-2. However, the paramagnetic metal impurity alone cannot fully explain the high spin-spin relaxivities. The paramagnetic[135] or superparamagnetic[134] properties of the SWNTs themselves also make some contribution to the r_2 spin-spin relaxivity. It is also noted that the diamagnetic control, $Lu_3N@C_{80}@SWNT(OH)_x$, also exhibited modest r_1 and r_2 relaxivities. This could be attributed to free radical defect sites on carbon nanotube walls.

($mM^{-1}s^{-1}$)

	r_1 (0.35T)	r_2 (0.35T)	r_1 (9.4T)	r_2 (9.4T)
$Gd_3N@C_{80}@SWNT(OH)_x$ (Carbolex nanotubes, Sample 1) (0.3-3μM)	171±24	719±85	21±6	866±33
$Gd_3N@C_{80}@SWNT(OH)_x$ (SWNT, Sample 2 nanotubes) (0.3-3μM)	166±33	265±28	26±2	508±28
$Lu_3N@C_{80}@SWNT(OH)_x$ Peapod (SWNT, Sample 2 nanotubes) (0.1-2 μM)	17±1	-	2±1	66±16
$Gd_3N@C_{80}(OH)_{\sim 26}(CH_2CH_2COOH)_{\sim 16}$[163]	154±7	204±22	76±3	231±25
$Gd_3N@C_{80}$[DiPEG750$(OH)_x$] (1.1-17.4 μM)[202]	152±5	169±20	63.3±1.8	274±9

Table 1. The spin-lattice (r_1) and spin-spin (r_2) MRI relaxivity data of water-soluble peapods compared to water –soluble peapods reported before.

6.4 Conclusions

In summary, single wall carbon nanotube peapods encapsulating TNT EMFs have been successfully prepared and functionalized with hydroxyl group by HSVM. The resultant products were water miscible and stable. The peapods with $Gd_3N@C_{80}$ also exhibited much higher ^1H NMR relaxivity at 0.35 T and 9.4 T than commercial MRI contrast agents. This new nanomaterial platform is a good candidate for potential MRI contrast agents because of its high relaxivity, double carbon wall protection, and potential as a multimodal delivery platform.

Supporting Information

To analyze the residual metal impurities of both types of SWNTs, the following experiments were conducted. Both purified SWNTs-1 and SWNTs-2 were functionalized. Briefly, 1 mg SWNTs were mixed with 100 mg KOH and put into a stainless steel capsule with a stainless steel milling ball. The capsule was shaken vigorously for 2 h (SPEX 8000 Mixer/Mill, 1725 rpm). The product was washed with water and sonicated in 10 mL pure water for 20 mins. The obtained suspensions were analyzed by induced coupled plasma optical emission spectroscopy (ICP-OES, Perkin-Elmer Optima 5300DV). The concentration of Fe, Co and Ni were determined by ICP-OES at 238.204 nm (Fe), 231.604 nm (Ni) and 228.616 nm (Co). The results are listed below. From the table we can see that both purified SWNTs contain residual paramagnetic impurities even after purification. SWNTs-1 contains significantly more Ni than SWNTs-2. This explains the much higher spin-spin relaxivity for peapods made of SWNTs-1.

	Fe (mg/L)	Ni (mg/L)	Co (mg/L)
SWNTs-1	0.013	1.341	0.007
SWNTs-2	0.017	0.016	0.009

Table S1. The concentration of residual metal impurities in $SWNT(OH)_x$ solutions.

Chapter 7

In Vitro and *In Vivo* Studies of Single-Walled Carbon Nanohorns with Encapsulated Metallofullerenes and Exohedrally Functionalized Quantumd Dots

7.1 Introduction

Single-walled carbon nanohorns (SWNHs) were reported by Iijima's group in 1999. They have significant advantages over traditional carbon nanotubes for *in vivo* biotechnology because no metal catalyst is used in their production, and their aggregates are naturally within the size range of endocytosis. Recent research reports also indicate that SWNHs have low toxicity.[32, 220] These features make SWNHs uniquely suited for various medical applications, such as laser therapeutic agents,[157, 159] antiviral materials,[158] anticancer agents,[146, 147] etc. By encapsulating other species, SWNHs can also be used as drug delivery systems[145, 146, 148, 221-225] and magnetic resonance imaging (MRI) contrast agents.[226, 227] However, these medical applications are limited by the hydrophobic nature of the SWNHs. Many efforts have been made to disperse SWNHs in aqueous solution, both by covalent functionalization and noncovalent modification.[148, 187, 194, 197, 223, 228-231]

Recently, we developed a facile high speed vibration milling (HSVM) method to prepare water-dispersible SWNHs functionalized with carboxyl groups.[217] The carboxylated carbon materials can be further conjugated with other materials, such as quantum dots (QDs).[76, 232, 233] QDs are semiconducting nanocrystals for which the electronic and optical properties can be tuned by altering the size due to the quantum confinement effect.[234] The SWNH-QDs conjugate can be used for multiple functions such as bio-sensing.

In this chapter, we discuss the first successful encapsulation of trimetallic nitride template endohedral metallofullerenes (TNT-EMFs) inside SWNHs (SWNH peapods). Two kinds of TNT-EMFs were used for the encapsulation: $Gd_3N@C_{80}$ and $Lu_3N@C_{80}$. $Gd_3N@C_{80}$ can be used as MRI contrast agents, while $Lu_3N@C_{80}$ can be used as an X-ray contrast agent[235] and a radiotherapeutic agent.[236] The SWNH peapods were functionalized by the HSVM method and further conjugated with ZnS-capped CdSe (CdSe/ZnS) QDs. The materials were studied both *in vitro* and *in vivo*.

7.2 Experiments, Results and Discussion

SWNHs (estimated carbon purity ≥95%) were synthesized by Nd:YAG laser (λ=1.064 μm, 20 ms pulse width) vaporization of a carbon target into an argon atmosphere at 1100 ^{o}C. TNT-EMFs, $Gd_3N@C_{80}$ and $Lu_3N@C_{80}$, were produced and purified as previously reported.[20, 166] Succinic acid acyl peroxide was synthesized according to the literature.[3] CdSe/ZnS QDs (Emission: 577 nm, FWHM < 24 nm) were purchased from Ocean Nano Tech LLC.

The SWNH peapods were prepared by heating SWNHs at 650 ^{o}C in air for 10 min to remove amorphous carbon and open windows on the tips and walls. After cooling, TNT-EMFs were dissolved in CS_2 and dropped onto the SWNHs. The solvent was evaporated. The mixture of fullerenes and SWNHs was sealed in a quartz tube under 10^{-6} Torr. The tube was heated at 470^{o}C for 24 h. The product was sonicated in toluene for 10 min. The solution was filtered through a 0.45 μm poly(tetrafluoroethylene) (PTFE) membrane filter. The solid was washed with toluene until the extract was clear. The transmission electron microscopy (TEM) samples were prepared by dispersing SWNH peapods in 1,2-dichloroethane and dropped onto lacey carbon TEM grids.

High resolution TEM (HRTEM) images of $Lu_3N@C_{80}$@SWNHs are shown in Figure 1. In the bright field image (Figure 1a) at lower magnification, fullerene molecules appear to be small circles inside SWNHs. The high angle angular dark field (HAADF) image at higher magnification comfirmed the peapod structue. Due to the significant Z-contrast of HAADF, the Lu atoms appear to be bright spots inside SWNHs (grey area). When the fullerene molecule was at the right orientation, the Lu_3N cluster appears to be an equilateral triangle as the white circle shows. Similar results were also obtained for $Gd_3N@C_{80}$@SWNHs (See supporting information).

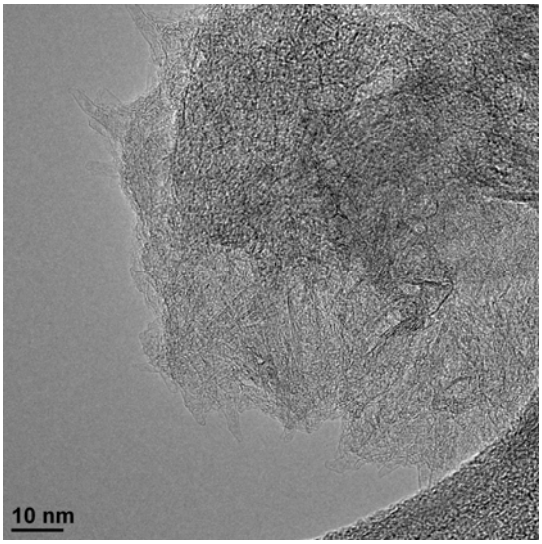

(a)

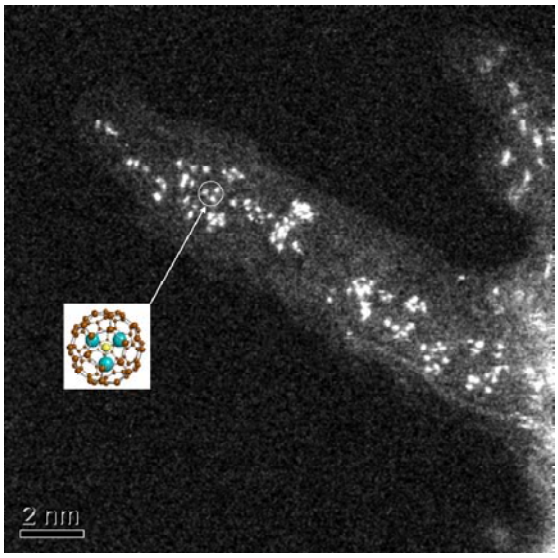

(b)

Figure 1. HRTEM image of $Lu_3N@C_{80}$@SWNHs (a) at low magnification and (b) high angle angular dark field image of $Lu_3N@C_{80}$@SWNHs at high magnification.

SWNH peapods were functionalized by the HSVM method.[217] The SWNH peapods were mixed with succinic acid acyl peroxide (mass ratio of SWNH peapods:peroxide = 1:100). The mixture was put into a stainless steel capsule with a stainless steel milling ball and shaken vigorously for 2 h (SPEX 8000 Mixer/Mill, 1725 rpm). The product was

treated with acetone and centrifuged. The supernatant was decanted. The washing procedure was repeated three times to remove excessive succinic acid acyl peroxide. The final solid product was washed with water twice and sonicated in pure water for 20 minutes. A dark suspension was obtained that was stable for several months.

CdSe/ZnS QDs were conjugated with $Gd_3N@C_{80}$@SWNHs. The method was similar to a published procedure as depicted in Scheme 1.[76] Prior to the conjugation of $Gd_3N@C_{80}$@SWNHs with QDs, the QDs surfaces were functionalized with amino groups. Briefly, QDs were suspended in chloroform via sonication for 30 min. Aqueous 1.0 M 2-aminoethanethiol hydrochloride (AET) was added to the QDs solution. Two layers were formed: the organic layer of chloroform-QDs suspension and the aqueous layer with AET. The mixture was stirred vigorously overnight and allowed to settle for a few minutes. An equal volume of phosphate-buffered saline solution (PBS) was then added, and the mixture was stirred overnight. The QDs were all transferred into the aqueous phase, which was collected and centrifuged. The precipitated QDs were then resuspended in PBS. To fabricate the $Gd_3N@C_{80}$@SWNH-QDs complexes, 1 mg of functionalized $Gd_3N@C_{80}$@SWNHs was suspended in 4 mL of PBS by sonication. N-(3-Dimethylaminopropyl)-N'-ethylcarbodiimide hydrochloride (EDC, 115mg) and N-hydroxysulfosuccinimide (Sulfo-NHS, 2.8 mg) were added, and the mixture was stirred for 5 min. Then 2 mL of functionalized QDs (2 mg/mL) in PBS were added and the resulting solution was stirred at 50 °C for 20 h. The $Gd_3N@C_{80}$@SWNH-QDs suspension was filtered through a 0.2 μm Nylon membrane. The solid was washed with pure water. In control experiments for both functionalized SWNH peapods and the

SWNH peapods conjugated with QDs, we have found no evidence for the diffusion of the TNT-EMFs out of the SWNHs. (See Supporting Information.)

Scheme 1 Depiction of conjugation of SWNHs with CdSe/ZnS QDs[a]

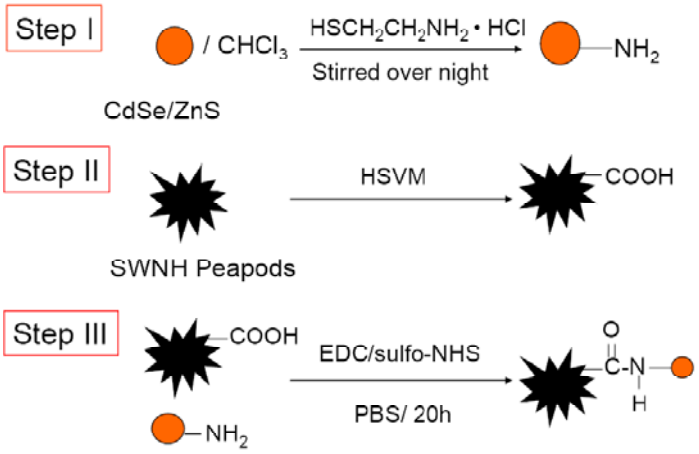

[a] The procedure contains three steps: I. Functionalization of QDs with AET; II. Functionalization of SWNHs peapods by HSVM method; III. Conjugation of SWNH peapods with QDs.

Since the encapsulated TNT-EMFs contain paramagnetic Gd^{3+} ions, they substantially increase the ^1H relaxation rates of water (or biological systems) and are potentially a new MRI contrast agent platform. The effect of these systems as potential MRI contrast agents was studied both *in vitro* and *in vivo*. The MRI experiments were performed on a 2.4 T/40 cm bore MR system (Biospec/Bruker). Tubes of different functionalized $Gd_3N@C_{80}$@SWNHs materials were imaged in a phantom well to obtain T_1-weighted (T_1W) images (T_R/T_E = 700/10 ms), T_2-weighted (T_2W) images (T_R/T_E = 6000/100 ms), and T_1-maps. The latter represents pure T_1 maps that are generated from a series of inversion-recovery spin-echo (T_1W) images. The Gd^{3+} concentrations of the

samples were determined by inductively coupled plasma mass spectrometry (ICP-MS) measurements.

Figure 2 shows the T_1-weighted, T_2-weighted and T_1 maps images of various SWNH-based materials, including our previously reported *in vitro* $Gd_3N@C_{80}(OH)_{\sim 26}(CH_2CH_2COOM)_{\sim 16}$[163] and the commercial Omniscan® agent at similar concentrations. The empty functionalized SWNHs (Figure 2A) shows no enhancement while the $Gd_3N@C_{80}(OH)_{\sim 26}(CH_2CH_2COOM)_{\sim 16}$ (Figure 2D) provides the highest contrast. The functionalized $Gd_3N@C_{80}$@SWNHs (Figure 2B) exhibited reduced contrast compared to $Gd_3N@C_{80}(OH)_{\sim 26}(CH_2CH_2COOM)_{\sim 16}$(Figure 2D), but the contrast is still significant. The reduced enhancement with the encapsulated fullerenes can be explained by the significant water exchange barrier between the encapsulated Gd^{3+} ions and bulk water molecules due to the additional graphitic layer of the SWNHs. This effective distance was increased further when QDs were conjugated (Figure 2C) to the surface of SWNHs, and thus led to even lower contrast enhancement.

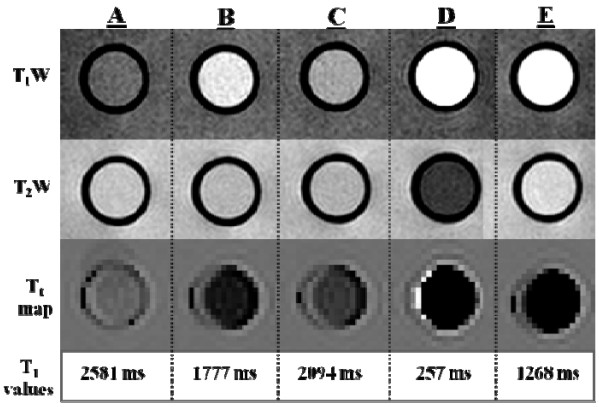

Figure 2. (Top row), T_1-weighted images (T_R/T_E = 700 ms/10 ms). Second row, T_2-weighted images (T_R/T_E = 6000 ms/100 ms). Third row, T_1-map images (T_R/T_E= 1500 ms/29 ms). Bottom row, T_1 values of (A) functionalized SWNHs, (B) functionalized $Gd_3N@C_{80}$@SWNHs, (C) $Gd_3N@C_{80}$@SWNH-QDs, (D) $Gd_3N@C_{80}(OH)_{\sim 26}(CH_2CH_2COOM)_{\sim 16}$, (E) Omniscan. The concentrations of Gd^{3+} for (B-E) are 0.102, 0.099, 0.102, and 0.102 mM, respectively. The T_1 values are averages from regions of interest (ROI) within the tubes.

To determine the ability of $Gd_3N@C_{80}$@SWNH-QDs to label cancer cells for diagnosis or permit intracellular uptake for potential drug delivery applications, *in vitro* cell cultures were imaged using QDs fluorescence by Prof. Rylander's group. A murine renal cancer cell line, RENCA, was cultured, and then the cells were allowed to adhere for 24 hours. $Gd_3N@C_{80}$@SWNH-QDs were added to the media to obtain a concentration of 0.025 mg/ml and introduced to cells for incubation durations of 24 and 48 h. Fluorescence and phase contrast images of RENCA cells were acquired before and following the 24 and 48 h incubation with $Gd_3N@C_{80}$@SWNH-QDs using a Leica fluorescence inverted microscope (CTR 6500, Leica Microsystems Inc., Bannockburn, IL) with a 20× objective. Figure 3 shows phase contrast and fluorescence images of RENCA cells without $Gd_3N@C_{80}$@SWNH-QDs inclusion (A, B) and following incubation for 24 h with $Gd_3N@C_{80}$@SWNH-QDs (D, E). Panels C and F of Figures 3 show fluorescent images of the previously mentioned samples superimposed on phase contrast images to permit enhanced visualization of the correlation between cellular structure and quantum dots fluorescence. A negligible fluorescence signal was detected in the sample without $Gd_3N@C_{80}$@SWNH-QDs. The fluorescence shown in the bottom of Figure 3C is associated with autofluorescence of debris. However, inclusion of $Gd_3N@C_{80}$@SWNH-QDs for 24 and 48 h (not shown) showed substantial and nearly identical levels of red fluorescence allowing imaging of the RENCA cells. The red fluorescence is entirely confined to the cell cytoplasm without any quantum dots visible in the extracellular media, providing evidence of cellular uptake. Due to the small size of the $Gd_3N@C_{80}$@SWNH-QDs, it is anticipated that significant cellular uptake occurs rapidly within minutes of $Gd_3N@C_{80}$@SWNH-QDs introduction. However, future experiments

measuring cellular uptake kinetics are required to confirm this hypothesis. Therefore, inclusion of $Gd_3N@C_{80}$@SWNH-QDs provide significant contrast enhancement based on their fluorescence signature necessary for imaging of RENCA cells and exhibit substantial levels of cellular uptake critical for clinical applications involving drug delivery.

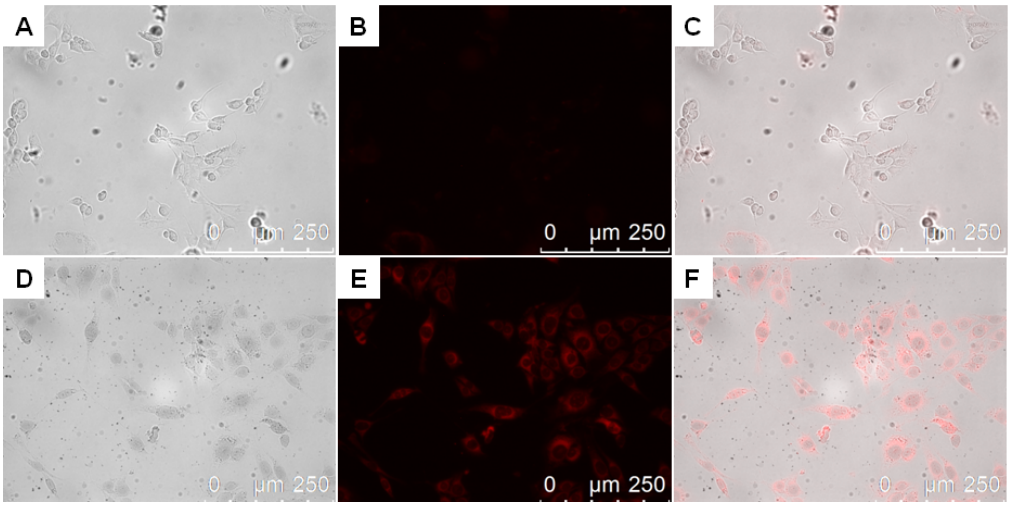

Figure 3. Phase contrast images of RENCA cells (A) without $Gd_3N@C_{80}$@SWNH-QDs inclusion and (D) following 24 h incubation with $Gd_3N@C_{80}$@SWNH-QDs. Fluorescence images of RENCA cells (B) without $Gd_3N@C_{80}$@SWNH-QDs inclusion and (E) following 24 h incubation with $Gd_3N@C_{80}$@SWNH-QDs. Fluorescent images superimposed on phase contrast images of identical samples (C) without $Gd_3N@C_{80}$@SWNH-QDs inclusion and (F) following 24 h incubation with $Gd_3N@C_{80}$@SWNH-QDs.

The *in vivo* investigation was performed by intratumoral infusion of $Gd_3N@C_{80}$@SWNH-QDs via convection enhanced delivery (CED) method into a U87 tumor bearing mouse by our collaborators, Prof. Panos P. Fatourous' group. The tumors were monitored by MRI scans with tail vein injections of OMNISCAN® before the tumor implantation. On the 11^{th} day after the tumor implantation, the $Gd_3N@C_{80}$@SWNH-QDs

were infused into the developed intra-cerebral tumor by CED using a microinjection pump (Bioanalytical Systems) at a flow rate of 0.2 μL/min for a total of 18 μL injected. The animals were scanned by MRI for baseline data immediately prior to intra-tumor infusion, and at time points of 0, 24, and up to 72 h post-infusion. Animals were then euthanized and the whole brains were extracted. Confocal microscopic images of the coronal sections were collected with a scan resolution of 1024 × 1024 pixels and a zoom factor of 1. This gave a field size of 750 μm × 750 μm. Fluorescence from DAPI and CdSe/ZnS QDs was generated by exciting the samples with a blue diode laser (405 nm). Due to the significant degree of broad spectrum autofluorescence within the tumor, the signal from the quantum dots was isolated from that of the overlying autofluorescence by collecting a lambda series of images across the spectrum and subsequently unmixing the signals using the Spectral Dye Separation module of the Leica confocal software (LCS ver. 2.5.1347a). A series of 30 images (bit depth = 12) was collected over a range of 300 nm (410 – 710 nm) using a detector window of 20 nm. Post-acquisition, the signals of DAPI, QD and autofluorescence were isolated using standard reference spectra for DAPI and Quantum Dots (Emission peak: 577 nm, FWHM 24 nm) and the collected spectrum for the tissue autofluorescence.

The *in vivo* data shown in Figure 4 clearly illustrate the brightening of the T_1-weighted MRI image in the region of infusion due to the contrast enhancement by the $Gd_3N@C_{80}$@SWNH-QDs. Figure 4A is a T_1W image of the tumor enhanced by OMNISCAN™ (tail vein injection) 10 days post tumor cell inoculation. Figure 4B is the baseline T_1W image obtained day 11 just prior to intratumoral infusion of the $Gd_3N@C_{80}$@SWNH-QDs, while Figure 4C was collected 3 h postinfusion showing

bright contrast at the infusion site within the tumor. The $Gd_3N@C_{80}$@SWNH-QDs were tracked by MRI 1 day postinfusion (Figure 4D) and 3 days post (Figure 4E), which demonstrates that the SWNHs have a significant lifetime within the tumor, remaining long enough for potential local drug delivery, therapy, and long-term diagnosis. Also, if radioactive $^{177}Lu_3N@C_{80}$ were co-encapsulated inside SWNHs, the materials could be used in dual modality for diagnosis and brachytherapy. Figure 4F is a high magnification composite confocal laser scanning microscope image of a region from a coronal section of the mouse brain (white square figure 4E) obtained following euthanization of the animal (3 days postinfusion). The red fluorescent signal of the QDs is seen within the bright contrast area on the MR image, Figure 4E (black arrow), which gives indication that the QDs remain bound to the SWNHs. This conjugation scheme can lead to further therapeutic agents remaining bound to the SWNHs, or with further ratio optimization, the QDs can be used as another tracking mode to investigate bio-distribution of the material by fluorescence imaging.

7.3 Conclusion

In conclusion, TNT-EMFs, $A_3N@C_{80}$ (A=Gd and Lu), were encapsulated into SWNHs for the first time. The SWNH peapods were functionalized with carboxyl groups by an HSVM method and conjugated with CdSe/ZnS QDs. *In vitro* and *in vivo* experiments demonstrate the potential of the SWNHs-based materials as multi-modal diagnostic MRI contrast agents.

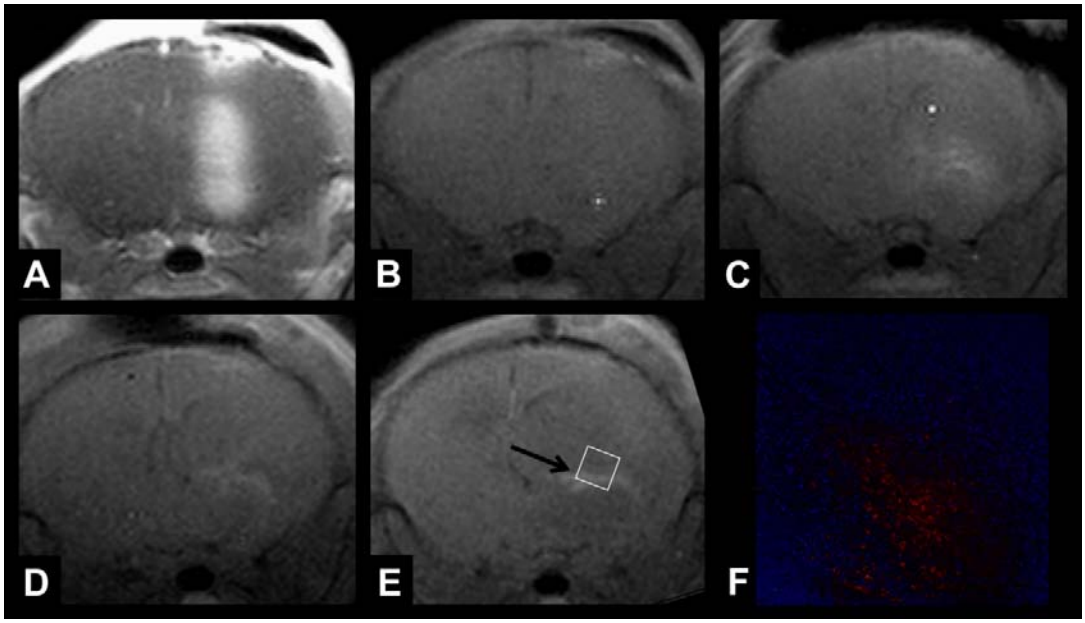

Figure 4. (A) T_1-weighted MRI image enhanced with OMNISCAN™ (I.V.) revealing the tumor in the right hemisphere. (B) Baseline T_1W image prior to infusion of $Gd_3N@C_{80}$@SWNH-QDs into a U87 tumor bearing mouse brain. T_1W images (C) 3 hours (D) 1 day, and (E) 3 days post infusion showing bright contrast at the infusion site. (F) Post-mortem confocal laser scanning microscopy image of a region(indicated by the white box in E) from a 50 μm coronal vibratome section of the same mouse brainFollowing lambda scanning, spectral dye separation and removal of the signal due to autofluorescence, the signals that are retained match the spectral profiles of DAPI (blue) and quantum dots (red).

Supporting Information

Part I. HRTEM Images of $Gd_3N@C_{80}$@SWNHs

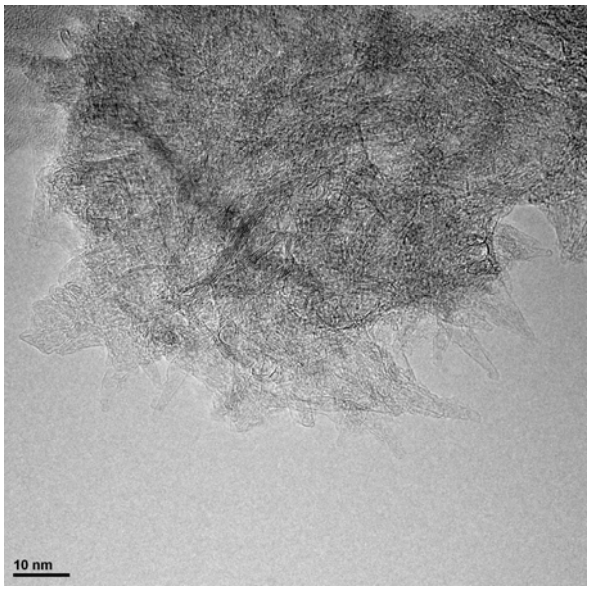

(a)

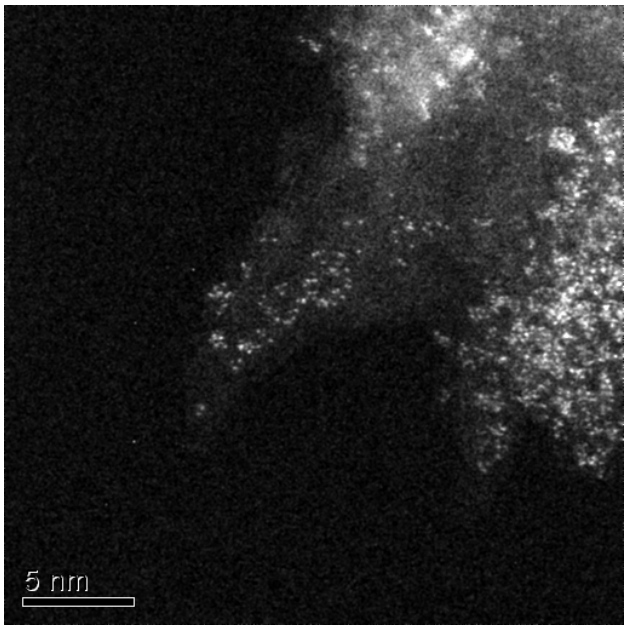

(b)

Figure S1. HRTEM image of $Gd_3N@C_{80}$@SWNHs (a) at low magnification and (b) high angle angular dark field image of $Gd_3N@C_{80}$@SWNHs at high magnification.

Part II. Studies of Diffusion of TNT-EMFs out of SWNHs

We have conducted experiments to determine if TNT-EMFs diffused out of single-walled carbon nanohorn (SWNH) peapods. In one experiment, we examined the long-term effect of diffusion of TNT-EMFs out of carboxylated SWNHs, and in a second experiment examined the short-term effect of diffusion of TNT-EMFs out of SWNHs conjugated with quantum dots.

1. In one experiment, $Lu_3N@C_{80}$SWNH was functionalized with –COOH and suspended in water by the high speed vibration milling (HSVM) method as described[217]. The concentration of Lu was 2.81 μg/mL, which was determined by inductively coupled plasma optical emission spectroscopy (ICP-OES, Perkin Elmer Optima 5300 DV) at 261.542 nm (a characteristic line of Lu). The suspension has been stored for about one and half years, and remains as a dark suspension. After storage for one and a half years, the suspension was filtered with a 0.2 μm Nylon membrane filter and the $Lu_3N@C_{80}$SWNH-COOH remained on the membrane filter. Based on previous experiments, the $Lu_3N@C_{80}$ TNT-EMFs can pass through the membrane filter. The filtrate was examined by ICP-OES at 261.542 nm. If TNT-EMFs diffused out of the SWNH-COOH, Lu should be detected in the filtrate. ICP-OES indicates that the concentration of Lu in the filtrate is 0.003 μg/mL, which is below the detection limit (0.01 μg/mL) of Lu by ICP-OES. In summary, we believe that no significant $Lu_3N@C_{80}$ diffused out of the carboxylated SWNH sample over this long time period.

2. In a second experiment we prepared some $Gd_3N@C_{80}$@SWNH peapods and functionalized them with carboxyls following the procedure described.[217] A sample of

empty SWNHs was also functionalized in the same manner as a control. Both samples were further conjugated with CdSe/ZnS quantum dots (QDs) as described, with a reaction lasting 20 hours at 50 ^{o}C. After cooling, the two solutions were filtered with 0.2 μm Nylon membrane filters and the filtrates were concentrated and examined for residual Gd by ICP-OES, which has a characteristic line at 342.247 nm. If $Gd_3N@C_{80}$ molecules diffused out of the SWNHs during the reaction, they should pass through the filter and be detected in the filtrate. The ICP results indicate that the concentration is 0.006 μg/mL for the filtrates of both the Gd-contained sample and the control sample. This concentration is below the detection limit of ICP-OES for Gd (0.05 μg/mL). Therefore, we believe that no significant $Gd_3N@C_{80}$ diffused out of the SWNHs during the 20-hour reaction period.

Note: The theoretical detection limits of ICP-OES were obtained from "ICP-OES and ICP-MS Detection Limit Guidance" from Evans Analytical Group, LLC. These detection limits assume that "there are no spectral interferences affecting the best isotope or wavelength for a given element".

Part III. TEM Images SWNH-QDs and $Gd_3N@C_{80}$@SWNHs-QDs

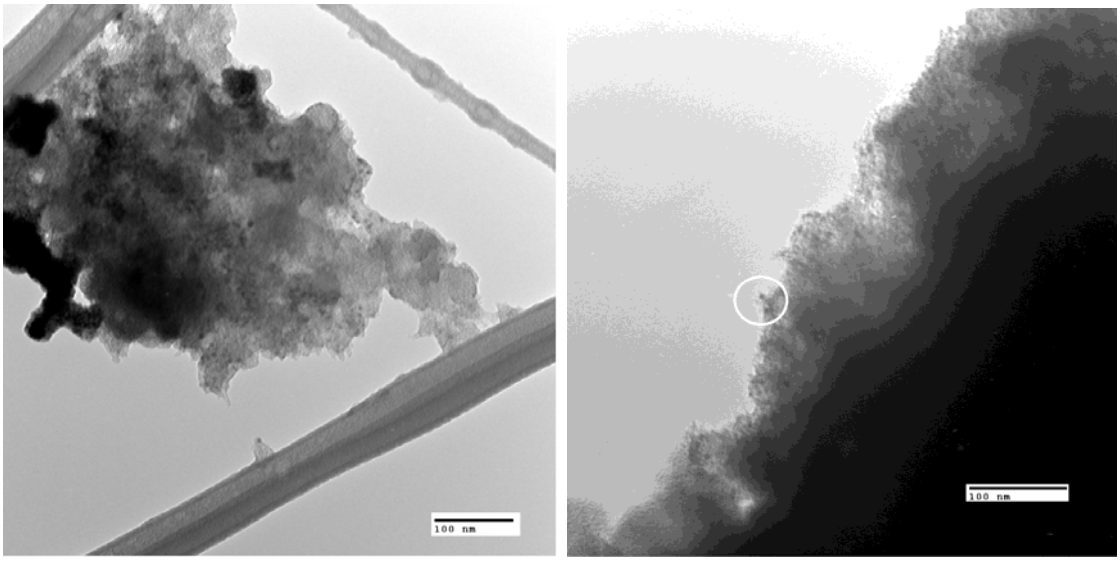

(a) (b)

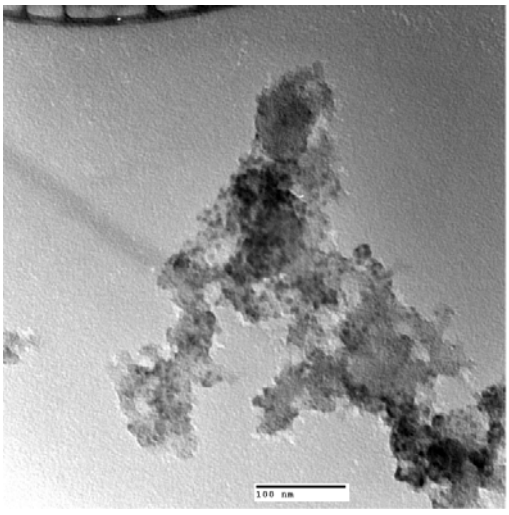

(c)

Figure S2. TEM Images of (a) SWNH-QDs, (b) $Gd_3N@C_{80}$@SWNH-QDs and (c) SWNH-QDs on supporting carbon film. QDs appear as black spots on the images. An individual QD can be observed attached to an individual carbon nanohorn as circled in (b). From (c), quantum dots were only observed on the carbon nanohorn aggregates. No free quantum dots were observed from.

Chapter 8

Summary and Future Work

8.1 Summary

This dissertation focuses on the biomedical applications of various carbon nanomaterials. Carbon nanomaterials were modified to be used as potential MRI contrast agents with other functions. $Gd_3N@C_{80}$ was functionalized by DiPEG to be water soluble. The molecular weight of PEG was tuned and the ^1H relaxivities were measured. We found that when the PEG chain was shortened (lower molecular weight), the water-soluble fullerenes aggregate more. Therefore, larger aggregates were formed and the relaxivities were increased. This research indicates that water soluble $Gd_3N@C_{80}$ is a good candidate for the application as an MRI contrast agent, and short functionalities are preferred. According to this result, $Gd_3N@C_{80}$ was also functionalized with both hydroxyl and carboxyl groups. The product has similar aggregate size and the relaxivities compared with $Gd_3N@C_{80}$[DiPEG 350$(OH)_x$] and $Gd_3N@C_{80}$[DiPEG 750$(OH)_x$].

To avoid possible alteration of the carbon cage, tubular carbon nanomaterials, including fullerenes, carbon nanotubes and nanohorns, were considered to encapsulate metallofullerenes. We developed a facile method, high speed vibration milling (HSVM) method, to functionalize tubular carbon nanomaterials. Using this method, tubular carbon materials react with succinic acyl peroxide and are functionalized with carboxyl groups. This method works pretty well for single-walled carbon nanohorns (SWNHs). We successfully encapsulated $Gd_3N@C_{80}$ and $Lu_3N@C_{80}$ inside SWNHs and functionalized

the SWNH peapods with carboxyl groups by the HSVM method. We also conjugated the Gd-doped SWNHs with CdSe/ZnS quantum dots. This new material can be used for dual purposes: MRI contrast agent and optical imaging agent. This research demonstrates the ability of SWNHs as a platform for multiple-purpose applications.

8.2 Future work

This dissertation demonstrates that SWNHs are good candidates for multipurpose platforms in biomedical applications. The function of SWNHs based materials depends on the moieties that are used to modify SWNHs. Here two future research efforts are proposed.

I. Tissue-targeting Diagnostic and Therapeutic Agents

It is known that β emitters have a relatively short penetration range and can provide localized ionizing radiation. If a β emitter, ^{177}Lu, is encapsulated inside TNT-EMFs, the new metallofullerenes can be used as radioactive therapeutic agents. Previously we have reported successful preparation of $^{177}Lu_xLu_{(3-x)}@C_{80}$ and its conjugation with a fluorescent tag labeled (tetramethyl-6-carboxyrhodamine (TAMRA)) tumor-targeting interlukin 13 (IL 13) peptide.[236] Considering the ability of SWNHs to encapsulate many molecules, $^{177}Lu_xLu_{(3-x)}N@C_{80}$ and $Gd_3N@C_{80}$ can be co-encapsulated inside SWNHs, and the resultant peapods can be functionalized by the HSVM method with carboxyl groups. Similar to our reported method,[236] TAMRA lableled IL 13 peptide can then be conjugated to the peapods. Therefore, the product can serve as both a fluorescent tagged tissue-targeting MRI contrast agent and a radioactive therapeutic agent. It is also reported

that SWNHs are laser therapeutic agents.[157, 158] Therefore, the SWNH-TAMRA-IL13 encapsulating $^{177}Lu_xLu_{(3-x)}N@C_{80}$ and $Gd_3N@C_{80}$ will totally have five functions. Besides IL 13, other tissue-targeting moieties or fluorescent tag can also be considered to modify the SWNH peapods.

II. Synthesis of QDs inside SWNHs

In Chapter 7, we discussed the SWNH peapods functionalized with CdSe/ZnS quantum dots. The Cd containing QDs may be potentially dangerous because Cd is toxic. Similar to the encapsulation of metallofullerenes, QDs are also considered to be encapsulated inside SWNHs. The typical size of commercial QDs is several nanometers, which is smaller than the diameter of SWNHs, making them difficult to encapsulated in SWNHs. The synthesis of QDs is based on the pyrolysis of organometallic agents injected into a hot coordinating solvent. The growth of QDs is initialized by temporal discrete nucleation and the size is controlled by the growth time.[237] Since SWNHs have large interior space, the nucleation may occur inside SWNHs. Therefore, QDs may be synthesized inside SWNHs and the size can be controlled by the size of SWNHs. Recent research indicates that CdSe QDs can be synthesized *in situ* inside multi-walled carbon nanotubes.[238] Although the diameter of SWNHs is much smaller than MWNTs, synthesis of QDs inside is still feasible. The QDs synthesized inside SWNHs may not have spherical shape, and their optical emission properties may also be different with QDs synthesized in solution. These properties will be studied and characterized. The QDs encapsulating SWNHs can also be modified by hydrophilic groups and other moieties for multiple purposes.

References:

1. Fatouros, P. P.; Corwin, F. D.; Chen, Z. J.; Broaddus, W. C.; Tatum, J. L.; Kettenmann, B.; Ge, Z.; Gibson, H. W.; Russ, J. L.; Leonard, A. P.; Duchamp, J. C.; Dorn, H. C., In vitro and in vivo imaging studies of a new endohedral metallofullerene nanoparticle. *Radiology* **2006**, 240, 756-764.

2. Liu, Z.; Kiessling, F.; Gatjens, J., Advanced Nanomaterials in Multimodal Imaging: Design, Functionalization, and Biomedical Applications. *J. Nanomater.* **2010**, 894303.

3. Peng, H. Q.; Alemany, L. B.; Margrave, J. L.; Khabashesku, V. N., Sidewall carboxylic acid functionalization of single-walled carbon nanotubes. *J Am Chem Soc* **2003**, 125, 15174-15182.

4. Long, B.; Wu, T. M.; Stellacci, F., Ultra-fast and scalable sidewall functionalisation of single-walled carbon nanotubes with carboxylic acid. *Chem. Commun.* **2008**, 2788-2790.

5. Shu, C. Y.; Ma, X. Y.; Zhang, J. F.; Corwin, F. D.; Sim, J. H.; Zhang, E. Y.; Dorn, H. C.; Gibson, H. W.; Fatouros, P. P.; Wang, C. R.; Fang, X. H., Conjugation of a water-soluble gadolinium endohedral fulleride with an antibody as a magnetic resonance imaging contrast agent. *Bioconjugate Chem.* **2008**, 19, 651-655.

6. Shu, C. Y.; Wang, C. R.; Zhang, J. F.; Gibson, H. W.; Dorn, H. C.; Corwin, F. D.; Fatouros, P. P.; Dennis, T. J. S., Organophosphonate functionalized Gd@C_{82} as a magnetic resonance imaging contrast agent. *Chem. Mater.* **2008**, 20, 2106-2109.

7. Whitney, J. R.; Sarkar, S.; Zhang, J. F.; Thao, D.; Young, T.; Manson, M. K.; Campbell, T. A.; Puretzky, A. A.; Rouleau, C. M.; More, K. L.; Geohegan, D. B.; Rylander, C. G.; Dorn, H. C.; Rylander, M. N., Single Walled Carbon Nanohorns as Photothermal Cancer Agents. *Lasers Surg. Med.* **2011**, 43, 43-51.

8. Kroto, H. W.; Heath, J. R.; Obrien, S. C.; Curl, R. F.; Smalley, R. E., C_{60} - Buckminsterfullerene. *Nature* **1985**, 318, 162-163.

9. Krätschmer, W.; Lamb, L. D.; Fostiropoulos, K.; Huffman, D. R., Solid C_{60} - a New Form of Carbon. *Nature* **1990**, 347, 354-358.

10. Heath, J. R.; Obrien, S. C.; Zhang, Q.; Liu, Y.; Curl, R. F.; Kroto, H. W.; Tittel, F. K.; Smalley, R. E., Lanthanum Complexes of Spheroidal Carbon Shells. *J. Am. Chem. Soc.* **1985**, 107, 7779-7780.

11. Chai, Y.; Guo, T.; Jin, C. M.; Haufler, R. E.; Chibante, L. P. F.; Fure, J.; Wang, L. H.; Alford, J. M.; Smalley, R. E., Fullerenes with Metals Inside. *J. Phys. Chem.* **1991**, 95, 7564-7568.

12. Liu, S. Y.; Sun, S. Q., Recent progress in the studies of endohedral metallofullerenes. *J. Organomet. Chem.* **2000**, 599, 74-86.

13. Weaver, J. H.; Chai, Y.; Kroll, G. H.; Jin, C.; Ohno, T. R.; Haufler, R. E.; Guo, T.; Alford, J. M.; Conceicao, J.; Chibante, L. P. F.; Jain, A.; Palmer, G.; Smalley, R. E., XPS Probes of Carbon-Caged Metals. *Chem. Phys. Lett.* **1992**, 190, 460-464.

14. Xu, Z. D.; Nakane, T.; Shinohara, H., Production and isolation of $Ca@C_{82}$ (I-IV) and $Ca@C_{84}$ (I,II) metallofullerenes. *J. Am. Chem. Soc.* **1996**, 118, 11309-11310.

15. Sun, D. Y.; Huang, H. J.; Yang, S. H.; Liu, Z. Y.; Liu, S. Y., A simple method for the selective enrichment of endohedral metallofullerenes. *Chem. Mater.* **1999**, 11, 374-377.

16. Cagle, D. W.; Thrash, T. P.; Alford, M.; Chibante, L. P. F.; Ehrhardt, G. J.; Wilson, L. J., Synthesis, characterization, and neutron activation of holmium metallofullerenes. *J. Am. Chem. Soc.* **1996**, 118, 8043-8047.

17. Shinohara, H.; Sato, H.; Ohkohchi, M.; Ando, Y.; Kodama, T.; Shida, T.; Kato, T.; Saito, Y., Encapsulation of a Scandium Trimer in C_{82}. *Nature* **1992**, 357, 52-54.

18. Wang, C. R.; Kai, T.; Tomiyama, T.; Yoshida, T.; Kobayashi, Y.; Nishibori, E.; Takata, M.; Sakata, M.; Shinohara, H., A scandium carbide endohedral metallofullerene: $(Sc_2C_2)@C_{84}$. *Angew. Chem. Int. Ed.* **2001**, 40, 397-399.

19. Liduka, Y.; Wakahara, T.; Nakahodo, T.; Tsuchiya, T.; Sakuraba, A.; Maeda, Y.; Akasaka, T.; Yoza, K.; Horn, E.; Kato, T.; Liu, M. T. H.; Mizorogi, N.; Kobayashi, K.; Nagase, S., Structural determination of metallofuIlerene Sc_3C_{82} revisited: A surprising finding. *J. Am. Chem. Soc.* **2005**, 127, 12500-12501.

20. Stevenson, S.; Rice, G.; Glass, T.; Harich, K.; Cromer, F.; Jordan, M. R.; Craft, J.; Hadju, E.; Bible, R.; Olmstead, M. M.; Maitra, K.; Fisher, A. J.; Balch, A. L.; Dorn, H. C., Small-bandgap endohedral metallofullerenes in high yield and purity. *Nature* **1999**, 401, 55-57.

21. Dunsch, L.; Yang, S., Metal nitride cluster fullerenes: Their current state and future prospects. *Small* **2007**, 3, 1298-1320.

22. Beavers, C. M.; Zuo, T. M.; Duchamp, J. C.; Harich, K.; Dorn, H. C.; Olmstead, M. M.; Balch, A. L., $Tb_3N@C_{84}$: An improbable, egg-shaped endohedral fullerene that violates the isolated pentagon rule. *J. Am. Chem. Soc.* **2006**, 128, 11352-11353.

23. Stevenson, S.; Phillips, J. P.; Reid, J. E.; Olmstead, M. M.; Rath, S. P.; Balch, A. L., Pyramidalization of Gd_3N inside a C_{80} cage. The synthesis and structure of $Gd_3N@C_{80}$. *Chem. Commun.* **2004**, 2814-2815.

24. Wang, X. L.; Zuo, T. M.; Olmstead, M. M.; Duchamp, J. C.; Glass, T. E.; Cromer, F.; Balch, A. L.; Dorn, H. C., Preparation and structure of $CeSc_2N@C_{80}$: An icosahedral carbon cage enclosing an acentric $CeSc_2N$ unit with buried f electron spin. *J. Am. Chem. Soc.* **2006**, 128, 8884-8889.

25. Chen, N.; Zhang, E. Y.; Wang, C. R., C_{80} encaging four different atoms: The synthesis, isolation, and characterizations of $ScYErN@C_{80}$. *J. Phys. Chem. B* **2006**, 110, 13322-13325.

26. Iijima, S., Helical Microtubules of Graphitic Carbon. *Nature* **1991**, 354, 56-58.

27. Iijima, S.; Ichihashi, T., Single-Shell Carbon Nanotubes of 1-Nm Diameter. *Nature* **1993**, 363, 603-605.

28. Bethune, D. S.; Kiang, C. H.; Devries, M. S.; Gorman, G.; Savoy, R.; Vazquez, J.; Beyers, R., Cobalt-Catalyzed Growth of Carbon Nanotubes with Single-Atomic-Layerwalls. *Nature* **1993**, 363, 605-607.

29. Saito, R.; Fujita, M.; Dresselhaus, G.; Dresselhaus, M. S., Electronic-Structure of Chiral Graphene Tubules. *Appl. Phys. Lett.* **1992**, 60, 2204-2206.

30. Iijima, S.; Yudasaka, M.; Yamada, R.; Bandow, S.; Suenaga, K.; Kokai, F.; Takahashi, K., Nano-aggregates of single-walled graphitic carbon nano-horns. *Chem. Phys. Lett.* **1999**, 309, 165-170.

31. Zhang, M.; Yamaguchi, T.; Iijima, S.; Yudasaka, M., Individual Single-Wall Carbon Nanohorns Separated from Aggregates. *J. Phys. Chem. C* **2009**, 113, 11184-11186.

32. Miyawaki, J.; Yudasaka, M.; Azami, T.; Kubo, Y.; Iijima, S., Toxicity of single-walled carbon nanohorns. *ACS Nano* **2008**, 2, 213-226.

33. Puretzky, A. A.; Styers-Barnett, D. J.; Rouleau, C. M.; Hu, H.; Zhao, B.; Ivanov, I. N.; Geohegan, D. B., Cumulative and continuous laser vaporization synthesis of single wall carbon nanotubes and nanohorns. *Appl. Phys. A-Mater.* **2008**, 93, 849-855.

34. Smith, B. W.; Monthioux, M.; Luzzi, D. E., Encapsulated C_{60} in carbon nanotubes. *Nature* **1998**, 396, 323-324.

35. Kataura, H.; Maniwa, Y.; Kodama, T.; Kikuchi, K.; Hirahara, K.; Suenaga, K.; Iijima, S.; Suzuki, S.; Achiba, Y.; Kratschmer, W., High-yield fullerene encapsulation in single-wall carbon nanotubes. *Synth. Met.* **2001**, 121, 1195-1196.

36. Suenaga, K.; Tence, M.; Mory, C.; Colliex, C.; Kato, H.; Okazaki, T.; Shinohara, H.; Hirahara, K.; Bandow, S.; Iijima, S., Element-selective single atom imaging. *Science* **2000**, 290, 2280-2282.

37. Okazaki, T.; Shimada, T.; Suenaga, K.; Ohno, Y.; Mizutani, T.; Lee, J.; Kuk, Y.; Shinohara, H., Electronic properties of $Gd@C_{82}$ metallofullerene peapods: $(Gd@C_{82})_n$@SWNTs. *Appl. Phys. A-Mater.* **2003**, 76, 475-478.

38. Smith, B. W.; Monthioux, M.; Luzzi, D. E., Carbon nanotube encapsulated fullerenes: a unique class of hybrid materials. *Chem. Phys. Lett.* **1999**, 315, 31-36.

39. Hirahara, K.; Bandow, S.; Suenaga, K.; Kato, H.; Okazaki, T.; Shinohara, H.; Iijima, S., Electron diffraction study of one-dimensional crystals of fullerenes. *Phys. Rev. B* **2001**, 64, 115420.

40. Suenaga, K.; Okazaki, T.; Hirahara, K.; Bandow, S.; Kato, H.; Taninaka, A.; Shinohara, H.; Iijima, S., High-resolution electron microscopy of individual metallofullerene molecules on the dipole orientations in peapods. *Appl. Phys. A-Mater.* **2003**, 76, 445-447.

41. Smith, B. W.; Luzzi, D. E.; Achiba, Y., Tumbling atoms and evidence for charge transfer in $La_2@C_{80}$@SWNT. *Chem. Phys. Lett.* **2000**, 331, 137-142.

42. Debarre, A.; Jaffiol, R.; Julien, C.; Richard, A.; Nutarelli, D.; Tchenio, P., Antenna effect in dimetallofullerene peapods. *Chem. Phys. Lett.* **2003**, 380, 6-11.

43. Khlobystov, A. N.; Porfyrakis, K.; Kanai, M.; Britz, D. A.; Ardavan, A.; Shinohara, H.; Dennis, T. J. S.; Briggs, G. A. D., Molecular motion of endohedral fullerenes in single-walled carbon nanotubes. *Angew. Chem. Int. Ed.* **2004**, 43, 1386-1389.

44. Suenaga, K.; Taniguchi, R.; Shimada, T.; Okazaki, T.; Shinohara, H.; Iijima, S., Evidence for the intramolecular motion of Gd atoms in a $Gd_2@C_{92}$ nanopeapod. *Nano Lett.* **2003**, 3, 1395-1398.

45. Kitaura, R.; Shinohara, H., Endohedral metallofullerenes and nano-peapods. *Jpn. J. Appl. Phys., Part 1* **2007**, 46, 881-891.

46. Berber, S.; Kwon, Y. K.; Tomanek, D., Microscopic formation mechanism of nanotube peapods. *Phys. Rev. Lett.* **2002**, 88, 185502.

47. Ulbricht, H.; Moos, G.; Hertel, T., Interaction of C_{60} with carbon nanotubes and graphite. *Phys. Rev. Lett.* **2003**, 90, 095501.

48. Yudasaka, M.; Ajima, K.; Suenaga, K.; Ichihashi, T.; Hashimoto, A.; Iijima, S., Nano-extraction and nano-condensation for C_{60} incorporation into single-wall carbon nanotubes in liquid phases. *Chem. Phys. Lett.* **2003**, 380, 42-46.

49. Simon, F.; Kuzmany, H.; Rauf, H.; Pichler, T.; Bernardi, J.; Peterlik, H.; Korecz, L.; Fulop, F.; Janossy, A., Low temperature fullerene encapsulation in single wall carbon nanotubes: synthesis of $N@C_{60}@SWCNT$. *Chem. Phys. Lett.* **2004**, 383, 362-367.

50. Britz, D. A.; Khlobystov, A. N.; Porfyrakis, K.; Ardavan, A.; Briggs, G. A. D., Chemical reactions inside single-walled carbon nano test-tubes. *Chem. Commun.* **2005**, 37-39.

51. Britz, D. A.; Khlobystov, A. N.; Wang, J. W.; O'Neil, A. S.; Poliakoff, M.; Ardavan, A.; Briggs, G. A., Selective host-guest interaction of single-walled carbon nanotubes with functionalised fullerenes. *Chem. Commun.* **2004**, 176-177.

52. Khlobystov, A. N.; Britz, D. A.; Wang, J. W.; O'Neil, S. A.; Poliakoff, M.; Briggs, G. A. D., Low temperature assembly of fullerene arrays in single-walled carbon nanotubes using supercritical fluids. *J. Mater. Chem.* **2004**, 14, 2852-2857.

53. Zhang, Y. M.; Chen, Y.; Yang, Y.; Liu, P.; Liu, Y., Supramolecular Architectures by Fullerene-Bridged Bis(permethyl-beta-cyclodextrin)s with Porphyrins. *Chem. Eur. J.* **2009**, 15, 11333-11340.

54. Camps, X.; Hirsch, A., Efficient cyclopropanation of C_{60} starting from malonates. *J. Chem. Soc., Perkin Trans. 1* **1997**, 1595-1596.

55. Feng, L.; Nakahodo, T.; Wakahara, T.; Tsuchiya, T.; Maeda, Y.; Akasaka, T.; Kato, T.; Horn, E.; Yoza, K.; Mizorogi, N.; Nagase, S., A singly bonded derivative of endohedral metallofullerene: $La@C_{82}CBr(COOC_2H_5)_2$. *J. Am. Chem. Soc.* **2005**, 127, 17136-17137.

56. Feng, L.; Wakahara, T.; Nakahodo, T.; Tsuchiya, T.; Piao, Q.; Maeda, Y.; Lian, Y.; Akasaka, T.; Horn, E.; Yoza, K.; Kato, T.; Mizorogi, N.; Nagase, S., The bingel monoadducts of $La@C_{82}$: Synthesis, characterization, and electrochemistry. *Chem. Eur. J.* **2006**, 12, 5578-5586.

57. Feng, L.; Tsuchiya, T.; Wakahara, T.; Nakahodo, T.; Piao, Q.; Maeda, Y.; Akasaka, T.; Kato, T.; Yoza, K.; Horn, E.; Mizorogi, N.; Nagase, S., Synthesis and characterization of a bisadduct of La@C_{82}. *J. Am. Chem. Soc.* **2006**, 128, 5990-5991.

58. Pinzon, J. R.; Zuo, T. M.; Echegoyen, L., Synthesis and Electrochemical Studies of Bingel-Hirsch Derivatives of $M_3N@I_h$-C_{80} (M = Sc, Lu). *Chem. Eur. J.* **2010**, 16, 4864-4869.

59. Pinzon, J. R.; Cardona, C. M.; Herranz, M. A.; Plonska-Brzezinska, M. E.; Palkar, A.; Athans, A. J.; Martin, N.; Rodriguez-Fortea, A.; Poblet, J. M.; Bottari, G.; Torres, T.; Gayathri, S. S.; Guldi, D. M.; Echegoyen, L., Metal Nitride Cluster Fullerene $M_3N@C_{80}$ (M = Y, Sc) Based Dyads: Synthesis, and Electrochemical, Theoretical and Photophysical Studies. *Chem. Eur. J.* **2009**, 15, 864-877.

60. Coleman, K. S.; Bailey, S. R.; Fogden, S.; Green, M. L. H., Functionalization of single-walled carbon nanotubes via the Bingel reaction. *J. Am. Chem. Soc.* **2003**, 125, 8722-8723.

61. Ashcroft, J. M.; Hartman, K. B.; Kissell, K. R.; Mackeyev, Y.; Pheasant, S.; Young, S.; Van der Heide, P. A. W.; Mikos, A. G.; Wilson, L. J., Single-molecule I_2@US-tube nanocapsules: A new X-ray contrast-agent design. *Adv. Mater.* **2007**, 19, 573-+.

62. Ashcroft, J. M.; Hartman, K. B.; Mackeyev, Y.; Hofmann, C.; Pheasant, S.; Alemany, L. B.; Wilson, L. J., Functionalization of individual ultra-short single-walled carbon nanotubes. *Nanotechnology* **2006**, 17, 5033-5037.

63. Worsley, K. A.; Moonoosawmy, K. R.; Kruse, P., Long-range periodicity in carbon nanotube sidewall functionalization. *Nano Lett.* **2004**, 4, 1541-1546.

64. Umeyama, T.; Tezuka, N.; Fujita, M.; Matano, Y.; Takeda, N.; Murakoshi, K.; Yoshida, K.; Isoda, S.; Imahori, H., Retention of intrinsic electronic properties of soluble single-walled carbon nanotubes after a significant degree of sidewall functionalization by the bingel reaction. *J Phys Chem C* **2007**, 111, 9734-9741.

65. Economopoulos, S. P.; Pagona, G.; Yudasaka, M.; Iijima, S.; Tagmatarchis, N., Solvent-free microwave-assisted Bingel reaction in carbon nanohorns. *J. Mater. Chem.* **2009**, 19, 7326-7331.

66. Li, T. B.; Huang, K. X.; Li, X. H.; Jiang, H. Y.; Li, J.; Yan, X. Z.; Li, J.; Zhao, S. K., Studies on the rapid preparation of fullerols and its formation mechanism. *Chem. J. Chinse U.* **1998**, 19, 858-860.

67. Li, J.; Takeuchi, A.; Ozawa, M.; Li, X. H.; Saigo, K.; Kitazawa, K., C_{60} Fullerol Formation Catalyzed by Quaternary Ammonium Hydroxides. *J. Chem. Soc., Chem. Commun.* **1993**, 1784-1785.

68. Cagle, D. W.; Kennel, S. J.; Mirzadeh, S.; Alford, J. M.; Wilson, L. J., In vivo studies of fullerene-based materials using endohedral metallofullerene radiotracers. *Proc. Natl. Acad. Sci. USA* **1999**, 96, 5182-5187.

69. Iezzi, E. B.; Cromer, F.; Stevenson, P.; Dorn, H. C., Synthesis of the first water-soluble trimetallic nitride endohedral metallofullerols. *Synth. Met.* **2002**, 128, 289-291.

70. Wang, S.; He, P.; Zhang, J. M.; Jiang, H.; Zhu, S. Z., Novel and efficient synthesis of water-soluble [60]fullerenol by solvent-free reaction. *Synth. Commun.* **2005**, 35, 1803-1808.

71. Pan, H.; Liu, L.; Guo, Z.-X.; Dai, L.; Zhang, F.; Zhu, D.; Czerw, R.; Carroll, D. L., Carbon nanotubols from mechanochemical reaction. *Nano Lett.* **2003**, 3, 29-32.

72. Cerar, J.; Cerkovnik, J.; Skerjanc, J., Water-soluble fullerenes. 1. Fullerenehexamalonic acid T_h-$C_{66}(COOH)_{12}$, an intermediate spherical electrolyte. *J. Phys. Chem. B* **1998**, 102, 7377-7381.

73. Lamparth, I.; Hirsch, A., Water-Soluble Malonic-Acid Derivatives of C_{60} with a Defined 3-Dimensional Structure. *J. Chem. Soc., Chem. Commun.* **1994**, 1727-1728.

74. Liu, J.; Rinzler, A. G.; Dai, H. J.; Hafner, J. H.; Bradley, R. K.; Boul, P. J.; Lu, A.; Iverson, T.; Shelimov, K.; Huffman, C. B.; Rodriguez-Macias, F.; Shon, Y. S.; Lee, T. R.; Colbert, D. T.; Smalley, R. E., Fullerene pipes. *Science* **1998**, 280, 1253-1256.

75. Kukovecz, A.; Kramberger, C.; Holzinger, M.; Kuzmany, H.; Schalko, J.; Mannsberger, M.; Hirsch, A., On the stacking behavior of functionalized single-wall carbon nanotubes. *J. Phys. Chem. B* **2002**, 106, 6374-6380.

76. Ravindran, S.; Chaudhary, S.; Colburn, B.; Ozkan, M.; Ozkan, C. S., Covalent coupling of quantum dots to multiwalled carbon nanotubes for electronic device applications. *Nano Lett* **2003**, 3, 447-453.

77. Hirsch, A., Functionalization of single-walled carbon nanotubes. *Angew. Chem. Int. Ed.* **2002**, 41, 1853-1859.

78. Bandow, S.; Rao, A. M.; Williams, K. A.; Thess, A.; Smalley, R. E.; Eklund, P. C., Purification of single-wall carbon nanotubes by microfiltration. *J. Phys. Chem. B* **1997**, 101, 8839-8842.

79. Duesberg, G. S.; Burghard, M.; Muster, J.; Philipp, G.; Roth, S., Separation of carbon nanotubes by size exclusion chromatography. *Chem. Commun.* **1998**, 435-436.

80. Cherukuri, P.; Gannon, C. J.; Leeuw, T. K.; Schmidt, H. K.; Smalley, R. E.; Curley, S. A.; Weisman, R. B., Mammalian pharmacokinetics of carbon nanotubes using intrinsic near-infrared fluorescence. *Proc. Natl. Acad. Sci. USA* **2006**, 103, 18882-18886.

81. Wu, Y.; Hudson, J. S.; Lu, Q.; Moore, J. M.; Mount, A. S.; Rao, A. M.; Alexov, E.; Ke, P. C., Coating single-walled carbon nanotubes with phospholipids. *J. Phys. Chem. B* **2006**, 110, 2475-2478.

82. Tasis, D.; Tagmatarchis, N.; Bianco, A.; Prato, M., Chemistry of carbon nanotubes. *Chem. Rev.* **2006**, 106, 1105-1136.

83. Ajayan, P. M.; Schadler, L. S.; Giannaris, C.; Rubio, A., Single-walled carbon nanotube-polymer composites: Strength and weakness. *Adv. Mater.* **2000**, 12, 750-+.

84. O'Connell, M. J.; Boul, P.; Ericson, L. M.; Huffman, C.; Wang, Y. H.; Haroz, E.; Kuper, C.; Tour, J.; Ausman, K. D.; Smalley, R. E., Reversible water-solubilization of single-walled carbon nanotubes by polymer wrapping. *Chem. Phys. Lett.* **2001**, 342, 265-271.

85. Hornak, J. P. The Basics of MRI. http://www.cis.rit.edu/htbooks/mri/ (04/01/2010),

86. Damadian, R. V., Tumor Detection by Nuclear Magnetic Resonance. *Science* **1971**, 171, 1151-1153.

87. Hollis, D. P.; Saryan, L. A.; Morris, H. P., A nuclear magnetic resonance study of water in two Morris hepatomas. *Johns Hopkins Med. J.* **1972**, 131, 441-444.

88. Lauterbur, P. C., Image Formation by Induced Local Interactions: Examples Employing Nuclear Magnetic Resonance. *Nature* **1973**, 242, 190-191.

89. Kumar, A.; Welti, D.; Ernst, R. R., NMR Fourier zeugmatography. *J. Magn. Reson.* **1975**, 18, 69-83.

90. de Haen, C., Conception of the first magnetic resonance imaging contrast agents: a brief history. *Top. Magn. Reson. Imag.* **2001**, 12, 221-30.

91. Zhang, S.; Ren, J.; Pei, F., Progress in research of magnetic resonance imaging contrast agents. *Prog. Chem.* **1995**, 7, 98-112.

92. Yan, G.; Zhuo, R., Research progress of magnetic resonance imaging contrast agents. *Chin. Sci. Bull.* **2001**, 46, 1233-1237.

93. Bottrill, M.; Nicholas, L. K.; Long, N. J., Lanthanides in magnetic resonance imaging. *Chem. Soc. Rev.* **2006**, 35, 557-571.

94. Aime, S.; Botta, M.; Terreno, E., Gd(III)-based contrast agents for MRI. *Adv. Inorg. Chem.* **2005**, 57, 173-237.

95. Toth, E.; Helm, L.; Merbach, A. E., Relaxivity of MRI contrast agents. *Top. Curr. Chem.* **2002**, 221, 61-101.

96. Kato, H.; Kanazawa, Y.; Okumura, M.; Taninaka, A.; Yokawa, T.; Shinohara, H., Lanthanoid Endohedral Metallofullerenols for MRI Contrast Agents. *J. Am. Chem. Soc.* **2003**, 125, 4391-4397.

97. Caravan, P.; Ellison, J. J.; McMurry, T. J.; Lauffer, R. B., Gadolinium(III) Chelates as MRI Contrast Agents: Structure, Dynamics, and Applications. *Chem. Rev.* **1999**, 99, 2293-2352.

98. Lauffer, R. B., Paramagnetic Metal Complexes as Water Proton Relaxation Agents for NMR Imaging: Theory and Design. *Chem. Rev.* **1987**, 87, 901-927.

99. Louie, A., Magnetic resonance imaging contrast agents in the study of development. In *Curr. Top. Dev. Biol.*, 2005; Vol. 70.

100. Luz, Z.; Meiboom, S., Proton Relaxation in Dilute Solutions of Cobalt (II) and Nickel (II) Ions in Methanol and the Rate of Methanol Exchange of the Solvation Sphere. *J. Chem. Phys.* **1964**, 40, 2686-2692.

101. Swift, T. J.; Connick, R. E., NMR-Relaxation Mechanisms of O^{17} in Aqueous Solutions of Paramagnetic Cations and the Lifetime of Water Molecules in the First Coordination Sphere. *J. Chem. Phys.* **1962**, 37, 307-320.

102. Aime, S.; Fedeli, F.; Sanino, A.; Terreno, E., A R_2/R_1 Ratiometric Procedure for a Concentration-Independent, pH-Responsive, Gd(III)-Based MRI Agent. *J. Am. Chem. Soc.* **2006**, 128, 11326-11327.

103. Bertini, I.; Luchinat, C., *Coord. Chem. Rev.* **1996**, 150, 1-295.

104. Banci, L.; Bertini, I.; Luchinat, C., *Nuclear and Electron Relaxation: the magnetic nucleus-unpaired electron coupling in solution* 1991.

105. Kowalewski, J.; Nordenskiöld, L.; Benetis, N.; Westlund, P.-O., Theory of nuclear spin relaxation in paramagnetic systems in solution *Prog. Nucl. Magn. Reson. Spectrosc.* **1985**, 17, 141-185.

106. Caravan, P., Strategies for increasing the sensitivity of gadolinium based MRI contrast agents. *Chem. Soc. Rev.* **2006**, 35, 512-523.

107. Lipad, G.; Szabo, A., Model-Free Approach to the Interpretation of Nuclear Magnetic Resonance Relaxation in Macromolecules. 2. Analysis of Experimental Results. *J. Am. Chem. Soc.* **1982**, 104, 4559-4570.

108. Lipad, G.; Szabo, A., Model-Free Approach to the Interpretation of Nuclear Magnetic Resonance Relaxation in Macromolecules. 1. Theory and Range of Validity. *J. Am. Chem. Soc.* **1982**, 104, 4546-4559.

109. Aime, S.; Botta, M.; Parker, D.; De Sousa, A. S., Relaxometric Determination of the Exchange Rate of the Coordinated Water Protons in a Neutral GdIII Chelate. *Chem. Eur. J.* **1997**, 3, 1499-1504.

110. Aime, S.; Barge, A.; Botta, M.; Parker, D.; De Sousa, A. S., Prototropic Ws Whole Water Exchange Contributions to the Solvent Relaxation Enhancement in the Aqueous Solution of a Cationic Gd^{3+} Macrocyclic Complex. *J. Am. Chem. Soc.* **1997**, 119, 4767-4768.

111. Kotek, J.; Lebduskova, P.; Hermann, P.; Vander Elst, L.; Muller, R. N.; Geraldes, C. F. G. C.; Maschmeyer, T.; Lukes, I.; Peters, J. A., Lanthanide(III) complexes of novel mixed carboxylic-phosphorus acid derivatives of diethylenetriamine: A step towards more efficient MRI contrast agents. *Chem. Eur. J.* **2003**, 9, 5899-5915.

112. Szilagyi, E.; Toth, E.; Brucher, E.; Merbach, A. E., Lanthanide(III)-1,4,7,10-tetraazacyclododecane-1,4,7,10-tetraacetic acid complexes in acidic medium: significant decrease in water exchange rate. *J. Chem. Soc., Dalton Trans.* **1999**, 2481-2486.

113. Andre, J. P.; Maecke, H. R.; Toth, E.; Merbach, A. A., Synthesis and physicochemical characterization of a novel precursor for covalently bound macromolecular MRI contrast agents. *J. Biol. Inorg. Chem.* **1999**, 4, 341-347.

114. La Mar, G. N.; Horrocks, W. D.; Holm, R. G., *NMR of Paramagnetic Molecules*. New York, 1973.

115. Strandberg, E.; Westlund, P.-O., 1H NMRD profile and ESR lineshape calculation for an isotropic electron spin system with S = 7/2. A generalized modified Solomon-

Bloembergen-Morgan theory for nonextreme-narrowing conditions. *J. Magn. Reson., Ser A* **1996**, 122, 179-191.

116. Benazeth, S.; Purans, J.; Chalbot, M.-C.; Nguyen-van-Duong, M. K.; Nicolas, L.; Keller, F.; Gaudemer, A., Temperature and pH dependence XAFS study of Gd(DOTA)- and $Gd(DTPA)_2$ complexes: solid state and solution structures. *Inorg. Chem.* **1998**, 37, 3667-3674.

117. Yamaguchi, T.; Nomura, M.; Wakita, H.; Otaki, H., An extended x-ray absorption fine structure study of aqueous rare earth perchlorate solutions in liquid and glassy states. *J. Chem. Phys.* **1988**, 89, 5153-9.

118. Astashkin, A. V.; Raitsimring, A. M.; Caravan, P., Pulsed ENDOR Study of Water Coordination to Gd^{3+} Complexes in Orientationally Disordered Systems. *J. Phys. Chem. A* **2004**, 108, 1990-2001.

119. Cossy, C.; Helm, L.; Powell, D. H.; Merbach, A. E., A change in coordination number from nine to eight along the lanthanide(III) aqua ion series in solution: a neutron diffraction study. *New J. Chem.* **1995**, 19, 27-35.

120. Wilson, L. J.; Cagle, D. W.; Thrash, T. P.; Kennel, S. J.; Mirzadeh, S.; Alford, J. M.; Ehrhardt, G. J., Metallofullerene drug design. *Coord. Chem. Rev.* **1999**, 190-192, 199-207.

121. Shu, C. Y.; Zhang, E. Y.; Xiang, J. F.; Zhu, C. F.; Wang, C. R.; Pei, X. L.; Han, H. B., Aggregation studies of the water-soluble gadofullerene magnetic resonance imaging contrast agent: $[Gd@C_{82}O_6(OH)_{16}(NHCH_2CH_2COOH)_8]_x$. *J. Phys. Chem. B* **2006**, 110, 15597-15601.

122. Shu, C. Y.; Gan, L. H.; Wang, C. R.; Pei, X. L.; Han, H. B., Synthesis and characterization of a new water-soluble endohedral metallofullerene for MRI contrast agents. *Carbon* **2006**, 44, 496-500.

123. Toth, E.; Bolskar, R. D.; Borel, A.; Gonzalez, G.; Helm, L.; Merbach, A. E.; Sitharaman, B.; Wilson, L. J., Water-soluble gadofullerenes: Toward high-relaxivity, pH-responsive MRI contrast agents. *J. Am. Chem. Soc.* **2005**, 127, 799-805.

124. Sitharaman, B.; Bolskar, R. D.; Rusakova, I.; Wilson, L. J., $Gd@C_{60}[C(COOH)_2]_{10}$ and $Gd@C_{60}(OH)_x$: Nanoscale Aggregation Studies of Two Metallofullerene MRI Contrast Agents in Aqueous Solution. *Nano Lett.* **2004**, 4, 2373-2378.

125. Bolskar, R. D.; Benedetto, A. F.; Husebo, L. O.; Price, R. E.; Jackson, E. F.; Wallace, S.; Wilson, L. J.; Alford, J. M., First soluble $M@C_{60}$ derivatives provide

enhanced access to metallofullerenes and permit in vivo evaluation of $Gd@C_{60}[C(COOH)_2]_{10}$ as a MRI contrast agent. *J. Am. Chem. Soc.* **2003**, 125, 5471-5478.

126. Kato, H.; Suenaga, K.; Mikawa, W.; Okumura, M.; Miwa, N.; Yashiro, A.; Fujimura, H.; Mizuno, A.; Nishida, Y.; Kobayashi, K.; Shinohara, H., Syntheses and EELS characterization of water-soluble multi-hydroxyl $Gd@C_{82}$ fullerenols. *Chem. Phys. Lett.* **2000**, 324, 255-259.

127. Wilson, L. J., Medical applications of fullerenes and metallofullerenes. *Electrochem. Soc. Interface* **1999**, 8, 24-28.

128. Wang, X. Synthesis and Functionalizations of Trimetallic Nitride Template Endohedral Metallofullerenes. M.S. Thesis, Virginia Polytechnic Institute and State University, Blackburg, 2006.

129. Sitharaman, B.; Wilson, L. J., Gadofullerenes and gadonanotubes: A new paradigm for high-performance magnetic resonance imaging contrast agent probes. *J. Biomed. Nanotechnol.* **2007**, 3, 342-352.

130. Sitharaman, B.; Kissell, K. R.; Hartman, K. B.; Tran, L. A.; Baikalov, A.; Rusakova, I.; Sun, Y.; Khant, H. A.; Ludtke, S. J.; Chiu, W.; Laus, S.; Toth, E.; Helm, L.; Merbach, A. E.; Wilson, L. J., Superparamagnetic gadonanotubes are high-performance MRI contrast agents. *Chem. Commun.* **2005**, 3915-3917.

131. Sitharaman, B.; Wilson, L. J., Gadonanotubes as new high-performance MRI contrast agents. *Int. J. Nanomed.* **2006**, 1, 291-295.

132. Hashimoto, A.; Yorimitsu, H.; Ajima, K.; Suenaga, K.; Isobe, H.; Miyawaki, A.; Yudasaka, M.; Iijima, S.; Nakamura, E., Selective deposition of a gadolinium(III) cluster in a hole opening of single-wall carbon nanohorn. *Proc. Natl. Acad. Sci. USA* **2004**, 101, 8527-8530.

133. Richard, C.; Doan, B. T.; Beloeil, J. C.; Bessodes, M.; Toth, E.; Scherman, D., Noncovalent functionalization of carbon nanotubes with amphiphilic Gd^{3+} chelates: Toward powerful T_1 and T_2 MRI contrast agents. *Nano Lett.* **2008**, 8, 232-236.

134. Ananta, J. S.; Matson, M. L.; Tang, A. M.; Mandal, T.; Lin, S.; Wong, K.; Wong, S. T.; Wilson, L. J., Single-Walled Carbon Nanotube Materials as T2-Weighted MRI Contrast Agents. *J. Phys. Chem. C* **2009**, 113, 19369-19372.

135. Chen, R. B.; Lu, B. J.; Tsai, C. C.; Chang, C. P.; Shyu, F. L.; Lin, M. F., Persistent currents in finite zigzag carbon nanotubes. *Carbon* **2004**, 42, 2873-2878.

136. Hilder, T. A.; Hill, J. M., Carbon nanotubes as drug delivery nanocapsules. *Curr. Appl. Phys.* **2008**, 8, 258-261.

137. Hilder, T. A.; Hill, J. M., Modelling the encapsulation of the anticancer drug cisplatin into carbon nanotubes. *Nanotechnology* **2007**, 18, 275704.

138. Hilder, T. A.; Hill, J. M., Probability of encapsulation of paclitaxel and doxorubicin into carbon nanotubes. *Micro & Nano Letters* **2008**, 3, 41-49.

139. Guo, Y.; Shi, D. L.; Cho, H. S.; Dong, Z. Y.; Kulkarni, A.; Pauletti, G. M.; Wang, W.; Lian, J.; Liu, W.; Ren, L.; Zhang, Q. Q.; Liu, G. K.; Huth, C.; Wang, L. M.; Ewing, R. C., In vivo imaging and drug storage by quantum-dot-conjugated carbon nanotubes. *Adv Funct Mater* **2008**, 18, 2489-2497.

140. Liu, Z.; Chen, K.; Davis, C.; Sherlock, S.; Cao, Q. Z.; Chen, X. Y.; Dai, H. J., Drug delivery with carbon nanotubes for in vivo cancer treatment. *Cancer Res.* **2008**, 68, 6652-6660.

141. Liu, Z.; Sun, X. M.; Nakayama-Ratchford, N.; Dai, H. J., Supramolecular chemistry on water-soluble carbon nanotubes for drug loading and delivery. *ACS Nano* **2007**, 1, 50-56.

142. Chen, J. Y.; Chen, S. Y.; Zhao, X. R.; Kuznetsova, L. V.; Wong, S. S.; Ojima, I., Functionalized Single-Walled Carbon Nanotubes as Rationally Designed Vehicles for Tumor-Targeted Drug Delivery. *J. Am. Chem. Soc.* **2008**, 130, 16778-16785.

143. Shiba, K., Functionalization of carbon nanomaterials by evolutionary molecular engineering: Potential application in drug delivery systems. *J Drug Target* **2006**, 14, 512-518.

144. Kase, D.; Shiba, K.; Jin, Z.; Kasuya, D.; Yudasaka, M.; Iijima, S. Toward development of nano-materials composed of artificial proteins and nano-carbons. Nanotechnology, IEEE-NANO, Third IEEE Conference, 2003; pp 386-389.

145. Murakami, T.; Ajima, K.; Miyawaki, J.; Yudasaka, M.; Iijima, S.; Shiba, K., Drug-Loaded Carbon Nanohorns: Adsorption and Release of Dexamethasone *in Vitro*. *Mol. Pharm.* **2004**, 1, 399-405.

146. Ajima, K.; Yudasaka, M.; Murakami, T.; Maigne, A.; Shiba, K.; Ijima, S., Carbon nanohorns as anticancer drug carriers. *Mol. Pharm.* **2005**, 2, 475-480.

147. Ajima, K.; Murakami, T.; Mizoguchi, Y.; Tsuchida, K.; Ichihashi, T.; Iijima, S.; Yudasaka, M., Enhancement of In Vivo Anticancer Effects of Cisplatin by Incorporation Inside Single-Wall Carbon Nanohorns. *ACS Nano* **2008**, 2, 2057-2064.

148. Matsumura, S.; Ajima, K.; Yudasaka, M.; Iijima, S.; Shiba, K., Dispersion of Cisplatin-Loaded Carbon Nanohorns with a Conjugate Comprised of an Artificial Peptide Aptamer and Polyethylene Glycol. *Mol. Pharm.* **2007**, 4, 723-729.

149. Kam, N. W. S.; O'Connell, M.; Wisdom, J. A.; Dai, H. J., Carbon nanotubes as multifunctional biological transporters and near-infrared agents for selective cancer cell destruction. *Proc. Natl. Acad. Sci. USA* **2005**, 102, 11600-11605.

150. O'Connell, M. J.; Bachilo, S. M.; Huffman, C. B.; Moore, V. C.; Strano, M. S.; Haroz, E. H.; Rialon, K. L.; Boul, P. J.; Noon, W. H.; Kittrell, C.; Ma, J. P.; Hauge, R. H.; Weisman, R. B.; Smalley, R. E., Band gap fluorescence from individual single-walled carbon nanotubes. *Science* **2002**, 297, 593-596.

151. Yang, D. J.; Zhang, Q.; Chen, G.; Yoon, S. F.; Ahn, J.; Wang, S. G.; Zhou, Q.; Wang, Q.; Li, J. Q., Thermal conductivity of multiwalled carbon nanotubes. *Phys. Rev. B* **2002**, 66, 165440.

152. Kim, J. W.; Shashkov, E. V.; Galanzha, E. I.; Kotagiri, N.; Zharov, V. P., Photothermal antimicrobial nanotherapy and nanodiagnostics with self-assembling carbon nanotube clusters. *Laser Surg Med* **2007**, 39, 622-634.

153. Torti, S. V.; Byrne, F.; Whelan, O.; Levi, N.; Ucer, B.; Schmid, M.; Torti, F. M.; Akman, S.; Liu, J.; Ajayan, P. M.; Nalamasu, O.; Carroll, D. L., Thermal ablation therapeutics based on CNx multi-walled nanotubes. *International Journal of Nanomedicine* **2007**, 2, 707-714.

154. Kim, J.-W.; Galanzha, E. I.; Shashkov, E. V.; Moon, H.-M.; Zharov, V. P., Golden carbon nanotubes as multimodal photoacoustic and photothermal high-contrast molecular agents. *Nat Nano* **2009**, 4, 688-694.

155. Wang, C.-H.; et al., In vitro photothermal destruction of neuroblastoma cells using carbon nanotubes conjugated with GD2 monoclonal antibody. *Nanotechnology* **2009**, 20, 315101.

156. Moon, H. K.; Lee, S. H.; Choi, H. C., In Vivo Near-Infrared Mediated Tumor Destruction by Photothermal Effect of Carbon Nanotubes. *ACS Nano* **2009**, 3, 3707-3713.

157. Miyako, E.; Nagata, H.; Hirano, K.; Makita, Y.; Nakayama, K.-i.; Hirotsu, T., Near-infrared laser-triggered carbon nanohorns for selective elimination of microbes. *Nanotechnology* **2007**, 18, 475103/1-475103/7.

158. Miyako, E.; Nagata, H.; Hirano, K.; Sakamoto, K.; Makita, Y.; Nakayama, K.-i.; Hirotsu, T., Photoinduced antiviral carbon nanohorns. *Nanotechnology* **2008**, 19, 075106/1-075106/6.

159. Zhang, M.; Murakami, T.; Ajima, K.; Tsuchida, K.; Sandanayaka Atula, S. D.; Ito, O.; Iijima, S.; Yudasaka, M., Fabrication of ZnPc/protein nanohorns for double photodynamic and hyperthermic cancer phototherapy. *Proc. Natl. Acad. Sci. USA* **2008**, 105, 14773-8.

160. Sieber, M. A.; Pietsch, H.; Walter, J.; Haider, W.; Frenzel, T.; Weinmann, H. J., A preclinical study to investigate the development of nephrogenic systemic fibrosis: A possible role for gadolinium-based contrast media. *Invest. Radiol.* **2008**, 43, 65-75.

161. Grobner, T., Gadolinium - a specific trigger for the development of nephrogenic fibrosing dermopathy and nephrogenic systemic fibrosis? *Nephrol., Dial., Transplant.* **2006**, 21, 1104-1108.

162. Mikawa, M.; Kato, H.; Okumura, M.; Narazaki, M.; Kanazawa, Y.; Miwa, N.; Shinohara, H., Paramagnetic water-soluble metallofullerenes having the highest relaxivity for MRI contrast agents. *Bioconjugate Chem.* **2001**, 12, 510-514.

163. Shu, C. Y.; Corwin, F. D.; Zhang, J. F.; Chen, Z. J.; Reid, J. E.; Sun, M. H.; Xu, W.; Sim, J. H.; Wang, C. R.; Fatouros, P. P.; Esker, A. R.; Gibson, H. W.; Dorn, H. C., Facile Preparation of a New Gadofullerene-Based Magnetic Resonance Imaging Contrast Agent with High ^{1}H Relaxivity. *Bioconjugate Chem.* **2009**, 20, 1186-1193.

164. MacFarland, D. K.; Walker, K. L.; Lenk, R. P.; Wilson, S. R.; Kumar, K.; Kepley, C. L.; Garbow, J. R., Hydrochalarones: A novel endohedral metallofullerene platform for enhancing magnetic resonance imaging contrast. *J. Med. Chem.* **2008**, 51, 3681-3683.

165. Zhang, E. Y.; Shu, C. Y.; Feng, L.; Wang, C. R., Preparation and characterization of two new water-soluble endohedral metallofullerenes as magnetic resonance imaging contrast agents. *J. Phys. Chem. B* **2007**, 111, 14223-14226.

166. Ge, Z. X.; Duchamp, J. C.; Cai, T.; Gibson, H. W.; Dorn, H. C., Purification of endohedral trimetallic nitride fullerenes in a single, facile step. *J. Am. Chem. Soc.* **2005**, 127, 16292-16298.

167. Krause, M.; Dunsch, L., Gadolinium nitride Gd_3N in carbon cages: The influence of cluster size and bond strength. *Angew. Chem. Int. Ed.* **2005**, 44, 1557-1560.

168. Yang, S. F.; Kalbac, M.; Popov, A.; Dunsch, L., Gadolinium-based mixed metal nitride clusterfullerenes $Gd_xSc_{3-x}N@C_{80}$ (x=1, 2). *Chemphyschem* **2006**, 7, 1990-1995.

169. Zhang, S.; Sun, D.; Li, X.; Pei, F.; Liu, S., Synthesis and solvent enhanced relaxation property of water-soluble endohedral metallofullerenols. *Fullerene Sci. Technol.* **1997**, 5, 1635-1643.

170. Laus, S.; Sitharaman, B.; Toth, E.; Bolskar, R. D.; Helm, L.; Asokan, S.; Wong, M. S.; Wilson, L. J.; Merbach, A. E., Destroying gadofullerene aggregates by salt addition in aqueous solution of $Gd@C_{60}(OH)_x$ and $Gd@C_{60}[C(COOH)_2]_{10}$. *J. Am. Chem. Soc.* **2005**, 127, 9368-9369.

171. Qian, M. C.; Ong, S. V.; Khanna, S. N.; Knickelbein, M. B., Magnetic endohedral metallofullerenes with floppy interiors. *Phys. Rev. B* **2007**, 75, 104424.

172. Laus, S.; Sitharaman, B.; Toth, E.; Bolskar, R. D.; Helm, L.; Wilson, L. J.; Merbach, A. E., Understanding paramagnetic relaxation phenomena for water-soluble gadofullerenes. *J. Phys. Chem. C* **2007**, 111, 5633-5639.

173. Lipari, G.; Szabo, A., Model-Free Approach to the Interpretation of Nuclear Magnetic-Resonance Relaxation in Macromolecules .1. Theory and Range of Validity. *J. Am. Chem. Soc.* **1982**, 104, 4546-4559.

174. Bekyarova, E.; Ni, Y. C.; Malarkey, E. B.; Montana, V.; McWilliams, J. L.; Haddon, R. C.; Parpura, V., Applications of Carbon Nanotubes in Biotechnology and Biomedicine. *J. Biomed. Nanotechnol.* **2005**, 1, 3-17.

175. Klumpp, C.; Kostarelos, K.; Prato, M.; Bianco, A., Functionalized carbon nanotubes as emerging nanovectors for the delivery of therapeutics. *Biochim. Biophys. Acta-Biomembranes* **2006**, 1758, 404-412.

176. Niyogi, S.; Hamon, M. A.; Hu, H.; Zhao, B.; Bhowmik, P.; Sen, R.; Itkis, M. E.; Haddon, R. C., Chemistry of Single-Walled Carbon Nanotubes. *Acc. Chem. Res.* **2002**, 35, 1105-1113.

177. Sun, Y.-P.; Fu, K.; Lin, Y.; Huang, W., Functionalized Carbon Nanotubes: Properties and Applications. *Acc. Chem. Res.* **2002**, 35, 1096-1104.

178. Islam, M. F.; Rojas, E.; Bergey, D. M.; Johnson, A. T.; Yodh, A. G., High weight fraction surfactant solubilization of single-wall carbon nanotubes in water. *Nano Lett.* **2003**, 3, 269-273.

179. Moore, V. C.; Strano, M. S.; Haroz, E. H.; Hauge, R. H.; Smalley, R. E.; Schmidt, J.; Talmon, Y., Individually suspended single-walled carbon nanotubes in various surfactants. *Nano Lett.* **2003**, 3, 1379-1382.

180. Richard, C.; Balavoine, F.; Schultz, P.; Ebbesen, T. W.; Mioskowski, C., Supramolecular self-assembly of lipid derivatives on carbon nanotubes. *Science* **2003**, 300, 775-778.

181. Chen, R. J.; Zhang, Y. G.; Wang, D. W.; Dai, H. J., Noncovalent sidewall functionalization of single-walled carbon nanotubes for protein immobilization. *J. Am. Chem. Soc.* **2001**, 123, 3838-3839.

182. Shvartzman-Cohen, R.; Nativ-Roth, E.; Baskaran, E.; Levi-Kalisman, Y.; Szleifer, I.; Yerushalmi-Rozen, R., Selective dispersion of single-walled carbon nanotubes in the presence of polymers: the role of molecular and colloidal length scales. *J. Am. Chem. Soc.* **2004**, 126, 14850-14857.

183. Sinani, V. A.; Gheith, M. K.; Yaroslavov, A. A.; Rakhnyanskaya, A. A.; Sun, K.; Mamedov, A. A.; Wicksted, J. P.; Kotov, N. A., Aqueous dispersions of single-wall and multiwall carbon nanotubes with designed amphiphilic polycations. *J. Am. Chem. Soc.* **2005**, 127, 3463-3472.

184. Didenko, V. V.; Moore, V. C.; Baskin, D. S.; Smalley, R. E., Visualization of individual single-walled carbon nanotubes by fluorescent polymer wrapping. *Nano Lett.* **2005**, 5, 1563-1567.

185. Star, A.; Stoddart, J. F.; Steuerman, D.; Diehl, M.; Boukai, A.; Wong, E. W.; Yang, X.; Chung, S. W.; Choi, H.; Heath, J. R., Preparation and properties of polymer-wrapped single-walled carbon nanotubes. *Angew. Chem. Int. Ed.* **2001**, 40, 1721-1725.

186. Zheng, M.; Jagota, A.; Semke, E. D.; Diner, B. A.; Mclean, R. S.; Lustig, S. R.; Richardson, R. E.; Tassi, N. G., DNA-assisted dispersion and separation of carbon nanotubes. *Nat. Mater.* **2003**, 2, 338-342.

187. Murakami, T.; Fan, J.; Yudasaka, M.; Iijima, S.; Shiba, K., Solubilization of Single-Wall Carbon Nanohorns Using a PEG-Doxorubicin Conjugate. *Mol. Pharm.* **2006**, 3, 407-414.

188. Dieckmann, G. R.; Dalton, A. B.; Johnson, P. A.; Razal, J.; Chen, J.; Giordano, G. M.; Munoz, E.; Musselman, I. H.; Baughman, R. H.; Draper, R. K., Controlled assembly of carbon nanotubes by designed amphiphilic peptide helices. *J. Am. Chem. Soc.* **2003**, 125, 1770-1777.

189. Ortiz-Acevedo, A.; Xie, H.; Zorbas, V.; Sampson, W. M.; Dalton, A. B.; Baughman, R. H.; Draper, R. K.; Musselman, I. H.; Dieckmann, G. R., Diameter-selective solubilization of single-walled carbon nanotubes by reversible cyclic peptides. *J. Am. Chem. Soc.* **2005**, 127, 9512-9517.

190. Zorbas, V.; Smith, A. L.; Xie, H.; Ortiz-Acevedo, A.; Dalton, A. B.; Dieckmann, G. R.; Draper, R. K.; Baughman, R. H.; Musselman, I. H., Importance of aromatic content for peptide/single-walled carbon nanotube interactions. *J. Am. Chem. Soc.* **2005**, 127, 12323-12328.

191. Ziegler, K. J.; Gu, Z. N.; Peng, H. Q.; Flor, E. L.; Hauge, R. H.; Smalley, R. E., Controlled oxidative cutting of single-walled carbon nanotubes. *J. Am. Chem. Soc.* **2005**, 127, 1541-1547.

192. Georgakilas, V.; Tagmatarchis, N.; Pantarotto, D.; Bianco, A.; Briand, J. P.; Prato, M., Amino acid functionalisation of water soluble carbon nanotubes. *Chem. Commun.* **2002**, 3050-3051.

193. Georgakilas, V.; Voulgaris, D.; Vazquez, E.; Prato, M.; Guldi, D. M.; Kukovecz, A.; Kuzmany, H., Purification of HiPCO carbon nanotubes via organic functionalization. *J. Am. Chem. Soc.* **2002**, 124, 14318-14319.

194. Tagmatarchis, N.; Maigne, A.; Yudasaka, M.; Iijima, S., Functionalization of carbon nanohorns with azomethine ylides: towards solubility enhancement and electron-transfer processes. *Small* **2006**, 2, 490-494.

195. Cioffi, C.; Campidelli, S.; Brunetti, F. G.; Meneghetti, M.; Prato, M., Functionalisation of carbon nanohorns. *Chem. Commun.* **2006**, 2129-2131.

196. Isobe, H.; Tanaka, T.; Maeda, R.; Noiri, E.; Solin, N.; Yudasaka, M.; Iijima, S.; Nakamura, E., Preparation, purification, characterization, and cytotoxicity assessment of water-soluble, transition-metal-free carbon nanotube aggregates. *Angew. Chem. Int. Ed.* **2006**, 45, 6676-6680.

197. Pagona, G.; Karousis, N.; Tagmatarchis, N., Aryl diazonium functionalization of carbon nanohorns. *Carbon* **2008**, 46, 604-610.

198. Pagona, G.; Tagmatarchis, N.; Fan, J.; Yudasaka, M.; Iijima, S., Cone-end functionalization of carbon nanohorns. *Chem. Mater.* **2006**, 18, 3918-3920.

199. Pagona, G.; Sandanayaka, A. S. D.; Araki, Y.; Fan, J.; Tagmatarchis, N.; Charalambidis, G.; Coutsolelos, A. G.; Boitrel, B.; Yudasaka, M.; Iijima, S.; Ito, O., Covalent functionalization of carbon nanohorns with porphyrins: Nanohybrid formation and photoinduced electron and energy transfer. *Adv. Funct. Mater.* **2007**, 17, 1705-1711.

200. Cioffi, C.; Campidelli, S.; Sooambar, C.; Marcaccio, M.; Marcolongo, G.; Meneghetti, M.; Paolucci, D.; Paolucci, F.; Ehli, C.; Rahman, G. M. A.; Sgobba, V.; Guldi, D. M.; Prato, M., Synthesis, characterization, and photoinduced electron transfer in functionalized single wall carbon nanohorns. *J. Am. Chem. Soc.* **2007**, 129, 3938-3945.

201. Harutyunyan, A. R.; Pradhan, B. K.; Chang, J. P.; Chen, G. G.; Eklund, P. C., Purification of single-wall carbon nanotubes by selective microwave heating of catalyst particles. *J. Phys. Chem. B* **2002**, 106, 8671-8675.

202. Zhang, J. F.; Fatouros, P. P.; Shu, C. Y.; Reid, J.; Owens, L. S.; Cai, T.; Gibson, H. W.; Long, G. L.; Corwin, F. D.; Chen, Z. J.; Dorn, H. C., High Relaxivity Trimetallic Nitride (Gd_3N) Metallofullerene MRI Contrast Agents with Optimized Functionality. *Bioconjugate Chem.* **2010**, 21, 610-615.

203. Hartman, K. B.; Laus, S.; Bolskar, R. D.; Muthupillai, R.; Helm, L.; Toth, E.; Merbach, A. E.; Wilson, L. J., Gadonanotubes as ultrasensitive pH-smart probes for magnetic resonance imaging. *Nano Lett.* **2008**, 8, 415-419.

204. Kitaura, R.; Shinohara, H., Carbon-nanotube-based hybrid materials. Nanopeapods. *Chem. - Asian J.* **2006**, 1, 646-655.

205. Li, B.; Shi, Z. J.; Lian, Y. F.; Gu, Z. N., Aqueous soluble single-wall carbon nanotube. *Chem. Lett.* **2001**, 598-599.

206. Warner, J. H.; Watt, A. A. R.; Ge, L.; Porfyrakis, K.; Akachi, T.; Okimoto, H.; Ito, Y.; Ardavan, A.; Montanari, B.; Jefferson, J. H.; Harrison, N. M.; Shinohara, H.; Briggs, G. A. D., Dynamics of Paramagnetic Metallofullerenes in Carbon Nanotube Peapods. *Nano Lett.* **2008**, 8, 1005-1010.

207. Warner, J. H.; Ito, Y.; Zaka, M.; Ge, L.; Akachi, T.; Okimoto, H.; Porfyrakis, K.; Watt, A. A. R.; Shinohara, H.; Briggs, G. A. D., Rotating Fullerene Chains in Carbon Nanopeapods. *Nano Lett.* **2008**, 8, 2328-2335.

208. Freiman, S.; Hooker, S.; Migler, K.; Arepalli, S., Measurement Issues in Single Wall Carbon Nanotubes. In National Institute of Standards and Technology: 2008.

209. Bandow, S.; Takizawa, M.; Hirahara, K.; Yudasaka, M.; Iijima, S., Raman scattering study of double-wall carbon nanotubes derived from the chains of fullerenes in single-wall carbon nanotubes. *Chem. Phys. Lett.* **2001**, 337, 48-54.

210. Kavan, L.; Dunsch, L.; Kataura, H.; Oshiyama, A.; Otani, M.; Okada, S., Electrochemical tuning of electronic structure of C_{60} and C_{70} fullerene peapods: In situ visible near-infrared and Raman study. *J. Phys. Chem. B* **2003**, 107, 7666-7675.

211. Ohno, Y.; Kurokawa, Y.; Kishimoto, S.; Mizutani, T.; Shimada, T.; Ishida, M.; Okazaki, T.; Shinohara, H.; Murakami, Y.; Maruyama, S.; Sakai, A.; Hiraga, K., Synthesis of carbon nanotube peapods directly on Si substrates. *Appl. Phys. Lett.* **2005**, 86, 023109(1-3).

212. Bandow, S.; Takizawa, M.; Kato, H.; Okazaki, T.; Shinohara, H.; Iijima, S., Smallest limit of tube diameters for encasing of particular fullerenes determined by radial breathing mode Raman scattering. *Chem. Phys. Lett.* **2001**, 347, 23-28.

213. Ren, Y. P.; Pastorin, G., Incorporation of hexamethylmelamine inside capped carbon nanotubes. *Adv. Mater.* **2008**, 20, 2031-2036.

214. Yao, M.; Stenmark, P.; Abou-Hamad, E.; Nitze, F.; Qin, J.; Goze-Bac, C.; Wågberg, T., Confined adamantane molecules assembled to one dimension in carbon nanotubes. *Carbon* **2011**, 49, 1159-1166.

215. Mrzel, A.; Hassanien, A.; Liu, Z.; Suenaga, K.; Miyata, Y.; Yanagi, K.; Kataura, H., Effective, fast, and low temperature encapsulation of fullerene derivatives in single wall carbon nanotubes. *Surf. Sci.* **2007**, 601, 5116-5120.

216. Kavan, L.; Kalbac, M.; Zukalova, M.; Dunsch, L., Electrochemical doping of chirality-resolved carbon nanotubes. *J. Phys. Chem. B* **2005**, 109, 19613-19619.

217. Shu, C.; Zhang, J.; Ge, J.; Sim, J. H.; Burke, B. G.; Williams, K. A.; Rylander, N. M.; Campbell, T.; Puretzky, A.; Rouleau, C.; Geohegan, D. B.; More, K.; Esker, A. R.; Gibson, H. W.; Dorn, H. C., A Facile High-speed Vibration Milling Method to Water-disperse Single-walled Carbon Nanohorns. *Chem. Mater.* **2010**, 22, 347-351.

218. Dellago, C.; Naor Mor, M.; Hummer, G., Proton transport through water-filled carbon nanotubes. *Phys. Rev. Lett.* **2003**, 90, 105902.

219. Hummer, G.; Rasaiah, J. C.; Noworyta, J. P., Water conduction through the hydrophobic channel of a carbon nanotube. *Nature* **2001**, 414, 188-190.

220. Lynch, R. M.; Voy, B. H.; Glass, D. F.; Mahurin, S. M.; Zhao, B.; Hu, H.; Saxton, A. M.; Donnell, R. L.; Cheng, M.-D., Assessing the pulmonary toxicity of single-walled carbon nanohorns. *Nanotoxicology* **2007**, 1, 157-166.

221. Xu, J. X.; Yudasaka, M.; Kouraba, S.; Sekido, M.; Yamamoto, Y.; Iijima, S., Single wall carbon nanohorn as a drug carrier for controlled release. *Chem. Phys. Lett.* **2008**, 461, 189-192.

222. Venkatesan, N.; Yoshimitsu, J.; Ito, Y.; Shibata, N.; Takada, K., Liquid filled nanoparticles as a drug delivery tool for protein therapeutics. *Biomaterials* **2005**, 26, 7154-7163.

223. Murakami, T.; Sawada, H.; Tamura, G.; Yudasaka, M.; Iijima, S.; Tsucbida, K., Water-dispersed single-wall carbon nanohorns as drug carriers for local cancer chemotherapy. *Nanomedicine* **2008**, 3, 453-463.

224. Utsumi, S.; Urita, K.; Kanoh, H.; Yudasaka, M.; Suenaga, K.; Iijima, S.; Kaneko, K., Preparing a magnetically responsive single-wall carbon nanohorn colloid by anchoring magnetite nanoparticles. *J. Phys. Chem. B* **2006**, 110, 7165-7170.

225. Yudasaka, M.; Murakami, T.; Ajima, K.; Miyawaki, J.; Shiba, K.; Iijima, S., Drug delivery system (DDS) applications of carbon nanotubes and carbon nanohorns. *Pharm Tech Jpn.* **2005**, 21, 2108-2112.

226. Miyawaki, J.; Yudasaka, M.; Imai, H.; Yorimitsu, H.; Isobe, H.; Nakamura, E.; Iijima, S., *In vivo* magnetic resonance imaging of single-walled carbon nanohorns by labeling with magnetite nanoparticles. *Adv. Mater.* **2006**, 18, 1010-1014.

227. Miyawaki, J.; Yudasaka, M.; Imai, H.; Yorimitsu, H.; Isobe, H.; Nakamura, E.; Iijima, S., Synthesis of Ultrafine Gd_2O_3 Nanoparticles Inside Single-Wall Carbon Nanohorns. *J. Phys. Chem. B* **2006**, 110, 5179-5181.

228. Rubio, N.; Herrero, M. A.; Meneghetti, M.; Diaz-Ortiz, A.; Schiavon, M.; Prato, M.; Vazquez, E., Efficient functionalization of carbon nanohorns via microwave irradiation. *J. Mater. Chem.* **2009**, 19, 4407-4413.

229. Mountrichas, G.; Ichihashi, T.; Pispas, S.; Yudasaka, M.; Iijima, S.; Tagmatarchis, N., Solubilization of Carbon Nanohorns by Block Polyelectrolyte Wrapping and Templated Formation of Gold Nanoparticles. *J. Phys. Chem. C* **2009**, 113, 5444-5449.

230. Pagona, G.; Rotas, G.; Petsalakis, I. D.; Theodorakopoulos, G.; Fan, J.; Maigne, A.; Yudasaka, M.; Iijima, S.; Tagmatarchis, N., Soluble functionalized carbon nanohorns. *J. Nanosci. Nanotechnol.* **2007**, 7, 3468-3472.

231. Pagona, G.; Fan, J.; Maigne, A.; Yudasaka, M.; Iijima, S.; Tagmatarchis, N., Aqueous carbon nanohorn-pyrene-porphyrin nanoensembles: Controlling charge-transfer interactions. *Diamond Relat. Mater.* **2007**, 16, 1150-1153.

232. Ravindran, S.; Chaudhary, S.; Ozkan, M.; Ozkan, C. S., Functionalization of carbon nanotubes for self assembly applications. In *Biomicroelectromech. Sys.*, 2003; Vol. 773, pp 95-99.

233. Zou, G. Z., Highly conjugated water soluble CdSe quantum dots to multiwalled carbon nanotubes. *Chin. Chem. Lett.* **2009**, 20, 356-357.

234. Alivisatos, A. P., Semiconductor clusters, nanocrystals, and quantum dots. *Science* **1996**, 271, 933-937.

235. Iezzi, E. B.; Duchamp, J. C.; Fletcher, K. R.; Glass, T. E.; Dorn, H. C., Lutetium-based trimetallic nitride endohedral metallofullerenes: New contrast agents. *Nano Lett.* **2002**, 2, 1187-1190.

236. Shultz, M. D.; Duchamp, J. C.; Wilson, J. D.; Shu, C.-Y.; Ge, J.; Zhang, J.; Gibson, H. W.; Fillmore, H. L.; Hirsch, J. I.; Dorn, H. C.; Fatouros, P. P., Encapsulation of a Radiolabeled Cluster Inside a Fullerene Cage, $^{177}Lu_xLu_{(3-x)}N@C_{80}$: An Interleukin-13-Conjugated Radiolabeled Metallofullerene Platform. *J. Am. Chem. Soc.* **2010**, 132, 4980-4981.

237. Murray, C. B.; Norris, D. J.; Bawendi, M. G., Synthesis and Characterization of Nearly Monodisperse Cde (E = S, Se, Te) Semiconductor Nanocrystallites. *J. Am. Chem. Soc.* **1993**, 115, 8706-8715.

238. Wang, L.; Niu, M.; Wu, Z., *In situ* growth of CdSe/CdS quantum dots inside and outside of MWCNTs. *Curr. Appl. Phys.* **2009**, 9, 1112-1116.